UNIVERSITY OF OKLAHOMA

GRADUATE COLLEGE

PERFORMANCE OF FIBER-REINFORCED ECO-FRIENDLY CONCRETE FOR BRIDGE STRUCTURES

A THESIS

SUBMITTED TO THE GRADUATE FACULTY

in partial fulfillment of the requirements for the

Degree of

MASTER OF SCIENCE

By

KODI WALLACE
Norman, Oklahoma
2016

PERFORMANCE OF FIBER-REINFORCED ECO-FRIENDLY CONCRETE FOR BRIDGE STRUCTURES

A THESIS APPROVED FOR THE
SCHOOL OF CIVIL ENGINEERING AND ENVIRONMENTAL SCIENCE

BY

_____
Dr. Jeffery Volz, Chair

_____
Dr. Royce Floyd

_____
Dr. Christopher Ramseyer

Acknowledgements

First and foremost I would like to thank my advisor, Dr. Jeffery Volz. His patience, kindness, and leadership throughout this process has helped make it a rewarding and successful experience.

I would like to thank my committee members, Dr. Royce Floyd and Dr. Chris Ramseyer, for their time and suggestions.

I would also like to thank the University of Oklahoma for the opportunity to pursue this degree, the scholarships that made it possible, and the experiences gained throughout this project.

Next, I would like to thank the lab technician, Mike Schmitz, and my fellow graduate students, Jonathan Drury, Corey Wirkman, Derek Garcias, Austin Messerli, Jake Choate, Hisham Tuwair, Nischal Pradhan, Mason Moore, and Alix Bradford. Their help and expertise with test setups, data collection, and the research in general were very much appreciated. I could have never completed the work without them.

I would like to thank my parents, Brian and Kim Wallace for all of the support and encouragement they have given me throughout all of my studies. It has made me into the person I am today and drove me to be the best I could be. Without them, this would not have been possible.

Last but not least, I would like to thank my boyfriend, Brandon Johns, for his support throughout my time in school. His patience, encouragement, and goofy jokes helped get me through the stressful times and made the good times much more enjoyable.

Table of Contents

List of Tables

List of Figures

Abstract

Concrete is the leading building material in the world due to its readily available materials, strength, durability, and relatively low cost. With cities growing at a more rapid pace, the demand for concrete is increasing. Buildings, bridges, and roadways are being constructed and repaired more often than they were twenty years ago. This means that the demand for concrete is rising as well. Unfortunately, there are environmental concerns with regard to the use of concrete. The Portland cement used to manufacture concrete produces large amounts of carbon dioxide emissions, equating to approximately 5% of man-made CO_2 emissions globally. In order to reduce the effects of Portland cement on the environment while still growing communities, lessening the amount of the Portland cement used in concrete could create a comparable concrete with lower environmental impact.

Reducing the amount of cementitious material in concrete can have negative ramifications. Cement takes on many different roles in a concrete mixture. Cement as part of the paste fills voids between aggregates, binds the aggregates together, and provides strength to the concrete as a whole. Reducing this part of the concrete could cause it to not perform as well as a standard concrete mix. The main objective of this research was to explore economically friendly concrete and its properties in structural design while working with local materials. This research was expected to develop an economically friendly concrete mix with a reduction in cementitious content and the use of aggregate optimization that would closely match a standard Oklahoma

Department of Transportation (ODOT) mix. Two economically friendly concrete mixes were compared to a standard ODOT Class AA mix in testing.

To evaluate shear capacity, nine full-scale beams were tested with six #7 flexural reinforcing bars. These beams were constructed using the *ACI 318-14 Building Code Requirements for Structural Concrete* and tested with a third point loading test frame. The eco-friendly concrete mixes performed at the same level as the ODOT Class AA mix design in terms of fresh and hardened concrete properties and shear strength. As a result, the use of an optimized aggregate distribution can help reduce the cementitious content of concrete mixes without sacrificing performance.

1. Introduction

1.1 Background and Justification

1.1.1 General. Concrete is the leading building material in the world due to its readily available material, strength, durability, and relatively low cost. With cities growing at a more rapid pace, the demand for concrete is increasing. Buildings, bridges, and roadways are being constructed and repaired more often than they were twenty years ago. This means that the demand for concrete is rising as well. Unfortunately, there are environmental concerns with regard to the use of concrete. The Portland cement used to produce concrete produces large amounts of carbon dioxide emissions, equating to approximately 5% of man-made CO_2 emissions globally (Rubenstein 2012).

In order to reduce the effects of Portland cement on the environment while still growing communities, lessening the amount of the Portland cement used in concrete could create a comparable concrete with lower environmental impact.

1.1.2 Benefits of Economically Friendly Concrete. Economically friendly concrete can have many benefits to society. By using a concrete mixture with less cementitious material, the long-term CO_2 emissions into the environment would be reduced. Using less Portland cement would also mean less expensive concrete since Portland cement is the single most expensive item in typical concrete.

1.1.3 Concerns of Economically Friendly Concrete.

Reducing the amount of cementitious material in concrete can negative ramifications. Portland cement takes on many different roles in a concrete mixture. Portland cement as a constituent of the paste fills voids between aggregates, binds the aggregates together, and provides strength to the concrete as a whole. Reducing this part of the concrete could cause it to not perform as well as a standard concrete mix.

1.2 Objectives and Scope of Work

The main objective of this research was to explore economically friendly concrete and its properties in bridge design while working with local materials. The main approach will focus on reducing cement content. This research was expected to develop an economically friendly concrete mix that would closely match a standard ODOT mix. Two economically friendly concrete mixes were compared to a standard ODOT Class AA mix in testing.

The following scope of work was carried out to fulfill this objective:

1. Review of relevant literature
2. Establish a plan for research
3. Obtain a control mix design and develop economically friendly concrete mixes
4. Fabricate testing apparatuses
5. Construct test specimens
6. Test specimens and record relevant data
7. Analyze results of the three mixes and compare
8. Compile conclusions and recommendations

9. Prepare this thesis in order to document the information gathered during this research

1.3 Research Plan

For this research, the shear behavior of reinforced concrete beams cast with an economically friendly concrete were compared to those constructed with a standard ODOT Class AA mix. To produce the economically friendly concrete, a combination of aggregate optimization and both micro- and macro-fibers were used to reduce the amount of Portland cement yet maintain performance.

For this research, tests were performed on small and large scale specimens along with material property tests including slump, air content, unit weight, compressive strength, modulus of elasticity, modulus of rupture, and splitting tensile strength. The small scale specimens were tested for compressive strength, split cylinder, modulus of elasticity, and modulus of rupture following the required ASTM guidelines. These tests are further discussed in Chapter 3. The full scale beam specimens were tested in shear using a third point loading method. There were three beams for each mix design used: ODOT Class AA, Eco-Bridge-Crete 1, and Eco-Bridge-Crete 2.

1.4 Outline

In this thesis, there are six chapters and an appendix. Chapter 1 goes through a background of economically friendly concrete, along with benefits and current uses. It

also contains objectives, scope of work, and a research plan. Chapter 2 discusses previous literature pertaining to aggregate optimization, shear, and Portland cement.

Chapter 3 shows an overall approach to obtaining mix designs for the two trial mixes in this research along with test methods used to produce fresh and hardened concrete properties. It then summarizes the finalized mix designs for each mix used. From there, Chapter 4 discusses the fabrication, test set-up, and procedure for the full-scale experimental beams.

Chapter 5 evaluates and analyzes the results of the specimens produced for this research. Finally, Chapter 6 presents findings, conclusions, and recommendations based on the research presented. Test data for all of the full-scale beam tests can be found in the appendices.

2. Literature Review

The following chapter contains the results of a detailed literature review of the topics pertinent to this study. These topics include Portland cement, aggregate optimization, synthetic fibers, and shear in reinforced concrete.

2.1 Portland Cement

Portland cement is the primary binder in grout, mortar, and concrete. The raw materials of Portland cement are 2/3 limestone material and 1/3 clay material comprising of silica, iron, and alumina (Mehta 2006). There are five types of Portland cement. In order, there is general purpose (Type I), moderate heat of hydration and sulfate resistance (Type II), high early strength (Type III), low heat (Type IV), and sulfate resistant (Type V). Due to its incredible versatility, availability, and relatively low cost, concrete is the most consumed synthetic material on the planet. It is second only to water as the most consumed material in the world. However, the production of Portland cement – the key ingredient in concrete – generates a significant amount of carbon dioxide (CO_2).

There is approximately 1.25 tons of CO_2 released for every ton of cement produced (Dokken 1996). Per the USGS (USGS 2015), in 2013 there were 181.7 million metric tons of cement produced in the United States. This includes Portland cement, masonry cement, and clinker. At 1.25 tons of CO_2 per ton of cement, there were 227.1 million metric tons of CO_2 released into the atmosphere from cement alone. There were 5,355 million metric tons of CO_2 produced in the United States that year (EIA 2014). That is

4.2% of the total amount of CO_2 released in the United States. Although that doesn't seem like a huge amount, it still represents a major industrial contributor to greenhouse gas emissions.

2.2 Cracking in Concrete

Cracking can be caused by numerous things. Non-structural cracks, including plastic cracking, hardened concrete cracking, and chemical cracking, are caused by the materials used, temperatures, exposure, etc. (Vic Roads 2010).

The original source and initial concrete temperatures have a large effect on drying shrinkage. "Controlling initial concrete temperatures and peak temperatures during hydration reduces thermal stresses and subsequent cracking" (Transportation Research Board 2006). Different types of concrete create different temperature rises during the setting of concrete. Cement that is slower setting should have a lower potential for drying shrinkage and cracking.

Water amounts in the concrete can be very important to cracking. Excessive water can cause cracking. When the concrete dries, excess water is evaporated. The more excess water, the more drying, and therefore more shrinkage. Shrinkage causes cracking. Plastic shrinkage cracks are caused by the surface of the concrete drying more rapidly than bleed water can get to the surface (Vic Roads 2010).

Aggregates also play a role in cracking. When optimized gradation is used with aggregates, cement content can be reduced due to the paste requirement being reduced. This will make the mixture more economical as well as give it a reduction in shrinkage and thermal stresses. Aggregate absorption can also cause shrinkage. "Generally, concretes made with high absorption aggregates tend to be more compressible, and this yield higher shrinkages" (Transportation Research Board 2006).

There are several types of admixtures for concrete. Some help with cracking, while others could potentially cause more cracking. Water-reducers minimize cracking by enabling a reduction in water content but still allowing for a workable mix. Retarders cause lower temperatures during hydration and a delayed set time which both decrease the susceptibility for cracking (Transportation Research Board 2006).

Fibers are known to hold the concrete together causing reductions in cracking and reducing the widths of cracks.

2.3 Durability of Concrete

"For durability provisions, the ACI 318 Building Code generally relies on the w/cm to reduce the permeation of water or chemical salts into the concrete that impacts its durability and service life" (Obla et al. 2005). For ACI, a maximum w/cm ratio of 50% is required for low permeability concrete and a minimum strength of 4,000 psi. These requirements alone will not ensure an adequate, durable concrete.

"Concrete durability is an example of a key aspect (measure) of performance that must be addressed in all specifications" (Transportation Research Board 2013). In order for a concrete to be durable, it must resist freeze/thaw and have a low permeability. In addition to that, shrinkage plays a role because cracking can allow moisture intrusion which will cause a less durable concrete.

When cracks form along the bottom of pavements, surface water can penetrate the concrete and saturate the present aggregate. When this happens, it allows for freeze/thaw to take place and further progress the cracks. This will create a less durable concrete.

2.4 Aggregate Optimization

"Concrete mixtures produced with a well-graded aggregate combination tend to reduce the need for water, provide and maintain adequate workability, require minimal finishing, and consolidate without segregation" (Iowa 2007). The Iowa Department of Transportation states that in order to efficiently receive an optimized aggregate for concrete, three charts need to be used. These charts are the workability chart, 0.45 power curve, and a percent-retained chart (Cook et al. 2013). Another chart, that has recently been constructed is the Tarantula chart.

Aggregate optimization is one way to reduce the cement content in a concrete mix design and still maintain a higher strength in the overall concrete. Ezgi Yurdakul (2010) optimized concrete mixtures for minimum cement content. In his five categories to

review, aggregates are present in each one. They play a different role in each category which shows the importance of an optimized aggregate in a low binder content mixture. Rached et al. (2010) goes on to discuss how aggregate shape along with the gradation plays a role in the amount of cement required to achieve the desired outcome. They say "poorly shaped and poorly graded aggregates typically have a lower packing density than well shaped and well graded aggregates, resulting in more paste being required to fill the voids between aggregates." They go on to say that the voids must be filled by making a more flowable paste which causes a higher *w/cm* ratio. A higher *w/cm* ratio causes a decreased compressive strength.

2.4.1 Shilstone Method. The workability chart, shown in **Figure 2.1**, is a gradation chart that uses a mathematically combined gradation. This chart is also known as the Shilstone Chart. Cook et. al. states:

> The Shilstone chart is made up of the coarseness factor and the workability factor. The two parameter equations control the percentage of sand, intermediate, and coarse aggregates. Shown in [**Equation 2.1]**, the workability factor changes the percentage of sand in the mixture. The ratio of large to intermediate aggregate for a given sand content is controlled by the coarseness factor shown by [**Equation 2.2]**.
>
> **[Equation 2.1]**
>
> Workability Factor (WF) = W + (2.5(C-564)/94)
>
> W= cumulative % passing the no. 8 sieve
>
> C= cementitious material content (lb/yd^3)

[Equation 2.2]

Coarseness Factor (CF) = (Q/R)*100

Q= cumulative % retained on the 3/8 sieve

R= cumulative % retained on the no. 8 sieve

The method of graphing workability forces a certain gradation on the blend of aggregate. This chart has five zones represented by the following:

I. Gap graded with little intermediate aggregate

II. Well graded

III. High intermediate content and low coarse

IV. Sandy extreme, and

V. Rocky extreme.

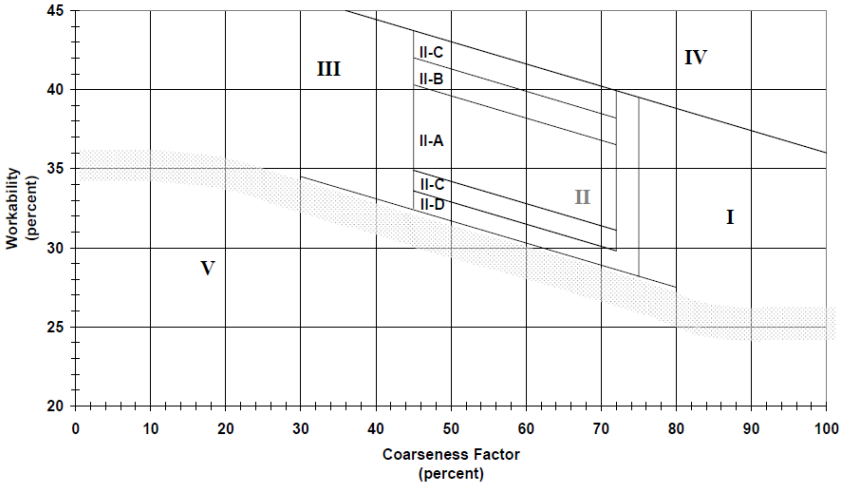

Figure 2.1: Workability Chart (Iowa 2007)

2.4.2 0.45 Power Curve Method. The 0.45 power curve uses percent passing and creates a "maximum density line". This curve is created by plotting the percent-passing on the y axis and sieve sizes on the x axis. The sieve sizes are raised to the 0.45 power. The maximum density lines runs "from the origin of the chart to the sieve one size larger than the first sieve to have 90 percent or less passing" (Iowa 2007). If the aggregate is well graded, the percent passing will closely follow the maximum density line, as shown in **Figure 2.2**. There are maximum and minimum passing boundary lines usually added at around +/- 10% of the maximum density line. The actual percent passing should fall within this line with the exception of the fines. The fines tend to fall out of the minimum zone. Cook et al. (2013) found this curve to not be useful, so they did not consider it in their study of optimized graded concrete for Oklahoma.

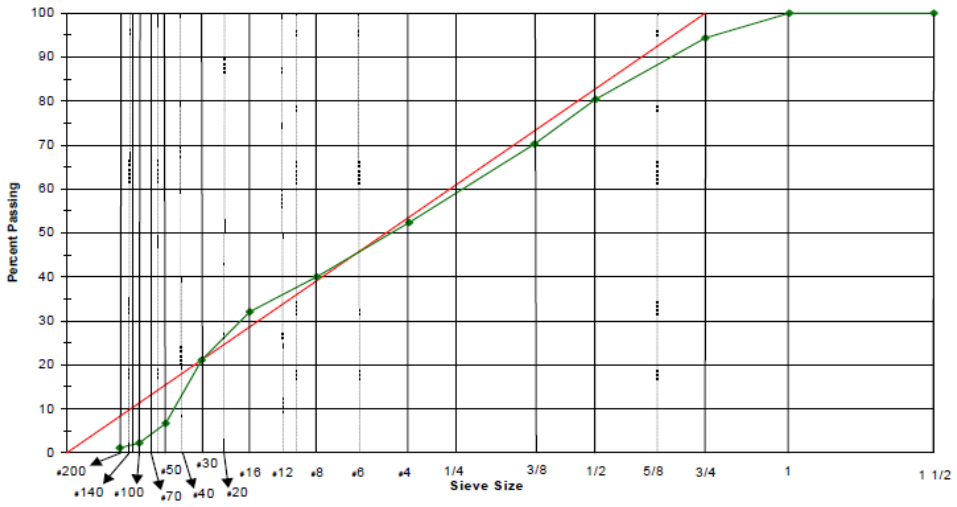

Figure 2.2: Power 45 Curve (Iowa 2007)

2.4.3 Percent-Retained Method. The percent-retained chart uses gradations based on the percent of aggregate retained on each sieve. There are boundary lines that the gradations should fall between. An example chart follows in **Figure 2.3**. This method is also called the 8/18 method because of the minimum and maximum boundaries. The lower boundary is at 8% retained, and the upper boundary is at 18% retained. In order to get the percent retained of the combined aggregates, each aggregate is graphed, and an average is determined, as shown in **Figure 2.4**.

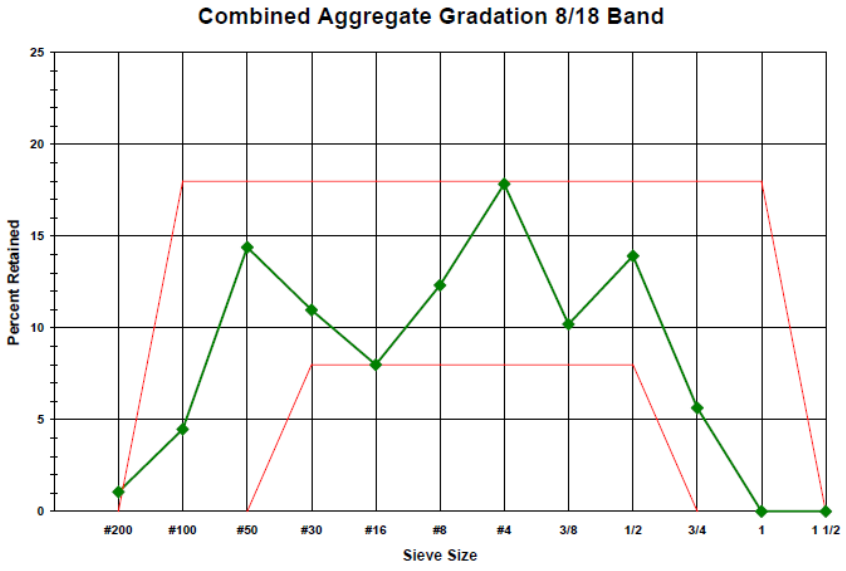

Figure 2.3: Percent-Retained Chart (Iowa 2007)

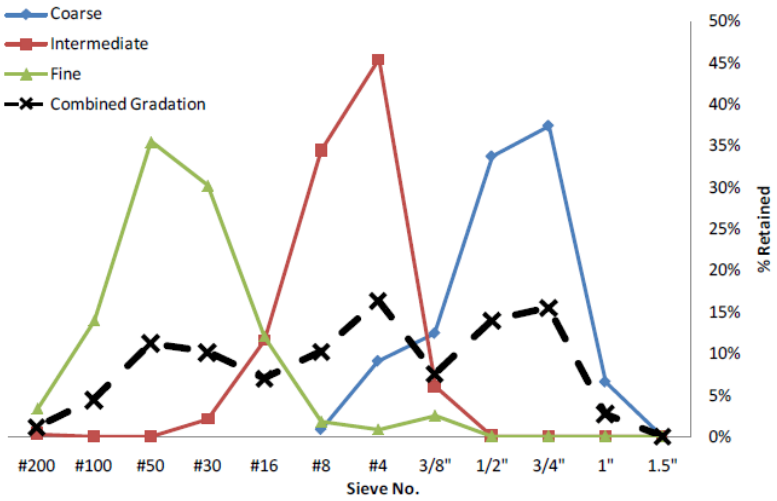

Figure 2.4: Combining Aggregate Gradations

2.4.4 Tarantula Method. Another method, produced in Oklahoma, is known as the Tarantula method. These limits were produced "by comparing the workability and aggregate gradation of more than 500 different mixtures with 8 different aggregate sources". This test uses a box test instead of slump to determine workability. This chart is similar to the percent retained chart, but the ideal limits mimic a tarantula silhouette, as seen in Figure 2.5. Recommended limits are 24% to 34% fine sands (#30-200) and greater than 15% for coarse sand (#8-30).

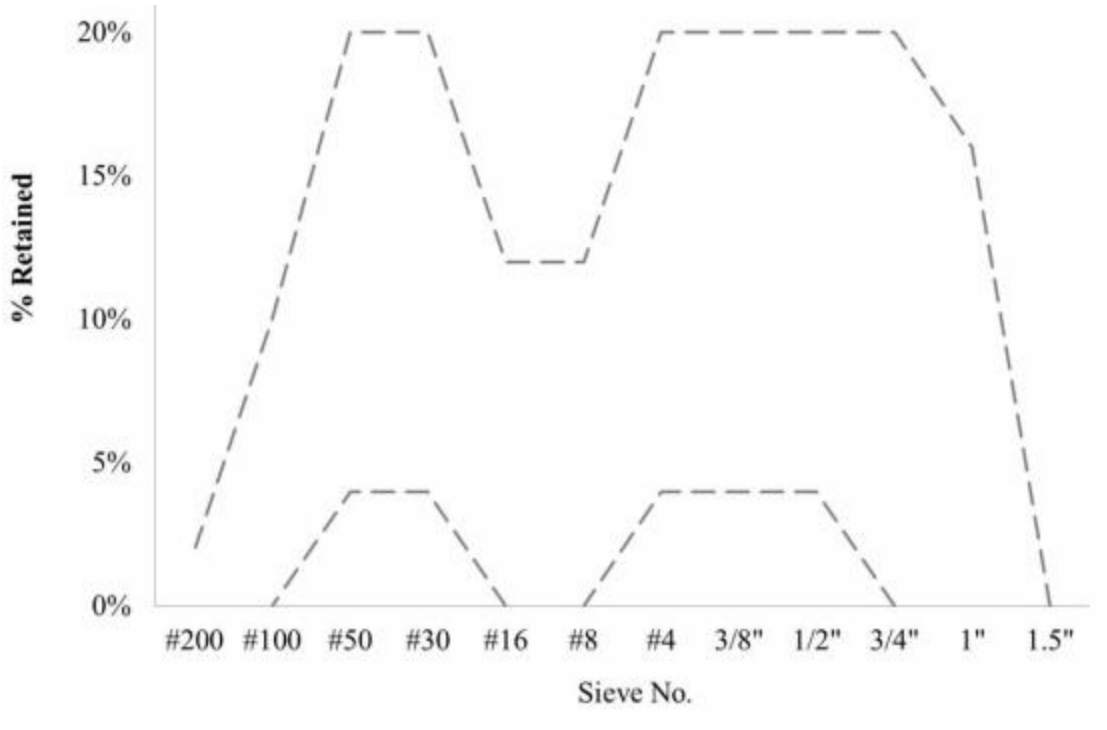

Figure 2.5: Tarantula Curve

2.5 Synthetic Fibers

Synthetic fibers can reduce the cracking from plastic settlement and shrinkage. These fibers mechanically block the micro shrinkage cracks caused by a stress existing which exceeds the concrete strength (NRMCA 1994). The fibers are uniformly distributed throughout the mix, lowering the chances of having capillaries form from bleed water rising to the surface. Capillaries are important because they can provide a location for cracking in the concrete at a later age. These two things combined create a lower permeability in the concrete.

For hardened concrete, synthetic fibers add shattering, abrasion, and impact force resistance along with the lowered permeability. The fibers bind the concrete together

tightly reducing shattering when the concrete is compressed. With the fibers reducing the number of bleed water capillaries, it creates a more uniform water/cement ratio on the surface. This, in turn, creates a better resistance to abrasion. Finally, the fibers create impact force resistance by absorbing shock due to their low modulus value. "Synthetic fibers help the concrete develop its optimum long-term integrity by the reduction of plastic shrinkage and shrinkage crack formation, lowered permeability, and increased resistance to abrading, shattering, and impact forces" (NRMCA 1994).

2.6 Factors Affecting Shear Behavior

Shear strength is controlled by the presence of web reinforcement, longitudinal reinforcement, coarse aggregate size, presence of axial loads, depth of the member, tensile strength of the concrete, and shear span to depth ratio, *a/d.* Some of these parameters are included in design equations and others are not.

Web reinforcement, typically called stirrups, is used to increase the shear strength of concrete beams and to ensure flexural failure. This is necessary due to the explosive and sudden nature of shear failures, compared with flexural failures which tend to be more ductile. Web reinforcement is normally provided as vertical stirrups and is spaced at varying intervals along a beam depending on the shear requirements. Alternatively, this reinforcement may be provided as inclined longitudinal bars. In general, small sized bars such as #3 and #4 are used in a U-shaped configuration that may be open or closed, or used as multiple legs.

Shear reinforcement has very little effect prior to the formation of diagonal cracks. However after cracking, the web reinforcement enhances the beam in the following ways (Nilson et al. 2004):

- The stirrups crossing the crack help in resisting the shear force.
- The stirrups restrict the growth of the cracks and reduce their penetration further into the compression zone.
- The stirrups oppose widening of the cracks, which helps to maintain aggregate interlock within the concrete.
- The presence of stirrups provides extra restraint against the splitting of concrete along the longitudinal bars due to their confinement effect.

The longitudinal reinforcement ratio, ρ_L , affects the extent and the width of the flexural cracks. If this ratio is small, the flexural cracks extend higher into the beam and open wider. When the crack width increases, the resistance components of shear decrease, because they are transferred either by dowel action or by shear stresses on the crack surfaces.

The coarse aggregate type and size noticeably affect the shear capacity, especially for beams without stirrups. Lightweight aggregate has a lower tensile strength than normal aggregate. The shear capacity of a concrete beam with no stirrups is directly related to the tensile strength, therefore, the failure due to mortar cracking, which is more desirable, could be preceded by aggregate failure instead. The aggregate size also affects the amount of shear stresses transferred across the cracks. Large diameter

aggregate increases the roughness of the crack surfaces, allowing higher shear stresses to be transferred (Wight and MacGregor 2009).

Researchers have concluded that axial compression serves to increase the shear capacity of a beam while axial tension greatly decreases the strength. As the axial compressive force is increased, the onset of flexural cracking is delayed, and the flexural cracks do not penetrate as far as into the beam (Wight and MacGregor 2009). The size of the beam affects the shear capacity at failure. If the overall depth of a beam is increased, it could result in a smaller shear force at failure. The reasoning is that when the overall depth of a beam increases, so do the crack width and crack spacing, causing loss of aggregate interlock. This condition is known as a size effect.

The tensile strength of the concrete, f_{ct}, also affects the shear strength. Because of the low tensile strength of the concrete, diagonal cracking develops along planes perpendicular to the planes of principal tensile stress. The shear strength of a reinforced concrete beam increases as the concrete material strength increases. The tensile strength of the concrete is known to have a great influence on the shear strength, but the concrete compressive strength, f'_c, is used instead in most shear strength formulas. This approach is used because tensile tests are more difficult to conduct and usually show greater scatter than compression tests.

The shear span to depth ratio, *a/d*, does not considerably affect the diagonal cracking for values larger than 2.5. The shear capacity increases as the shear span to depth ratio

decreases. This phenomenon is quite significant in deep beams ($a/d \leq 2.5$) because a portion of shear is transmitted directly to the support by an inclined strut or arch action. For deep beams, the initial diagonal cracking develops suddenly along almost the entire length of the test region (Wight and MacGregor 2009).

2.7 Shear Design Code Review

There are a variety of design code philosophies that can be found around the world for shear design. Some of these rely on empirical formulas for estimating the shear strength, such as the ACI 318-14 (2014), while others such as the AASHTO LRFD (2014) rely more on concrete models such as the modified compression field theory (MCFT). This section will detail three selected design codes.

2.7.1 American Concrete Institute, ACI 318-14.

The ACI 318-14 method is most commonly used for shear design in the United States, and is based on a 45 degree truss model. The shear strength is based on an average shear stress distribution across the entire cross section, and is composed of a concrete component, V_c, and a steel component, V_s. The basic equations for normal-weight, non-prestressed reinforced concrete are listed in **Equations 2.3 to 2.7**.

$$V_u \leq V_n = V_c + V_s \qquad \textbf{(Eq. 2.3)}$$

$$V_c = \left(1.9\sqrt{f'_c} + 2500\rho_w \frac{V_u d}{M_u}\right) b_w d \leq 3.5\sqrt{f'_c} b_w d \quad \textbf{(Eq. 2.4)}$$

$$\text{Simplified version: } V_c = 2\sqrt{f'_c} b_w d \quad \textbf{(Eq. 2.5)}$$

$$A_{v,min} = 0.75\sqrt{f'_c}\frac{b_w s}{f_{yt}} \geq 50\frac{b_w s}{f_{yt}} \quad \textbf{(Eq. 2.6)}$$

$$V_s = \frac{A_v f_{yt} d}{s} \quad \textbf{(Eq. 2.7)}$$

$\emptyset$ is the strength reduction factor equal to 0.75 and not shown in **Equation 2.3**, V_n is the nominal shear strength, V_u is the ultimate shear strength, $\rho_w = \frac{A_s}{b_w d}$, A_s is the area of longitudinal reinforcement, b_w is the width of the web, d is the distance from the extreme compression fiber to the center of gravity of the steel, M_u is the factored moment at the section, f'_c is the concrete compressive strength (psi), f_{yt} is the yield strength of the transverse reinforcement (psi), s is the spacing of the transverse reinforcement, and A_v is the area of shear reinforcement. The following condition must be maintained $\frac{V_u d}{M_u} \leq 1.0$.

The ACI 318-14 presents a procedure for calculating the failure shear strength for concrete beams without shear reinforcement. The simplified method is presented in **Equation 2.5**. Some research data indicate that **Equation 2.4** overestimates the influence of f'_c and underestimates the influence of ρ_w and $\frac{V_u d}{M_u}$. This is why, for most

designs, it is convenient to assume that the second term of this equation equals $0.1\sqrt{f'_c}$ and use **Equation 2.5** to calculate the shear contribution of the concrete.

2.7.2 AASHTO LRFD Bridge Design Specifications. The AASHTO LRFD (2014) method is known as the Sectional Design Model, and is based on the MCFT. The nominal shear resistance, V_n, can be computed by **Equations 2.8** to **2.12**.

$$V_n = V_c + V_s + V_p \quad \textbf{(Eq. 2.8)}$$

$$V_{n,max} = 0.25 f'_c b_v d_v + V_p \quad \textbf{(Eq. 2.9)}$$

$$V_c = 0.0316 \beta \sqrt{f'_c} b_v d_v \quad \textbf{(Eq. 2.10)}$$

$$V_s = \frac{A_v f_y d_v \cot\theta}{s} \quad \textbf{(Eq. 2.11)}$$

$$A_{v,min} \geq 0.0316 \sqrt{f'_c} \frac{b_v s}{f_y} \quad \textbf{(Eq. 2.12)}$$

where, V_p is the vertical component of the prestressing force, b_v is the effective width of the web taken as the minimum web width within the depth, d_v is the effective shear depth taken as the greater of $0.9d$ or $0.72h$, β is the factor indicating the ability of diagonal cracked concrete to transmit tension, θ is the angle of inclination of the diagonal compressive struts, f'_c is the concrete compressive strength (ksi), and f_y is the yield strength of the transverse reinforcement (ksi).

For sections containing at least the minimum amount of transverse reinforcement, the values of β and θ may be found using **Table 2.1**. The designer selects the row corresponding to the shear design stress ratio $\frac{v}{f'_c} = \frac{V_u}{b_v d_v f'_c}$, and selects the column corresponding to the longitudinal strain (ε_x) at mid-depth. The longitudinal strain may be computed using **Equation 2.13**.

Table 2.1 Values of θ and β for Sections with Transverse Reinforcement

(AASHTO LRFD 2007)

$\frac{v_u}{f'_c}$		$\varepsilon_x \times 1000$										
		≤ -0.20	≤ -0.10	≤ -0.05	≤0	≤0.125	≤0.25	≤0.50	≤0.75	≤1.00	≤1.50	≤2.00
≤0.075	θ	22.3°	20.4°	21.0°	21.8°	24.3°	26.6°	30.5°	33.7°	36.4°	40.8°	43.9°
	β	6.32	4.75	4.10	3.75	3.24	2.94	2.59	2.38	2.23	1.95	1.67
≤0.100	θ	18.1°	20.4°	21.4°	22.5°	24.9°	27.1°	30.8°	34.0°	36.7°	40.8°	43.1°
	β	3.79	3.38	3.24	3.14	2.91	2.75	2.50	2.32	2.18	1.93	1.69
≤0.125	θ	19.9°	21.9°	22.8°	23.7°	25.9°	27.9°	31.4°	34.4°	37.0°	41.0°	43.2°
	β	3.18	2.99	2.94	2.87	2.74	2.62	2.42	2.26	2.13	1.90	1.67
≤0.150	θ	21.6°	23.3°	24.2°	25.0°	26.9°	28.8°	32.1°	34.9°	37.3°	40.5°	42.8°
	β	2.88	2.79	2.78	2.72	2.60	2.52	2.36	2.21	2.08	1.82	1.61
≤0.175	θ	23.2°	24.7°	25.5°	26.2°	28.0°	29.7°	32.7°	35.2°	36.8°	39.7°	42.2°
	β	2.73	2.66	2.65	2.60	2.52	2.44	2.28	2.14	1.96	1.71	1.54
≤0.200	θ	24.7°	26.1°	26.7°	27.4°	29.0°	30.6°	32.8°	34.5°	36.1°	39.2°	41.7°
	β	2.63	2.59	2.52	2.51	2.43	2.37	2.14	1.94	1.79	1.61	1.47
≤0.225	θ	26.1°	27.3°	27.9°	28.5°	30.0°	30.8°	32.3°	34.0°	35.7°	38.8°	41.4°
	β	2.53	2.45	2.42	2.40	2.34	2.14	1.86	1.73	1.64	1.51	1.39
≤0.250	θ	27.5°	28.6°	29.1°	29.7°	30.6°	31.3°	32.8°	34.3°	35.8°	38.6°	41.2°
	β	2.39	2.39	2.33	2.33	2.12	1.93	1.70	1.58	1.50	1.38	1.29

$$\varepsilon_x = \frac{\frac{M_u}{d_v} + 0.5N_u + 0.5\left(V_u - V_p\right)\cot\theta - A_{ps}f_{po}}{2\left(E_s A_s + E_p A_p\right)} \qquad \textbf{(Eq. 2.13)}$$

For sections containing less than the minimum amount of transverse reinforcement, the values of β and θ may be found using **Table 2.2**. The designer selects the row corresponding to an equivalent spacing parameter (s_{xe}), and selects the column corresponding to the longitudinal strain at mid-depth. The equivalent spacing may be computed using **Equation 2.14**. The longitudinal strain for this case may be computed using **Equation 2.15**.

Table 2.2 Values of θ and β for Sections with Less Than Minimum Transverse Reinforcement (AASHTO LRFD 2007)

s_{xe} (in.)		$\varepsilon_x \times 1000$										
		≤ -0.20	≤ -0.10	≤ -0.05	≤0	≤0.125	≤0.25	≤0.50	≤0.75	≤1.00	≤1.50	≤2.00
≤ 5	θ	25.4°	25.5°	25.9°	26.4°	27.7°	28.9°	30.9°	32.4°	33.7°	35.6°	37.2°
	β	6.36	6.06	5.56	5.15	4.41	3.91	3.26	2.86	2.58	2.21	1.96
≤ 10	θ	27.6°	27.6°	28.3°	29.3°	31.6°	33.5°	36.3°	38.4°	40.1°	42.7°	44.7°
	β	5.78	5.78	5.38	4.89	4.05	3.52	2.88	2.50	2.23	1.88	1.65
≤ 15	θ	29.5°	29.5°	29.7°	31.1°	34.1°	36.5°	39.9°	42.4°	44.4°	47.4°	49.7°
	β	5.34	5.34	5.27	4.73	3.82	3.28	2.64	2.26	2.01	1.68	1.46
≤ 20	θ	31.2°	31.2°	31.2°	32.3°	36.0°	38.8°	42.7°	45.5°	47.6°	50.9°	53.4°
	β	4.99	4.99	4.99	4.61	3.65	3.09	2.46	2.09	1.85	1.52	1.31
≤ 30	θ	34.1°	34.1°	34.1°	34.2°	38.9°	42.3°	46.9°	50.1°	52.6°	56.3°	59.0°
	β	4.46	4.46	4.46	4.43	3.39	2.82	2.19	1.84	1.60	1.30	1.10
≤ 40	θ	36.6°	36.6°	36.6°	36.6°	41.2°	45.0°	50.2°	53.7°	56.3°	60.2°	63.0°
	β	4.06	4.06	4.06	4.06	3.20	2.62	2.00	1.66	1.43	1.14	0.95
≤ 60	θ	40.8°	40.8°	40.8°	40.8°	44.5°	49.2°	55.1°	58.9°	61.8°	65.8°	68.6°
	β	3.50	3.50	3.50	3.50	2.92	2.32	1.72	1.40	1.18	0.92	0.75
≤ 80	θ	44.3°	44.3°	44.3°	44.3°	47.1°	52.3°	58.7°	62.8°	65.7°	69.7°	72.4°
	β	3.10	3.10	3.10	3.10	2.71	2.11	1.52	1.21	1.01	0.76	0.62

$$s_{xe} = \frac{1.38 s_x}{a_g + 0.63} \quad \textbf{(Eq. 2.14)}$$

$$\varepsilon_x = \frac{\frac{M_u}{d_v} + 0.5N_u + 0.5\left(V_u - V_p\right)\cot\theta - A_{ps}f_{po}}{E_s A_s + E_p A_p} \quad \textbf{(Eq. 2.15)}$$

If either value computed for ε_x is negative, the user should use **Equation 2.16** to compute the longitudinal steel strain instead.

$$\varepsilon_x = \frac{\frac{M_u}{d_v} + 0.5N_u + 0.5\left(V_u - V_p\right)\cot\theta - A_{ps}f_{po}}{2\left(E_c A_c + E_s A_s + E_p A_p\right)} \quad \textbf{(Eq. 2.16)}$$

where, A_c is the area of concrete on the flexural tension side, A_p is the area of prestressing steel on the flexural tension side, A_s is the area of non-prestressed steel on the flexural tension side, f_{po} is computed by the modulus of elasticity of the prestressing tendons (E_p) times the locked difference in strain at ultimate load between the prestressing tendons and the surrounding concrete, N_u is the factored axial force, s_x is the crack spacing parameter, and a_g is the maximum aggregate size in inches.

A simplified procedure is presented in the AASHTO LRFD (2014) where the values of β and θ can be calculated using the following expressions shown in **Equations 2.17** and **2.18**. The parameter s_{xe} can be calculated using **Equation 2.14**.

$$\beta = \frac{4.8}{1 + 750\varepsilon_x} \cdot \frac{51}{39 + s_{xe}} \quad \textbf{(Eq. 2.17)}$$

$$\theta = 29 + 3500\varepsilon_x \quad \textbf{(Eq. 2.18)}$$

2.7.3 Canadian Standards Association, CSA A23.3-04. The Canadian Standards Association method, also based on MCFT, gives the following **Equations 2.19** to **2.26** to calculate the shear strength of a section using their general method. Note that the equations are given in psi and in. units, with the same notation defined in previous sections.

$$V_n = V_c + V_s + V_p \quad \textbf{(Eq. 2.19)}$$

$$V_{n,max} = 0.25f'_c b_v d_v + V_p \quad \textbf{(Eq. 2.20)}$$

$$V_c = \beta\sqrt{f'_c} b_v d_v \quad \textbf{(Eq. 2.21)}$$

$$s_{ze} = \frac{35s_z}{15 + a_g} \quad \textbf{(Eq. 2.22)}$$

The term a_g should be taken as zero if f'_c exceeds 10,150 psi. The crack spacing parameter s_z can be taken as d_v or as the maximum distance between layers of

distributed longitudinal reinforcement, whichever is less. Each layer of reinforcement must have an area at least equal to $0.003 b_v s_z$. However, $s_{ze} \geq 0.85 s_z$.

$$\varepsilon_x = \frac{\frac{M_u}{d_v} + 0.5N_u + V_u - V_p - A_{ps} f_{po}}{2\left(E_s A_s + E_p A_p\right)} \quad \textbf{(Eq. 2.23)}$$

$$V_s = \frac{A_v f_y d_v \cot\theta}{s} \quad \textbf{(Eq. 2.24)}$$

$$\theta = 29 + 7000\varepsilon_x \quad \textbf{(Eq. 2.25)}$$

$$A_{v,min} \geq 0.06\sqrt{f'_c}\frac{b_v s}{f_y} \quad \textbf{(Eq. 2.26)}$$

3. Concrete Mix Designs

3.1 Introduction

For this research, three mix designs were studied for shear strength. The control mix design used was an ODOT Class AA mix. The two eco-friendly mix designs used aggregate optimization techniques to reduce the total cement content yet maintain the same performance as the control mix. In addition to limiting the cement content, the eco-friendly mixes included both micro- and macro-synthetic fibers to improve durability and performance, thus increasing the potential service life and thus sustainability of the material. Initial mix designs were developed by collegues at Missouri College of Science and Technology.

3.2 Aggregate Testing

3.2.1 Gradation. Before trial mix designs began, the aggregate underwent testing to verify compliance with ASTM and ODOT specifications. The aggregates used were #67 crushed rock, 3/8" chip, and natural sand. A sieve analysis was performed on each aggregate to determine gradation. The analyses included two samples, which were averaged to obtain a representative distribution for the source material. **Tables 3.1** and **3.2** show the fine and coarse aggregate gradations, respectively, along with the required gradation from *ASTM C33/C33M-16 Standard Specification for Concrete Aggregates*. Along with the fine and coarse aggregates used in both mixes, a 3/8" limestone chip was analyzed for the purpose of optimizing the aggregate gradations of the eco-friendly mixes. Most aggregate passed the 3/8" sieve

but did not pass the #4 sieve, which was anticipated for a 3/8” chip. This is shown in **Table 3.3**.

Table 3.1: Fine Aggregate Gradation

Fine Aggregate: Natural Sand			
Sieve	**Opening (mm)**	**% Passing, Sample**	**% Passing, Required**
3/8"	9.5	100	100
#4	4.75	99.18	95 to 100
#8	2.36	94.67	80 to 100
#16	1.18	79.88	50 to 85
#30	0.6	47.39	25 to 60
#50	0.3	13.97	5 to 30
#100	0.15	1.58	0 to 10
#200	0.075	0.27	0 to 3
Pan	0	0	0

Table 3.2: Coarse Aggregate Gradation

Coarse Aggregate: #67 Crushed Limestone			
Sieve	**Opening (mm)**	**% Passing, Sample**	**% Passing, Required**
1.5"	37.5	100.0	100
1"	25	100	100
3/4"	19	95.13	90 to 100
3/8"	9.5	31.76	25 to 55
#4	4.75	3.44	0 to 10
#8	2.36	1.39	0 to 5
Pan	0	0	0

Table 3.3: 3/8" Chip Gradation

Coarse Aggregate: 3/8" Limestone Chip			
Sieve	**Opening, mm**	**% Passing, Sample**	**% Passing, Required**
1.5"	37.5	100	100
1"	25	100	100
3/4"	9.5	100	100
3/8"	4.75	95	85 to 100
#4	2.35	14.7	10 to 30
#8	2	4.1	0 to 10
#16	1.18	2.4	0 to 5
#30	0.6	1.6	--
#50	0.3	1.2	--
#100	0.15	0.7	--
#200	0.075	0.3	--
Pan	-	0	0

3.2.2 Absorption. Absorption was also performed on the three types of aggregates. To test absorption, a sample was submerged in water then dried in towel to achieve a saturated surface dried, SSD, state. It was then weighed at the saturated surface dried, SSD, state. The sample was then dried in an oven and then reweighed to obtain the OD weight. **Equation 3.1** was then used to determine the absorption.

$$Absorption = \frac{SSD - OD}{OD} \qquad \textbf{(Eq. 3.1)}$$

This test was performed on two samples of each aggregate and averaged. These values are shown in **Table 3.4**.

Table 3.4: Aggregate Absorptions

Aggregate	Average Absorption
#67 Coarse	0.86%
3/8" Chip	1.01%
Fine Aggregate	0.70%

3.2.3 Specific Gravity. Specific gravity was determined for the #67, 3/8" chip, and sand. For the coarse aggregate, *ASTM C127: Standard Test Method for Relative Density (Specific Gravity) and Absorption of Coarse Aggregate* was used. A samples were oven dried and cooled to room temperature. The samples were then immersed in water for 24 hours. After, the samples were moved to a cloth for drying off surface water. The samples were then reweighed. Once this was finished, the samples were submerged in water and reweighed. Using **Equation 3.2**, the specific gravity of the #67 and 3/8" chip were 2.69 and 2.67, respectively. For the natural sand, *ASTM C128-15: Standard Test Method for Relative Density (Specific Gravity) and Absorption of Fine Aggregate* was used. A sample of sand was spread out and stirred to achieve a saturated surface dried state. Then a pycnometer was filled partially with water, fines were added, then the pycnometer was agitated per the ASTM standard. It was then heated to 23˚C and weighed. Using **Equation 3.3**, where B is the mass of the pycnometer fill with water and C is the mass of the pycnometer fill with the specimen and water, the specific gravity for the natural sand was 2.65.

$$SG = \frac{Oven\ dried\ Mass}{(Oven\ dried\ mass - Submerged\ mass)} \quad \textbf{(Eq. 3.2)}$$

$$SG(SSD) = \frac{SSD\ Mass}{B + SSD\ Mass - C} \quad \textbf{(Eq. 3.3)}$$

3.2.4 LA Abrasion Test. The LA Abrasion test was performed on the coarse aggregates based on *ASTM C131: Standard Test Method for Resistance to Degradation of Small-Size Coarse Aggregate by Abrasion and Impact in the Los Angeles Machine*. A sample of both coarse aggregates was oven dried then weighed. Once dried, each sample was put into the LA Abrasion machine to run the test. After the machine had completed its cycle, the sample was then washed, oven dried, and reweighed. **Equation 3.4** was used to determine the percentage loss of the sample. This test resulted in a loss percentage of 26% and 22% for the #67 and 3/8" chip, respectively.

$$\%\ Loss = \frac{Original\ Mass - Final\ Mass}{Final\ Mass}\ x\ 100 \quad \textbf{(Eq. 3.4)}$$

3.2.5 ODOT Limits. For the Class AA ODOT mix used for the control specimens in this research, aggregate was chosen based on the limits outlined by ODOT. For coarse aggregates, ODOT specifies that the percent passing be as follows: 100% passing the 1 ½" sieve, 95-100% passing the 1" sieve, and 0-3% passing the No. 200 sieve. For the fine aggregates, ODOT specifies that the percent passing be as follows: 100% passing the ½" sieve and 0-3% passing the No. 200 sieve. For the LA abrasion test, ODOT limits the maximum percentage to 40%.

3.3 Concrete Properties and Small Specimen Testing

3.3.1 Fresh Concrete Properties. The three fresh concrete properties measured for all three mixes were unit weight, air content, and slump. For the unit weight test, *ASTM C138/C138M-14 Standard Test Method for Density (unit Weight, Yield, and Air Content (Gravimetric) of Concrete* was used. The air content bucket was weighed empty, then filled with concrete in three lifts. Each lift was tamped 25 times and tapped with a mallet. Once the last lift was rodded, the top was smoothed off and the edges cleaned. The bucket was then weighed again full of concrete, and the unit weight was determined using **Equation 3.5**:

$$D = \frac{(\text{Weight of Full Bucket} - \text{Weight of Empty Bucket})}{\text{Volume of Bucket}} \qquad \textbf{(Eq. 3.5)}$$

Next, the air content was measured following *ASTM C231/C231M-14 Standard Test Method for Air Content of Freshly Mixed Concrete by the Pressure Method*. Using the concrete from the unit weight test already in the bucket, the air meter lid was placed on the bucket and secured by the four buckles. The air meter was brought up to the correct initial pressure, then water was added to one of the petcocks until continually flowing out the opposite petcock. The petcocks were then closed. Next, the air was released into the concrete while the base was struck with a rubber mallet. The gauge reading was recorded.

For the slump flow test, *ASTM C143/C143M-15 Standard Test Method for Slump of Hydraulic-Cement Concrete* was followed. A dampened slump cone was placed on a base plate. Concrete was added to the cone in three lifts and tamped 25 times between each lift. After the last lift was rodded, the top was smoothed off and concrete cleared out around the cone. The cone was then lifted vertically at a constant rate within 3-5 seconds. The cone was then turned upside down and placed next to the concrete cone. A measurement was taken from the top of the metal cone to the top center of the concrete cone.

3.3.2 Concrete Compressive Strength. For each mix, cylinders were made to test for compressive strength, f_c, at 1, 3, 7, 14, 21, and 28 days. It was also tested on the day of full-scale beam specimen testing. Cylinders were made using molds with a diameter of 4 in. and depth of 8 in. for the control mix and the first trial mix. For the second trial mix, molds with a diameter of 6 in. and depth of 12 in. were used due to the length of the macrofibers used in this mix. The cylinders cast with the full scale beams were cured with the beams to ensure they underwent the same conditions. The cylinders were ground on each side, so no caps or pads were used during testing. Testing was done per *ASTM C39/C39M-15a Standard Test Method for Compressive Strength of Cylindrical Concrete Specimens*. Three specimens were tested at each time interval to get an average compressive strength. The average data points were then plotted. **Figure 3.1** shows a cylinder that has been set up for compressive strength testing.

Figure 3.1: Compressive Strength Test Setup

3.3.3 Concrete Modulus of Elasticity. The modulus of elasticity, MOE, was determined at 28 days for each mix using the same size cylinders that were used for compressive strength. This test was done in accordance with *ASTM C469/C469M-14 Standard Test Method for Static Modulus of Elasticity and Poisson's Ratio of Concrete in Compression*. The specimens were placed in a compressometer and subjected to 40% of the compressive strength three times each. The strains were recorded automatically.

This data was then analyzed and averaged between the three runs. A modulus of elasticity test setup can be seen in **Figure 3.2**.

Figure 3.2: Modulus of Elasticity Test Setup

3.3.4 Concrete Splitting Tensile Strength. Splitting tensile strength testing was performed on three cylinders at 28 days. Cylinders were placed in the Forney machine one at a time on their side and loaded until failure. This setup can be seen in **Figure 3.3**.

Figure 3.3: Splitting Tensile Test

The splitting tensile strength test, f_{tsp}, followed *ASTM C496/C496M-11 Standard Test Method for Splitting Tensile Strength of Cylindrical Concrete Specimens*. **Equation 3.6** was used to calculate the splitting tensile strength, where *P* is the peak load, *L* is the length of the cylinder, and *D* is the diameter of the cylinder.

$$f_{tsp} = \frac{2P}{\pi LD} \qquad \textbf{(Eq. 3.6)}$$

3.3.5 Concrete Modulus of Rupture. Small beams were cast to measure the modulus of rupture, f_r, using *ASTM C78/C78M-15b Standard Test Method for Flexural Strength of Concrete (Using Simple Beam with Third-Point Loading)*. The small beams measured 6 in. x 6 in. x 24 in. Third point loading was applied at a span length of 18 in. **Equation 3.7** was used to determine the modulus of rupture, where P is the peak load, L is the length of the beam, b is the beam width, and d is the beam depth. Three specimens were tested to determine an average value.

$$f_r = \frac{PL}{bd^2} \qquad \textbf{(Eq. 3.7)}$$

3.4 Control Concrete Mix Design

The ODOT Class AA mix design requirements were selected for the control concrete. The minimum cement content, air content, *w/c* ratio, slump, and minimum 28 day compressive strength requirements for the ODOT Class AA mix are shown in **Table 3.5**. Fly ash can also be substituted for cement by up to 20% by weight. Burlap is an acceptable agent for curing of the concrete.

Table 3.5: ODOT Limits

Minimum Cement Content (lb/yd3)	Air Content (%)	w/c Ratio	Slump (in)	Minimum 28 Day Compressive Strength (psi)
564	6.5 ± 1.5	0.25-0.44	2 ± 1	4000

A standard Dolese Class AA mix was selected with a target strength of 5,000 psi. For this mix, the cement content was 470 lb/yd^3, fly ash was added at 20% by mass for a total of 118 lb/yd^3, the water-to-cement ratio was 0.40, the design air content was 6.5%, and the target slump was 5 in. There was roughly 40% fine aggregates by volume, 4.4 oz./yd^3 of AEA air entrainer, and 26.7 oz./yd^3 of Glenium 7500. The mix specifications are shown in **Table 3.6**.

Table 3.6: Control Mix Design Specifications

Concrete Mix Design per yd^3 (Dolese Class AA Mix)			
Cement	470	lb	
Class F Fly Ash	118	lb	(20% by mass)
w/cm	0.4		
Fine Agg.	1323	lb	sand
Coarse Agg.	1857	lb	#67
AEA (AE-90)	4.4	oz	0.75 oz/cwt
WRA (G 7500)	26.7	oz	4.53 oz/cwt

Several laboratory trial mixes were completed to verify the performance of the mix design shown in **Table 3.6**. The trial mixes had compressive strengths above 5,000 psi and met the ODOT Class AA air content and slump requirements.

3.5 Aggregate Optimization

For the Eco-Bridge-Crete mixes, the aggregate gradation was optimized in order to reduce the paste content yet maintain performance. Three approaches were used to

finalize the aggregate proportions: Shilstone chart, percent retained chart, and the power 45 chart. For each of these methods, the volume percentages of each type of aggregate are used. A spreadsheet was developed to set up quantities and percentages of each component of the concrete mix. From there, the data was placed into the three charts. Once the charts were created and linked back to the data, the percentages could then be changed to optimize the aggregate amounts. This process required an iterative approach and it was realized that not all of the three methods could necessarily be met with one gradation. The approach balanced the sometimes competing interests of each method. The finalized optimized aggregate percentages are shown in **Table 3.7**. These percentages were chosen as the closest percentages to optimum for a combination of the three graphs.

Table 3.7: Optimized Aggregate Percentages

Aggregate Percentages	
#67 Crushed Rock	35.0%
3/8" Chip	20.0%
Sand	45.0%
Total	100.0%

3.5.1 Shilstone. The Shilstone chart, often referred to as a coarseness/workability chart, uses a percentage ratio of sieve gradations to classify aggregates. **Figure 3.4** shows the five different zones of the chart. Zone I is referred to as gap graded concrete with low amounts of intermediate materials. Zone II consists of well-graded concrete; this is the optimal zone. Zone III has excessively more

intermediate aggregate than coarse aggregate. Zones IV and V are zones that are extremely sandy or rocky, respectively. The blue box shown in **Figure 3.4** is considered the ideal region. The X axis is determined by **Equation 3.8** for the coarseness factor, where *Q* is the cumulative percent retained on the 3/8" sieve and *R* is the cumulative percent retained on the No. 8 sieve. The Y axis is calculated from the workability factor, *WF*, shown in **Equation 3.9** where *W* is the cumulative % passing the No. 8 sieve and *C* is the cementitious material content of the mix in lb/yd^3. The 564 number comes from a standard 6-sack mix that uses six sacks of cement, which totals 564 lbs. To use the chart for other mixes, the workability factor can be changed by a percentage depending on the number of bags used.

$$CF = \frac{Q}{R} * 100 \qquad \textbf{(Eq. 3.8)}$$

$$WF = W + (\frac{2.5(C - 564)}{94}) \qquad \textbf{(Eq. 3.9)}$$

Using the percentages noted in the previous section, the aggregate combination charted just slightly above Zone II, into the Zone IV region, shown in **Figure 3.4**.

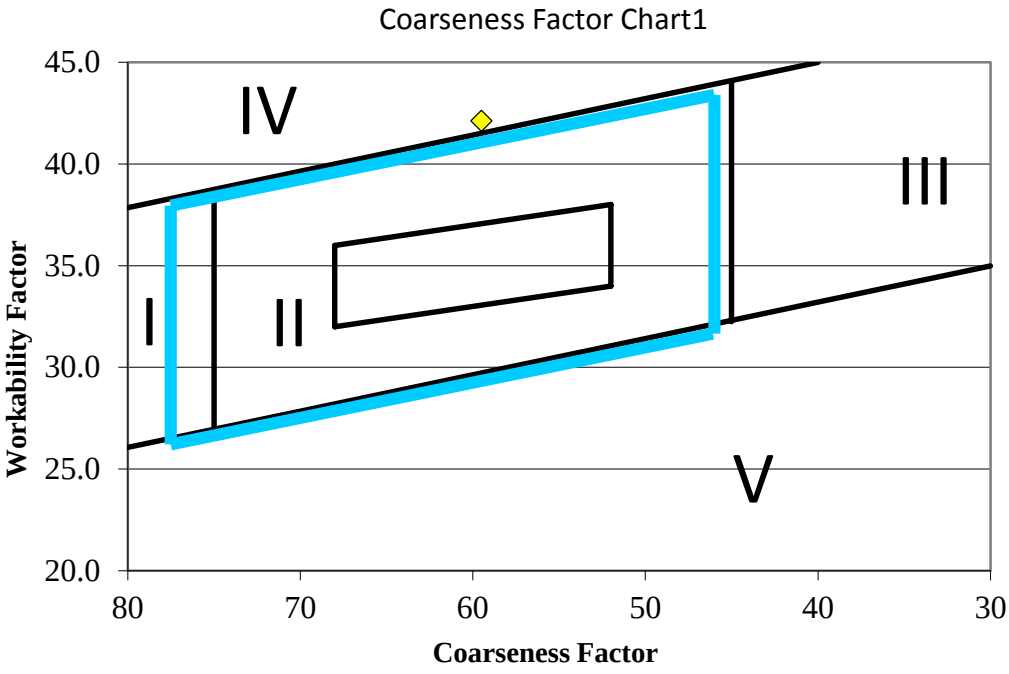

Figure 3.4: Shilstone Chart

3.5.2 Percent Retained. The percent retained chart uses the cumulative percent retained from a sieve analysis to determine the optimized aggregate gradation. The X axis comes from the sieve sizes, and the Y axis is the percent retained. The chart uses two lines representing 5-12% and 18-22% retainment. These are said to be the optimum maximum and minimum values for concrete. Aggregate gradations that stay between these markers are said to be optimal. The chart used for this research uses lines at 8% and 18% as typical limitations. As shown in **Figure 3.5**, the percentages used fall mostly in between the lines with 2 points going beyond. The upper point, referencing the 3/8 in. sieve rises above the line, however, it is still below the 22% maximum that can be used. For the No. 8 sieve, the graphs dips down to just below 5%.

This is deemed acceptable considering the different percentages used and other graph progressions.

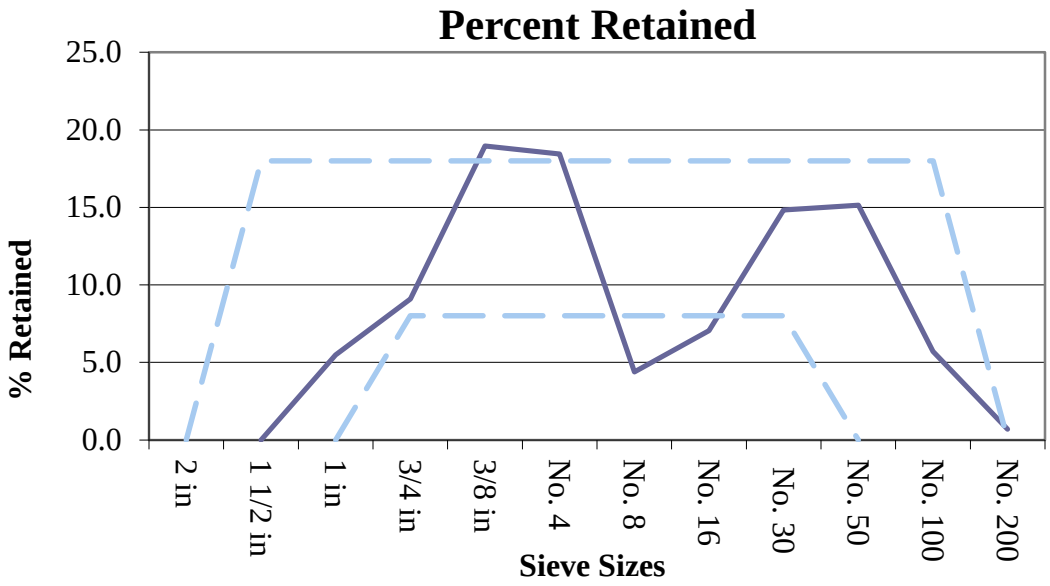

Figure 3.5: Percent Retained Chart

3.5.3 Power 45. The Power 45 curve also uses a cumulative gradation of aggregates. A line is drawn from the 0 point to the nominal maximum size. This is the "maximum density line". From this, minimum and maximum density lines are drawn starting at zero and reaching a sieve size one lower and one higher than the nominal maximum size, respectively. **Figure 3.6** shows the optimized aggregate for this research go slightly below and slightly above the lines. This variation outside of the limits would require an alteration to the percentage of sand, which tended to push the values outside of the optimal Shilstone and percent retained limits. It was felt that the

gradation chosen in **Table 3.7** offered an acceptable balance between the three methods.

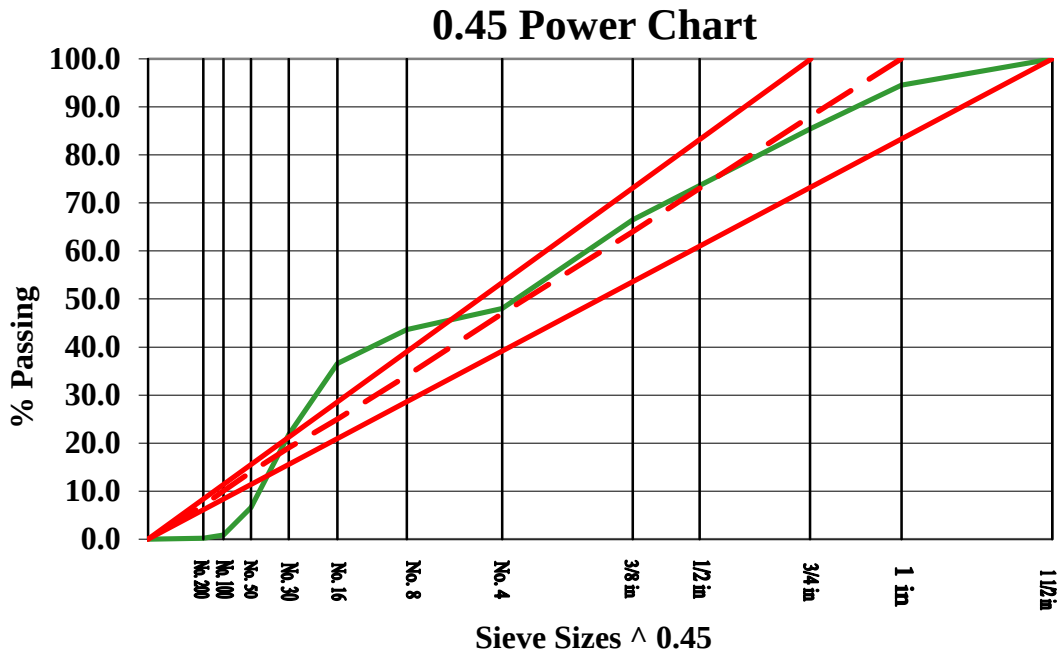

Figure 3.6: Power 45 Chart

3.6 Economical and Crack-Free High Performance Concrete

3.6.1 Aggregate Gradation & Limiting Cement Content. For the Eco-Bridge-Crete mixes, the aggregate was sieved for gradation and optimized as discussed in Section 3.5. The goal was to reduce the cement content while still maintaining the required properties.

3.6.2 Micro Fibers. The micro fibers used in the Eco-Bridge-Crete mixes were MasterFiber M 100 monofilament microsynthetic fibers by BASF. The fibers are

made from ultra-thin monofilament homopolymer polypropylene and measure 0.75 in. in length. They quickly spread uniformly through the concrete and are designed to have a high tensile strength and high modulus of elasticity. These fibers were used to reduce shrinkage cracking, reduce plastic settlement, increase durability of the concrete by reducing permeability, and keeping cracks small. The recommended dosage is 0.50 lb/yd^3, which is what was used in the mixes.

3.6.3 Macro Fibers. The macro fibers used in the Eco-Bridge-Crete mixes were MasterFiber MAC Matrix macrosynthetic fibers by BASF. This is an embossed fiber made from a polypropylene resin blend and measure 2.1 in. in length. These are used to control shrinkage, temperature, and settlement cracking in concrete and are created to have excellent flexural performance and finishability. Some benefits of these fibers include crack control, reduction in transportation stresses, increased toughness, increased shatter resistance, and improved green strengths. The recommended dosage is 3 to 5 lb/yd^3. More information on these fibers can be found in Appendix B.

3.6.4 Trial Laboratory Mixes. Using the optimized aggregate gradation, several laboratory trial mixes were developed and tested. The goal was to reduce the cement content while still maintaining the 5,000 psi target strength as well as the air content and slump requirements. Initially, the trial mixes did not include the micro- and macro-fibers. An initial mix design was developed that reduced the cement content 20% from the Class AA mix design. However, the subsequent addition of the fibers required higher paste contents to achieve the desired degree of workability. Therefore,

some cement was added back in making the total reduction 12%. After several attempts, the final eco-friendly mix designs are shown in **Tables 3.8** and **3.9**. The only difference between the two mixes involved the fibers. The Eco-Bridge-Crete 1 mix used only the micro-fibers while the Eco-Bridge-Crete 2 mix used both the micro- and macro-fibers.

Table 3.8: Eco-Bridge-Crete 1 Design Specifications

Concrete Mix Design 1 Per Cubic Yard			
Cement	414	lb	
Class F Fly Ash	103	lb	(20% by mass)
w/cm	0.40		
Fine Agg.	1415	lb	sand
Coarse Agg. 1	989	lb	#67
Coarse Agg. 2	565	lb	3/8 chip
AEA (AE-90)	2.585	oz	.67 oz/cwt
WRA (G 7500)	36.19	oz	7 oz/cwt
Micro-fibers	0.50	lb	0.5 lb/yd^3

Table 3.9: Eco-Bridge Crete 2 Design Specifications

Concrete Mix Design Per Cubic Yard			
Cement	414	lb	
Class F Fly Ash	103	lb	(20% by mass)
w/cm	0.4		
Fine Agg.	1415	lb	sand
Coarse Agg. 1	989	lb	#67
Coarse Agg. 2	565	lb	3/8 chip
AEA (AE-90)	2.585	oz	0.67 oz/cwt
WRA (G 7500)	36.19	oz	7 oz/cwt
Micro-fibers	0.5	lb	0.5 lb/yd^3
Macro-fibers	3.0	lb	3.0 lb/yd^3

3.7 Summary of Concrete Mix Designs

The final mix designs for use in the full-scale test specimens are shown in **Tables 3.10**, **3.11**, and **3.12** for the Control, Eco-Bridge-Crete 1, and Eco-Bridge-Crete 2 mix designs, respectively.

Table 3.10: Finalized Mix Designs per Cubic Yard

Mix Design	Cement (lb)	Class F Fly Ash (lb)	w/cm ratio	Natural Sand (lb)	#67 Crushed Stone (lb)	3/8" Chip (lb)	AEA (AE-90) (oz)	WRA (G 7500) (oz)	Micro-Fibers (lb/yd^3)	Macro-Fibers (lb/yd^3)
Control	470	118	0.4	1,323	1,857	0	4.4	26.7	0	0
Eco-Bridge-Crete 1	414	103	0.4	1,415	989	565	2.585	36.19	0.5	0
Eco-bridge-Crete 2	414	103	0.4	1,415	989	565	2.585	36.19	0.5	3

4. Full-Scale Experimental Program

4.1. Introduction

The objective of this study was to investigate the shear performance of two eco-friendly concretes. The experimental program consisted of a total of nine tests performed on full-scale reinforced concrete (RC) beam specimens. The following section discusses the beam specimen design, fabrication, test setup, and test procedure.

4.2. Specimen Design

The beam span, cross section, and loading arrangement were chosen to maintain a slender beam with a shear span-to-depth ratio larger than 3.0, avoiding any deep beam effects. The beams used in this program were 14 ft. long with a cross section of 12 in. x 18 in. The reinforcement was designed in accordance with *ACI 318-11 Building Code Requirements for Structural Concrete*. The longitudinal reinforcement consisted of six ASTM A615-09, Grade 60, deformed #7 bars. This amount of steel was selected to provide a typical flexural reinforcement ratio of 0.0198 as well as ensure a shear failure of the specimens. Each #7 bar contained a standard 90° hook at each end to prevent pullout in the event of longitudinal splitting cracks near the beam ends, which are common in beams that fail due to shear.

Transverse reinforcement consisted of 15, ASTM A615-09, Grade 60, #3 U-shaped stirrups with standard 180° hooks. Stirrups were spaced 2 in. on center at the ends of the beam and 7 in. on center within the center portion of the beam. This reinforcement layout provided two shear test regions, with each region measuring approximately 4 ft.

in length and reinforced for flexure only (i.e., no stirrups). Two ASTM A615-09, Grade 60, deformed #4 straight bars were placed at the top to anchor the stirrups and help stabilize the reinforcing cage. Schematic diagrams of the beam cross section and elevation are shown in **Figures 4.1** and **4.2**, respectively.

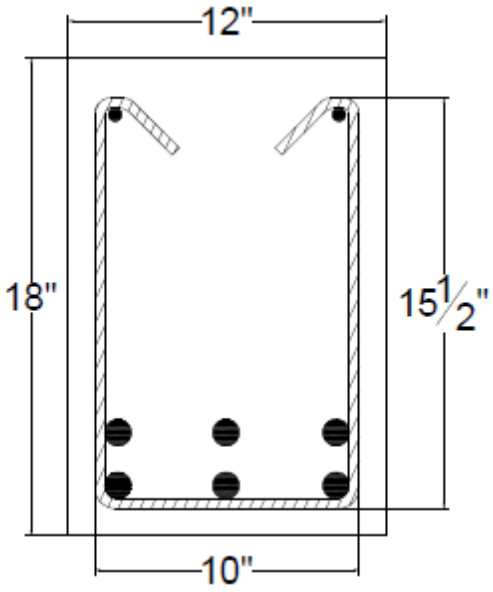

Figure 4.1: Schematic of Specimen Profile

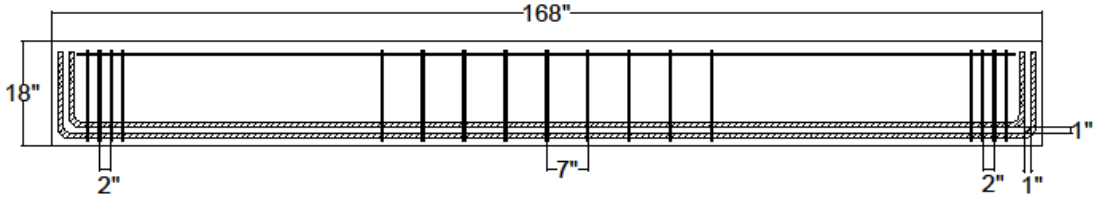

Figure 4.2: Schematic of Specimen Plan

4.3. Specimen Fabrication

The reinforcing bars were purchased from a local concrete detailing company and were already cut and bent prior to delivery to the lab. To construct the cages, the longitudinal reinforcing bars were placed upside down on top of sawhorses. A 10-in.-long section of #8 bar was placed between the two sets of longitudinal bars to create the correct vertical clear spacing. The stirrups were then placed at the appropriate locations and secured with wire ties. Once every joint was tied, the top bars were threaded into the cages from one end along the hooks of the stirrups and wire tied in place. Steel chairs measuring 1 in. were placed on the underneath and sides of the cage to ensure proper concrete cover. A completed reinforcing cage is shown in **Figures 4.3** and **4.4**.

Once the cage construction was complete, strain gauges were then installed on two of the longitudinal reinforcing bars near midspan. Once the placement of the strain gauges was decided, a small grinder was used to create a flat surface and then a Dremel was used to create a smooth surface. After being ground, the bar was cleaned with alcohol and a clean paper towel to remove any debris. The gauges were then attached to the steel using cyanoacrylate adhesive (**Figure 4.5**) and then coated with a two-part epoxy adhesive. After the outer adhesive cured, the gauges were wrapped in a buthyl rubber tape and then wrapped again in aluminum foil tape for protection during the concrete pour (**Figure 4.6**). The wires for the two strain gauges were fed to the top of each cage and secured to the reinforcing steel with zip ties as shown in **Figure 4.6**.

Figure 4.3: Completed Reinforcing Cage

Figure 4.4: Completed Reinforcing Cage

Figure 4.5: Strain Gauge Adhered to Longitudinal Bar

Figure 4.6: Completed Strain Gauges

The forms used for this program were steel framed with walls constructed of wood. Wedge bolts were fastened with wire ties to hold the frames together. These forms were coated with a form release agent to help with demolding. The cages were set in the forms, and steel straps were placed across the top to minimize movement during concrete placement, as shown in **Figure 4.7**. The strain gauge wires extending out of the forms were covered in plastic and secured on the outside of the forms for protection.

Figure 4.7: Forms for Full Scale Beam

The mix designs used to construct the beam specimens were sent to the local concrete batch plant, and the concrete was delivered to the lab. After the concrete arrived, a slump test was performed to verify if the desired slump was achieved. Afterwards, a wheelbarrow was filled with concrete to be used for the air content test and for making the appropriate number of compressive strength cylinders, splitting tensile strength cylinders, modulus of elasticity cylinders, and modulus of rupture beams. The only

deviation from this procedure was during the Eco-Crete 1 and Eco-Crete 2 concrete placements. For these two mixes, the admixtures and fibers were weighed and added to the concrete truck in the lab and allowed to mix before the final slump was verified. As the small specimens were being prepared, a concrete bucket attached to the crane was used for transporting the concrete from the truck to the beam forms (**Figure 4.8**). The beams were filled in two layers. After the first layer was poured, the concrete was vibrated to reduce air pockets and ensure proper consolidation. As the vibrator approached the vicinity of the strain gauges, extra care was taken in order to keep the strain gauges from being damaged. Once the last layer was poured and vibrated, the top was screeded and smoothed with finishing trowels (**Figure 4.9**). During the finishing process, premade steel hooks were vibrated into the top of the beams for transporting the specimens.

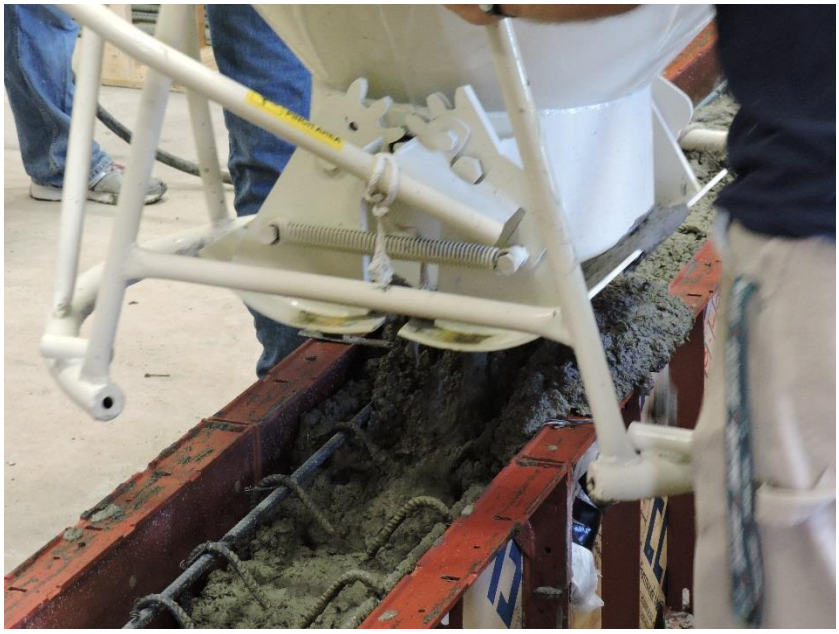

Figure 4.8: Concrete Pour

Figure 4.9: Screeding

The beams and small specimens were moist cured for seven days. The small specimens were placed in the area between the beams in order to maintain everything in the same curing environment. The beams and small specimens were covered with saturated burlap and plastic, and they were maintained in this moist environment throughout the seven day curing period. The beams and small specimens were demolded between two and seven days and re-covered with the wet burlap and plastic until reaching the full seven day curing time. After seven days, the beams and small specimens were uncovered and allowed to cure the remaining time within the lab environment.

4.4. Specimen Test Setup

The goal of the testing program was to test the beam specimens as close to the design strength as possible. The strength was monitored periodically to determine the most

appropriate time for testing. Once the beams neared design strength, one side of each beam was coated with white paint to provide a background for marking the propagation of cracks during the test. Small metal angles were adhered to the midpoint on both sides of the beams and were used for recording the midspan deflections.

A third-point loading arrangement was selected to test the beams in order to provide two, constant shear test regions for each beam. A schematic of the test setup is shown in **Figure 4.10**. Using an overhead crane, the beams were loaded into the test frame. The beams were carefully aligned in all directions to ensure proper loading. The lower pin and roller were set at 1 ft. from the end of the beam during placement. After the beam was centered, the top rollers were placed at the third point locations. Sand was placed under the top roller plates to create a level surface and reduce any gaps. A steel spreader beam was used to transfer the load from the hydraulic jack to the test specimens. A 100 kip load cell was placed on top of the spreader beam in order to monitor the load being applied during the testing process. A photograph of a test specimen within the test fixture is shown in **Figure 4.11**. String pots were attached to the metal angles placed at midspan in order to monitor the beam's deflection (**Figure 4.12**). The load cell, two string pots, and two strain gauges were connected to the data acquisition system.

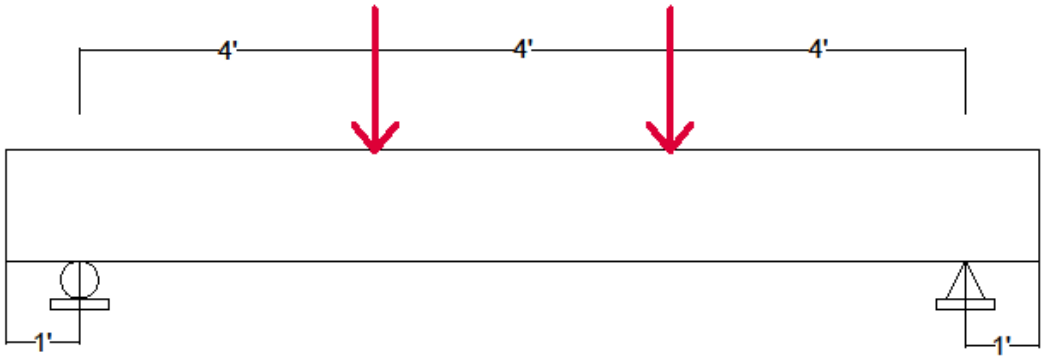

Figure 4.10: Third Point Loading Schematic

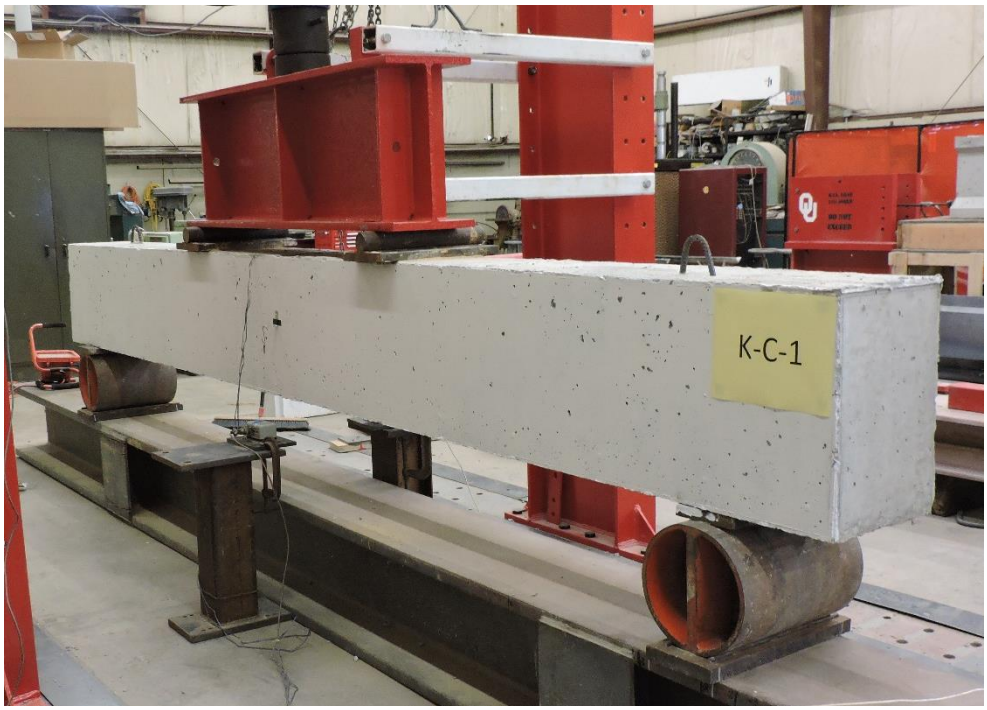

Figure 4.11: Test Setup

Figure 4.12: String Pot Setup

4.5. Specimen Test Procedure

Before beginning load application, the data acquisition software was set up to record the data received from the load cell, string pots, and strain gauges. The test protocol involved applying load in increments of 10 kips up to a total load of 50 kips. The load was then increased in increments of 5 kips until failure. The load was decreased to a 5 kip increase so the cracks could be looked at more frequently closer to failure. After each load step, crack propagation patterns were traced and the end of the cracks were labeled with the current load amount (**Figure 4.13**).

Each beam failure was determined when there was a significant drop in load, a load audible pop, and visual observation of the concrete in the test region undergoing severe

cracking as shown in **Figure 4.14**. At this point, the data acquisition system was stopped, the data was saved, photographs were taken of the failure, and the beam was removed from the test setup. This process was repeated for every beam.

Figure 4.13 Crack Propagation

Figure 4.14: Shear Failure Example

5. Test Results, Behavior, and Analysis

5.1. General

The objective of this study was to investigate the shear performance of two eco-friendly concretes. The full-scale testing program consisted of a total of nine tests performed on reinforced concrete beams designed to fail in shear. One set of beams cast from a standard ODOT Class AA mix served as control specimens. Identical sets of eco-friendly concrete beams were cast to determine the response and behavior of this material relative to the control concrete. Each set of beams consisted of three individual specimens. The following section discusses the fresh and hardened concrete properties; full-scale specimen test results and behavior; and analysis of the test results relative to selected design standards and a database of shear test results.

5.2. Fresh and Hardened Concrete Properties

The following section contains the fresh and hardened property test results for the control and two eco-friendly concrete mixes.

5.2.1. Fresh Concrete Properties. The unit weight, air content, and slump were determined during batching of the full scale beams in accordance with the procedures outline in Chapter 3. These results are shown in **Table 5.1**.

Table 5.1: Fresh Concrete Properties

Mix	Unit Weight (lb/yd^3)	Air Content (%)	Slump (in)
Control Mix	144	6.0	6.0
Eco-Bridge-Crete 1	141	7.2	3.0
Eco-Bridge-Crete 2	143	3.6	5.2

5.2.2 Hardened Concrete Properties. During batching, small-scale specimens were made to test compressive strength, modulus of elasticity, splitting tensile strength, and modulus of rupture as outlined in Chapter 3. The change in compressive strength for each individual mix as a function of time is shown in **Figures 5.1-5.3**. A compilation of the individual compressive strength results is shown in **Figure 5.4**.

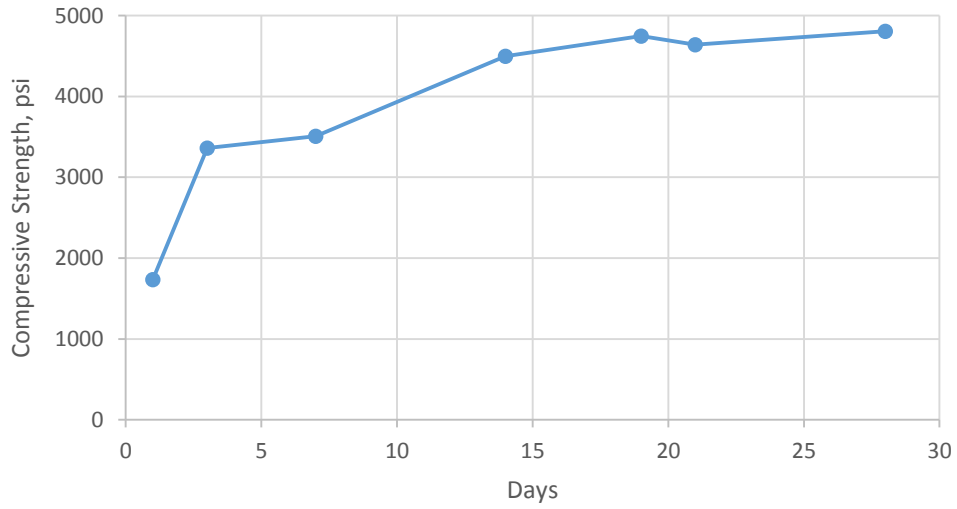

Figure 5.1: Control Mix Compressive Strength

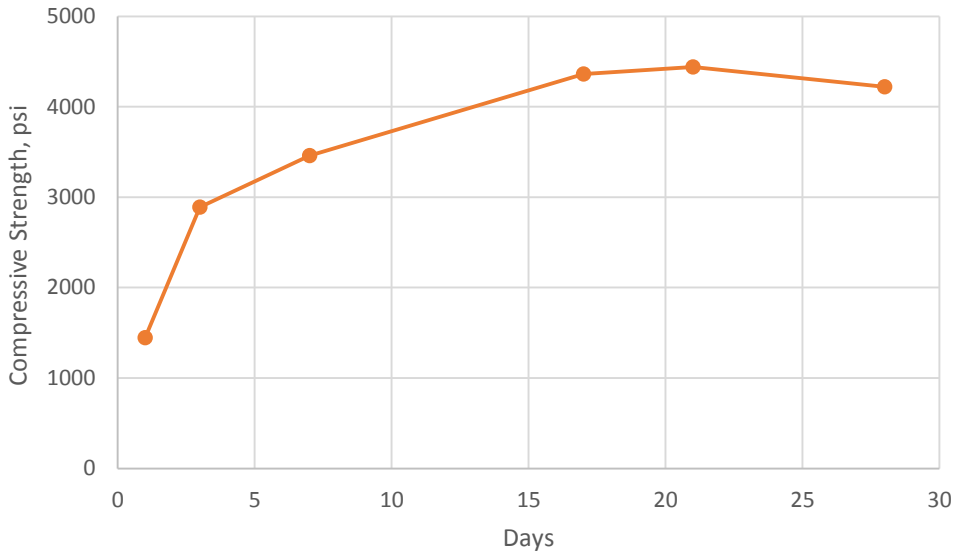

Figure 5.2: Eco-Bridge-Crete 1 Compressive Strength

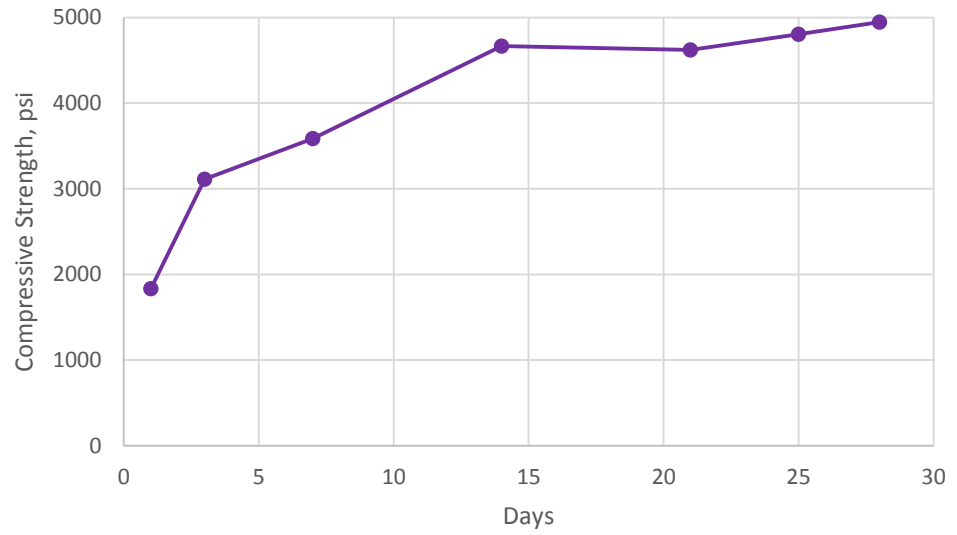

Figure 5.3: Eco-Bridge-Crete 2 Compressive Strength

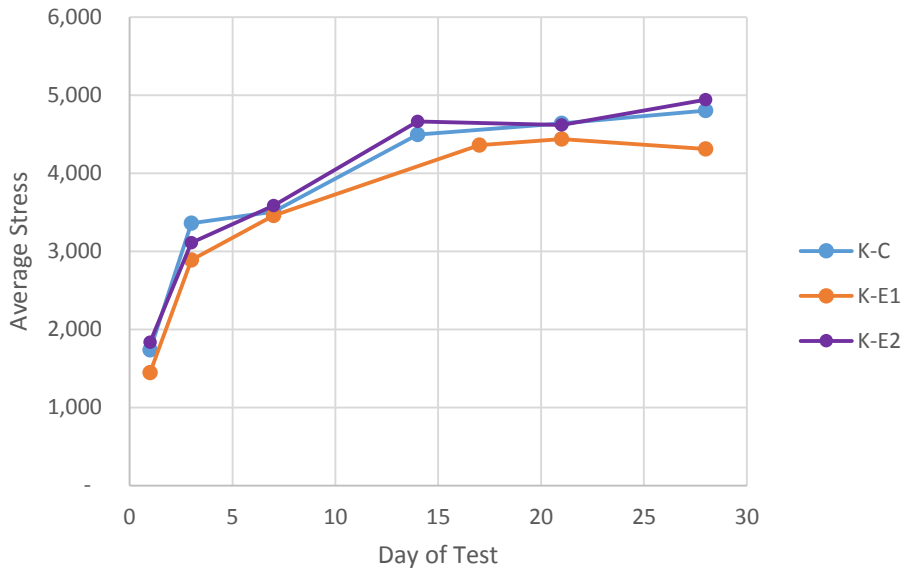

Figure 5.4: Compiled Compressive Strengths

The moduli of rupture, splitting tensile strengths, and moduli of elasticity are shown in **Table 5.2**. Following that, in **Figure 5.5** are the normalized charts for each.

Table 5.2: Small Specimen Test Results

Mix	Modulus of Rupture (psi)	Splitting Tensile Strength (psi)	Modulus of Elasticity (psi)
Control Mix	835	352	4,250,000
Eco-Bridge-Crete 1	676	365	3,600,000
Eco-Bridge-Crete 2	712	392	4,050,000

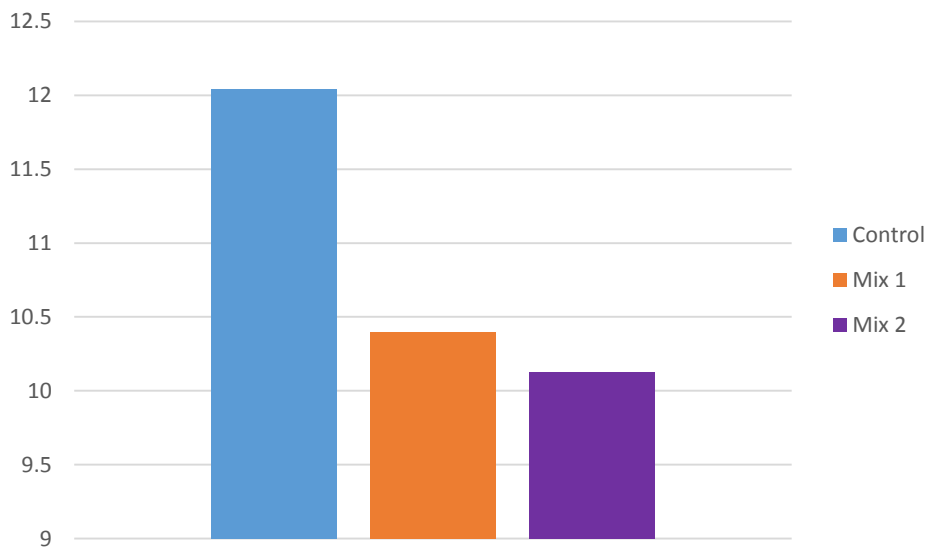

(a) Normalized Modulus of Rupture

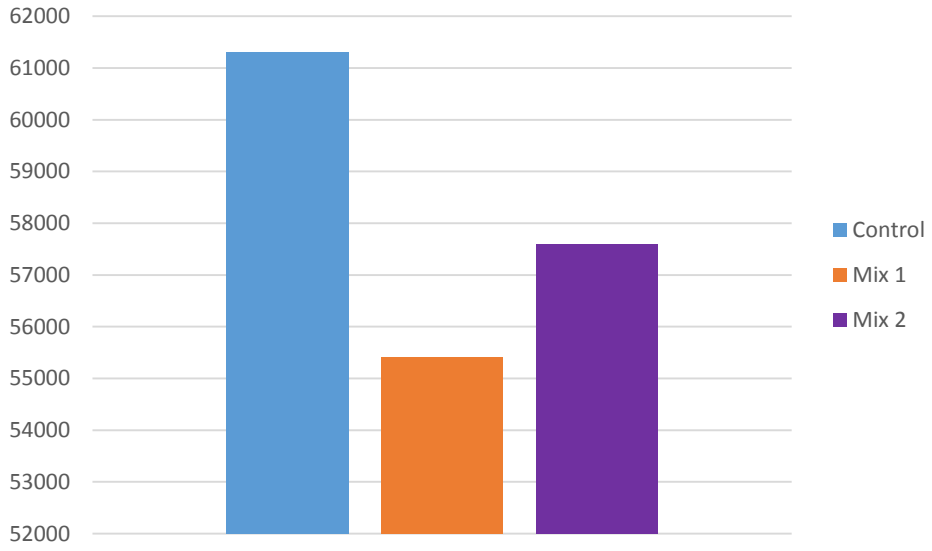

(b) Normalized Modulus of Elasticity

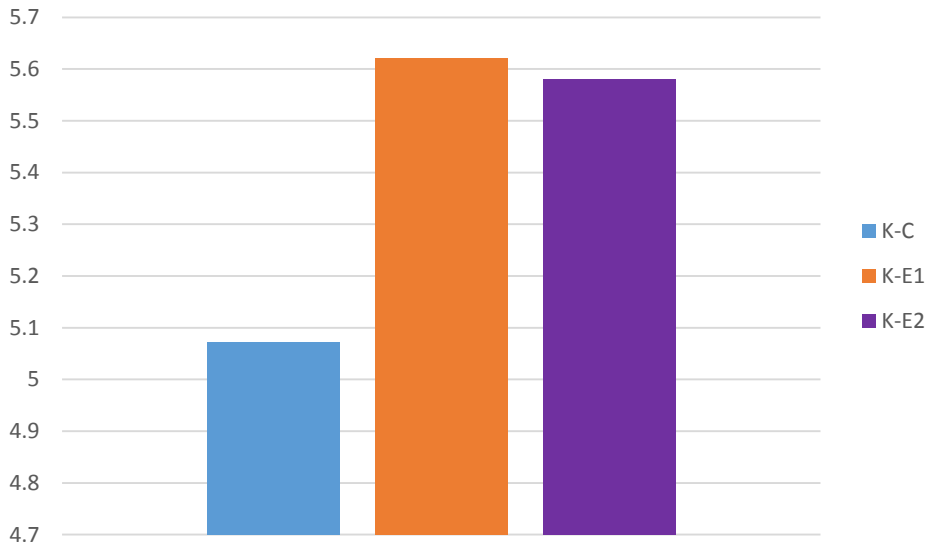

(c) Normalized Splitting Tensile Strength

Figure 5.5: Normalized Hardened Concrete Properties

5.3. Reinforcing Bar Tension Test Results

In order to determine the ultimate stress, yield stress, and modulus of elasticity of the flexural reinforcing bars used in the full-scale beam specimens, tension tests were performed in accordance with ASTM E 8-09 *Standard Test Methods for Tension Testing of Metallic Materials*. This test was performed on three 36 in. lengths of #7 reinforcing bars. Each specimen was clamped at each end in a 200 kip capacity load frame and loaded until rupture. Throughout testing, both strain and load were recorded. For each specimen, the yield stress of the bar was determined from the 0.2% strain offset of the stress versus strain plot. The modulus of elasticity was also determined for each bar using the slope of the linear portion of the stress strain curve. Table 5.3 shows the results of the #7 reinforcing bar tension test.

Table 5.3 #7 Reinforcing Bar Tension Test Results

Specimen	Yield Stress (ksi)	Average Yield Stress (ksi)	Ultimate Stress (ksi)	Average Ultimate Stress (ksi)	Modulus of Elasticity (ksi)	Average Modulus of Elasticity (ksi)
1	77.97	78.24	109.28	109.12	28,396	28,623
2	78.46		109.13		28,779	
3	78.28		108.96		28,694	

5.4. Test Results and Behavior of Full-Scale Specimens

Third-point loading was used to test the full-scale beams to evaluate shear capacity of the three different mixes. Three beams were tested for each mix design. The results of both Eco-Bridge-Crete mixes were compared to the control mix.

Table 5.4 summarizes the compressive strength at time of testing, f'_c, total load, shear force at failure, V_{test}, average shear stress at failure, $V_{test}/b_w d$, ratio of the average shear stress to compressive strength, V'_{test}/f'_c, and ratio of the average shear stress to the square root of the compressive strength, $V'_{test}/\sqrt{f'_c}$. The average shear stress varied from 155 to 179 psi with a mean of 165 psi for the control beams, from 141 to 192 psi with a mean of 171 psi for the Eco-Bridge-Crete 1 beams, and from 166 to 196 psi with a mean of 183 psi for the Eco-Bridge-Crete 2 beams. Normalized as a percentage of compressive strength, the average shear stress varied from 3.3% to 3.8% for the control beams, from 3.2% to 4.3% for the Eco-Bridge-Crete 1 beams, and from 3.4% to 4.1% for the Eco-Bridge-Crete 2 beams. Similar relative behavior is shown in the last column

of **Table 5.4** where the average shear stress is normalized with respect to the square root of compressive strength.

Table 5.4: Test Data at Failure

Mix Design	Beam ID	f'c (psi)	Total Load (kips)	V_{test}=Total Load/2 (kips)	$V'_{test} = V_{test}/b_w d$ (psi)	$V'_{test}/f'c$ (%)	$V'_{test}/\sqrt{f'c}$
Control	K-C-1	4747	64.98	32.49	179	3.8	2.6
	K-C-2		58.96	29.48	162	3.4	2.4
	K-C-3		56.42	28.21	155	3.3	2.3
Eco-Bridge-Crete 1	K-E1-1	4437	69.77	34.89	192	4.3	2.9
	K-E1-2		65.24	32.62	180	4.1	2.7
	K-E1-3		51.31	25.66	141	3.2	2.1
Eco-Bridge-Crete 2	K-E2-1	4805	60.09	30.05	166	3.4	2.4
	K-E2-2		71.03	35.52	196	4.1	2.8
	K-E2-3		68.11	34.06	188	3.9	2.7

Figure 5.5 shows the load-deflection behavior for the test specimens of each mix, where the deflection was measured at midspan. As can be seen in the graph, each beam displayed a linear elastic behavior until failure. The drops seen in the graph through the elastic region indicate pauses in load application for crack registration. For K-E1-3, since there was a significant difference from the other beams, there may have been an error with the data acquisition system.

Tables 5.5-5.7 show the crack registration for each load level per beam and mix design. In general, cracks typically began on the tension face of the beam within the central constant moment region, followed by additional flexural cracks forming between the load and support regions as the load was increased. Upon further increasing the applied load, flexural cracks in the shear test regions formed inclined flexure-shear cracks. The formation of the inclined flexure-shear cracks did not result in immediate failure, and additional load was required prior to failure. In general, the critical flexure-shear crack typically extended from the beam support to the loading point on the top side of the beam, as shown in **Figures 5.6-5.8** for each specimen.

The load-deflection behavior, cracking behavior, and formation of a critical flexure-shear crack indicate that all nine specimens failed in shear.

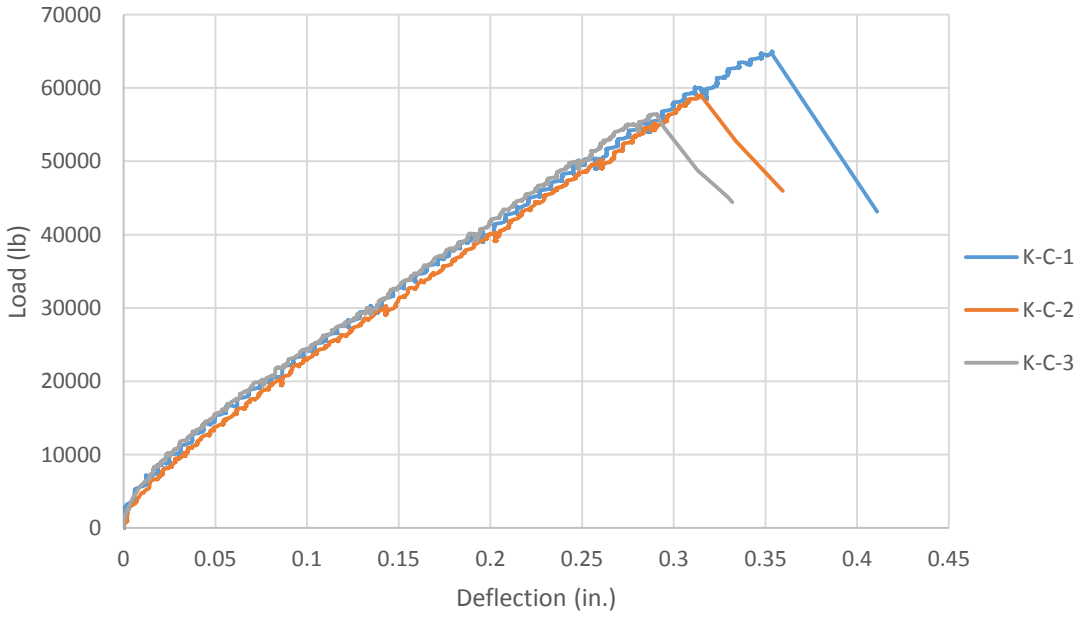

(a) Control Beam Load-Deflection Curve

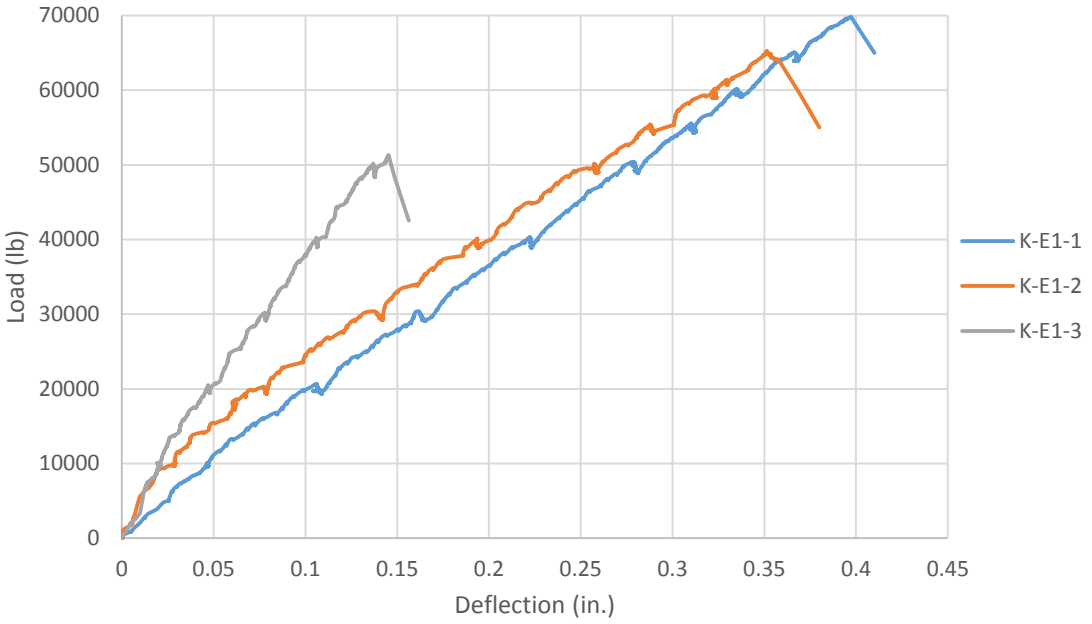

(b) Eco-Bridge-Crete 1 Load-Deflection Curve

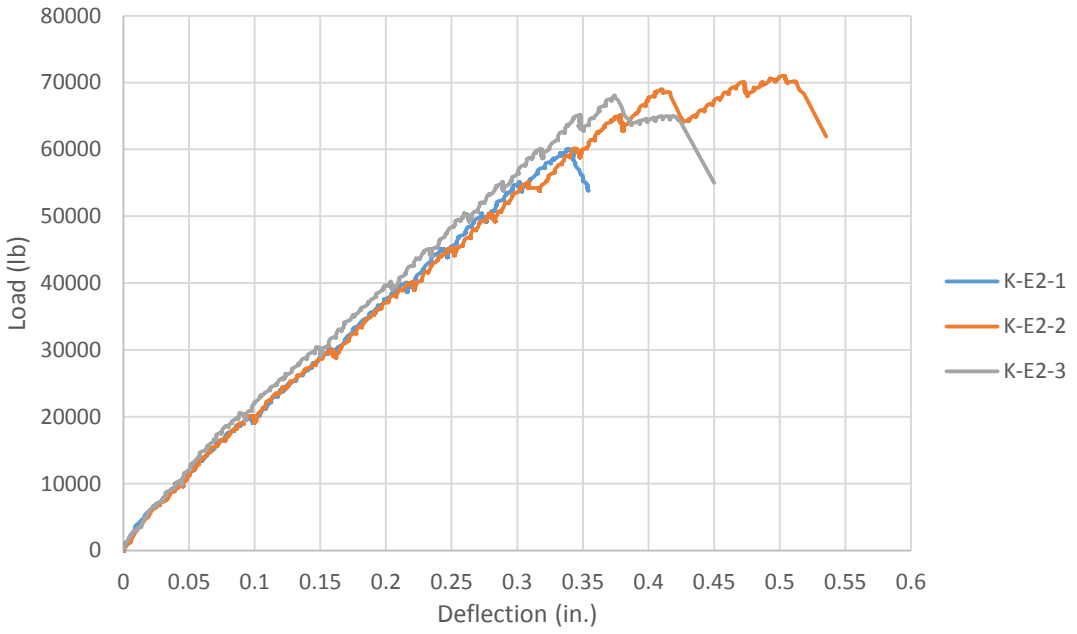

(c) Eco-Bridge-Crete 2 Load-Deflection Curve

Figure 5.6: Load Deflection Curves

Table 5.5: Crack Registration for Control Mix

Load (lbs)	Comments		
	K-C-1	K-C-2	K-C-3
10,000	No cracking	No cracking	No cracking
20,000	No cracking	No cracking	No cracking
30,000	No cracking	Small flexural cracks beginning	Flexural cracks forming
40,000	Small flexural cracks beginning	Cracks continue	Cracking continues
50,000	Cracks continue	Cracks continue	Shear cracks forming
55,000	Cracks continue	Shear cracks forming	Cracks continue
60,000	Shear cracks forming	Shear Failure - 58,957 lbs	Shear Failure - 56,423 lbs
65,000	Shear Failure - 64,979 lbs		

Table 5.6: Crack Registration for Eco-Bridge-Crete 1

Load (lbs)	Comments		
	K-E1-1	**K-E1-2**	**K-E1-3**
10,000	No cracking	Minor flexural cracks beginning	No cracking
20,000	Small flexure cracks beginning	Development of existing cracks, new cracks forming	Flexural cracks beginning
30,000	Cracking continues	Cracking continues	Cracking continues
40,000	Cracking continues	Cracking continues	Cracking continues
50,000	Shear cracks forming	Shear cracks forming	Shear cracks develop
55,000	Shear cracks forming	Shear cracks becoming visible	Shear Failure - 51,307 lbs
60,000	Shear cracks getting larger	Shear cracks continue	
65,000	Shear cracks getting larger	Shear cracks getting larger	
70,000	Shear failure - 65,949 lbs	Shear Failure - 65,238 lbs	

Table 5.7: Crack Registration for Eco-Bridge-Crete 2

Load (lbs)	Comments		
	K-E2-1	**K-E2-2**	**K-E2-3**
10,000	No Cracking	No cracking	No cracking
20,000	Small flexural cracks beginning	No cracking	No cracking
30,000	Cracking continues	Small flexural cracks beginning	Small flexural cracks beginning
40,000	Cracking continues	Cracking continues	Cracking continues
45,000	Slight diagonal in cracking	Cracking continues	Cracking continues
50,000	Cracking continues	Cracking continues	Cracking continues
55,000	Cracking continues	Cracking continues	Cracking continues
60,000	Shear Failure - 60,085 lbs	Shear cracks forming	Cracking continues
65,000		Shear cracks getting larger	Shear cracks forming
70,000		Shear Failure - 71,031 lbs	Shear Failure - 68,108 lbs

(a) K-C-1 Failure Crack

(b) K-C-2 Failure Crack

(c) K-C-3 Failure Crack

Figure 5.7: Control Mix Failure Cracks

(a) K-E1-1 Failure Crack

(b) K-E1-2 Failure Crack

(c) K-E1-3 Failure Crack

Figure 5.8: Eco-Bridge-Crete 1 Failure Cracks

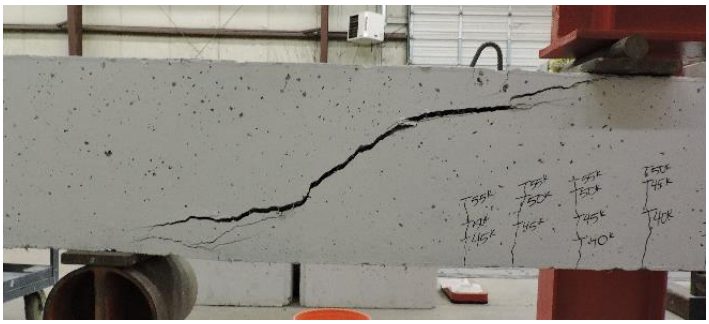

(a) K-E2-1 Failure Crack

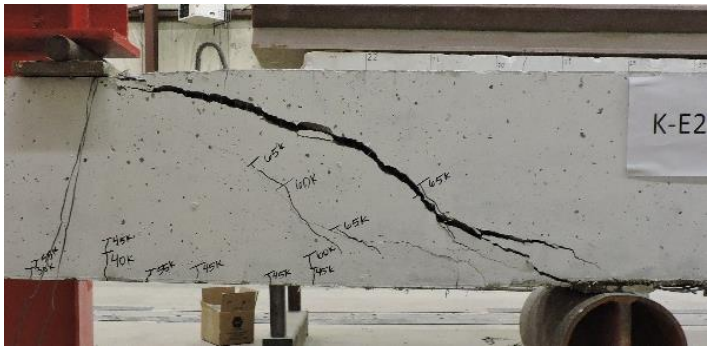

(b) K-E2-2 Failure Crack

(c) K-E2-3 Failure Crack

Figure 5.9: Eco-Bridge-Crete 2 Failure Cracks

As shown in **Table 5.8**, the steel stresses at failure do not exceed the yield strength of the flexural steel, further verifying that the specimens failed in shear.

Table 5.8: Calculated Steel Stresses at Failure Based on Measured Strains

Mix Design	Beam ID	Streel Stress at Failure (front)	Steel Stress at Failure (back)
Control	K-C-1	44.94	45.51
	K-C-2	39.21	40.07
	K-C-3	41.79	39.79
Eco-Bridge-Crete 1	K-E1-1	51.81	56.96
	K-E1-2	52.38	51.24
	K-E1-3	36.92	40.07
Eco-Bridge-Crete 2	K-E2-1	48.09	48.95
	K-E2-2	54.67	57.53
	K-E2-3	43.51	46.37

5.5 Statistical Data Analysis

Statistical tests were used to evaluate whether there is any statistically significant difference between the normalized shear strengths of the three different mix designs. To compare the test results, the shear stress at failure must be adjusted to reflect the different compressive strengths of the specimens. The shear strength of a beam is generally a function of the square root of the compressive strength of the concrete. Therefore, to normalize the data for comparison, the shear strengths were divided by the square root of compressive strength (see **Table 5.4**).

The paired *t*-test is a statistical technique used to compare two population means. This test assumes that the differences between pairs are normally distributed. If this assumption is violated, the paired *t*-test may not be the most powerful test. Both Kolmogorv-Smirnov and Anderson-Darling tests showed that the data – the differences between the shear capacities of each mix design – follow a normal distribution. Therefore, the paired *t*-tests could be performed. Three separate analyses were performed comparing two sets of test data: Control versus Eco-Bridge-Crete 1; Control versus Eco-Bridge-Crete 2; and Eco-Bridge-Crete 1 versus Eco-Bridge-Crete 2. The following hypothesis was used for the paired *t*-tests: the means of the shear capacities are equal. The results of the statistical analysis showed that the *P* values were greater than 0.05 in all cases. This confims the null hypothesis at the 0.05 significance level (or 95% confidence interval). In other words, the normalized shear capacities of the three differenct concrete mixes are essentially equal (*i.e.*, not statistically significantly different).

5.6 Comparison of Test Results with Shear Provisions of Selected Standards

The shear capacity of each beam was determined pre-testing using **Equation 5.1** from *ACI 318-11 (11.2.1.1)*. This equation was chosen because there is no reinforcement in the shear region of the beams. After testing, the shear capacity was determined based on the failure load. The shear is assumed to be half of the failure load since it was a simply supported beam loaded at the third points. **Equation 5.2** was used to determine

the percentage of shear over the pre-testing calculation for each beam, and then an average for each set was calculated.

$$V_c = 2\lambda\sqrt{f'_c}b_w d \qquad \textbf{(Eq. 5.1)}$$

$$\%\ Over = \frac{\mathrm{V}'}{V_c} \qquad \textbf{(Eq. 5.2)}$$

Table 5.9 shows the ratio of experimental-to-code predicted capacity for the selected design standard for all of the beams. In comparing the mixes, they all exceed the design standard, indicating the existing code provisions conservatively predict the shear strength of the Class AA beams along with the eco-friendly beams.

For the control beams, the tested shear strength exceeded the code capacity between 12.8% and 29.9%, giving an average of 20.2% above the required shear strength. For the Eco-Bridge-Crete 1 beams, the tested shear strength exceeded the code capacity between 6.1% and 44.3%, giving an average of 28.4% above the required shear strength. For the Eco-Bridge-Crete 2 beams, tested shear strength exceeded the code capacity between 19.4% and 41.1%, giving an average of 32.0% above the required shear strength. On average, the Eco-Bridge-Crete beams exceeded the code capacity more than the control mix, indicating the Eco-Bridge-Crete beams exceeded the code predicted strengths by a larger margin.

Table 5.9: Shear Capacity Data

Mix Design	Specimen	V_c (lb)	V_{test}=Load/2 (lb)	Test vs. Calculated Capacity		
				V_{test}/V_c	% over V_c	Avg. % over V_c
Control	K-C-1	25,010	32,490	1.30	29.9	20.2
	K-C-2		29,479	1.18	17.9	
	K-C-3		28,212	1.13	12.8	
Eco-Bridge-Crete 1	K-E1-1	24,180	34,886	1.44	44.3	28.4
	K-E1-2		32,619	1.35	34.9	
	K-E1-3		25,654	1.06	6.1	
Eco-Bridge-Crete 2	K-E2-1	25,162	30,043	1.19	19.4	32.0
	K-E2-2		35,516	1.41	41.1	
	K-E2-3		34,054	1.35	35.3	

5.7 Comparison of Test Results with Shear Test Database

Figure 5.9 presents the normalized shear strength (ACI Equation 11-3 noted previously) versus longitudinal reinforcement ratio for the beams of this study as well as the wealth of shear-test data available in the literature (Reineck et al. 2003). **Figure 5.9(a)** contains all nine shear test results while **Figure 5.9(b)** contains the average for each concrete type. Given the significant scatter of the database of previous shear-test results, it is somewhat difficult to draw definitive conclusions on the current test values. Nonetheless, visually, **Figure 5.9** seems to indicate that the test results fall within the central portion of the data and follow the same general trend of increasing shear strength as a function of increasing longitudinal reinforcement ratio.

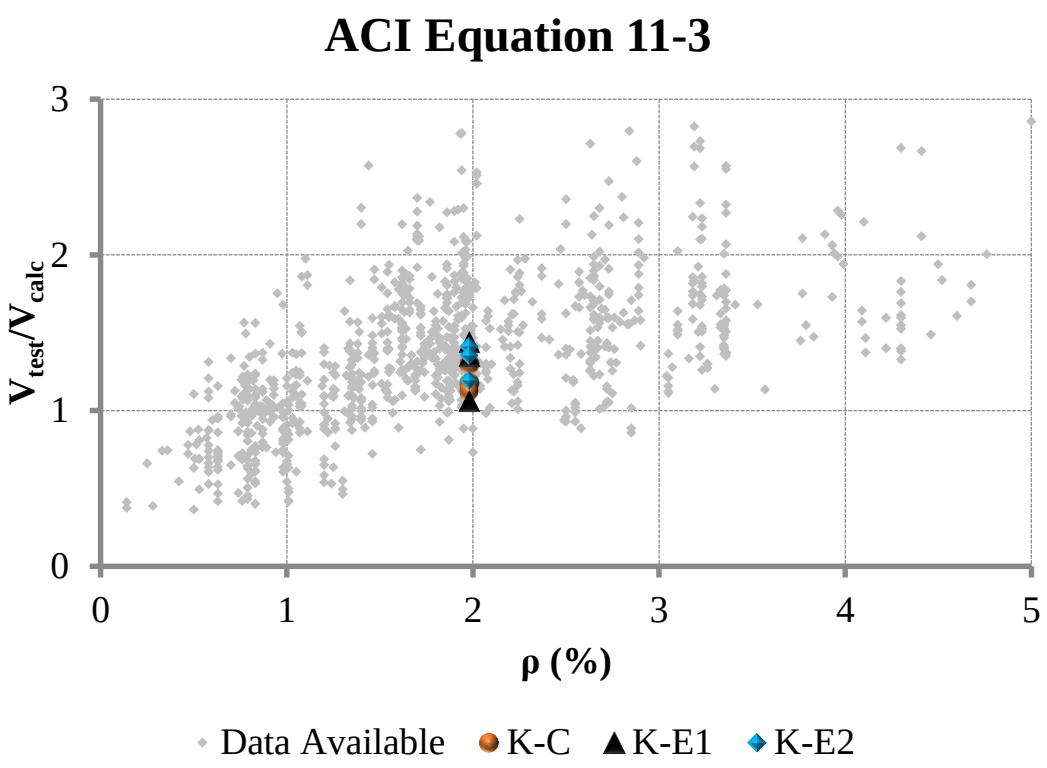

(a) Normalized Shear Strength versus ρ (Reineck et al. 2013)

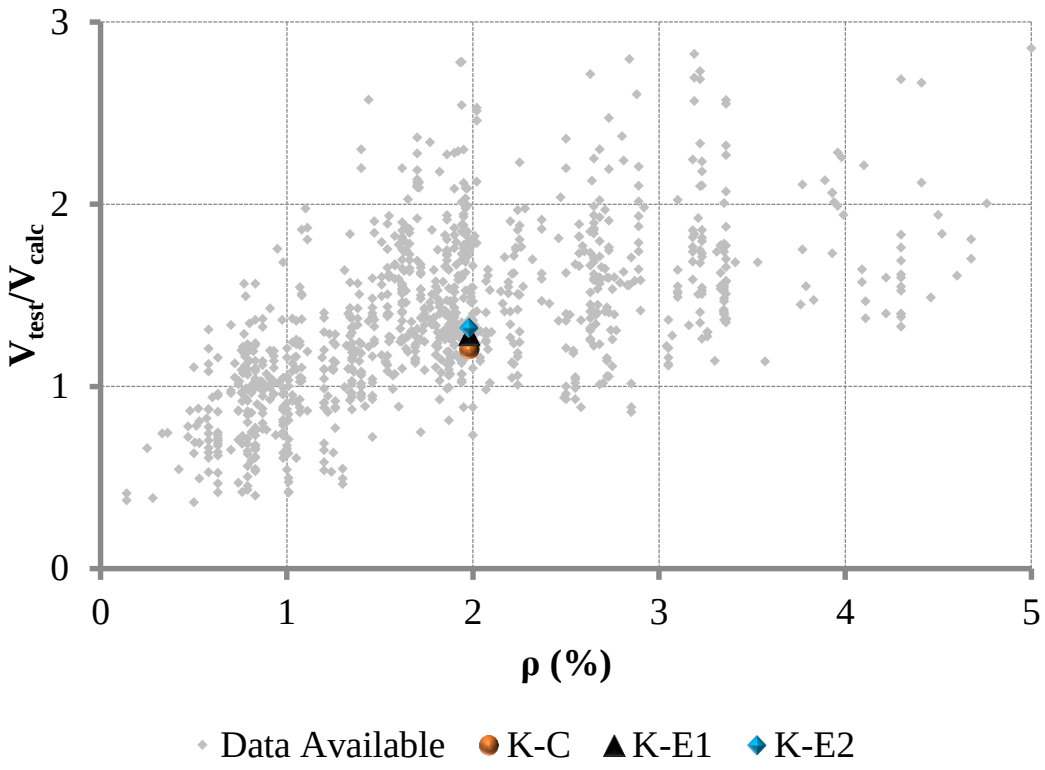

(b) Normalized Shear Strength Averages versus ρ (Reineck et al. 2013)

Figure 5.10: Normalized Shear Strength versus ρ

Because the span-to-depth ratio plays a significant role in the shear strength of beams, **Figure 5.10** presents the normalized shear strength of the beams of this study versus the span-to-depth ratio, a/d, with the same extensive database of shear-test results. **Figure 5.10(a)** contains all nine shear test results while **Figure 5.10(b)** contains the average for each concrete type. Again, given the significant scatter of the database of previous shear-test results, it is somewhat difficult to draw definitive conclusions on the current test values. Nonetheless, visually, **Figure 5.10** seems to indicate that the test results fall within the central portion of the data and follow the same general trend of decreasing shear strength as a function of increasing span-to-depth ratio.

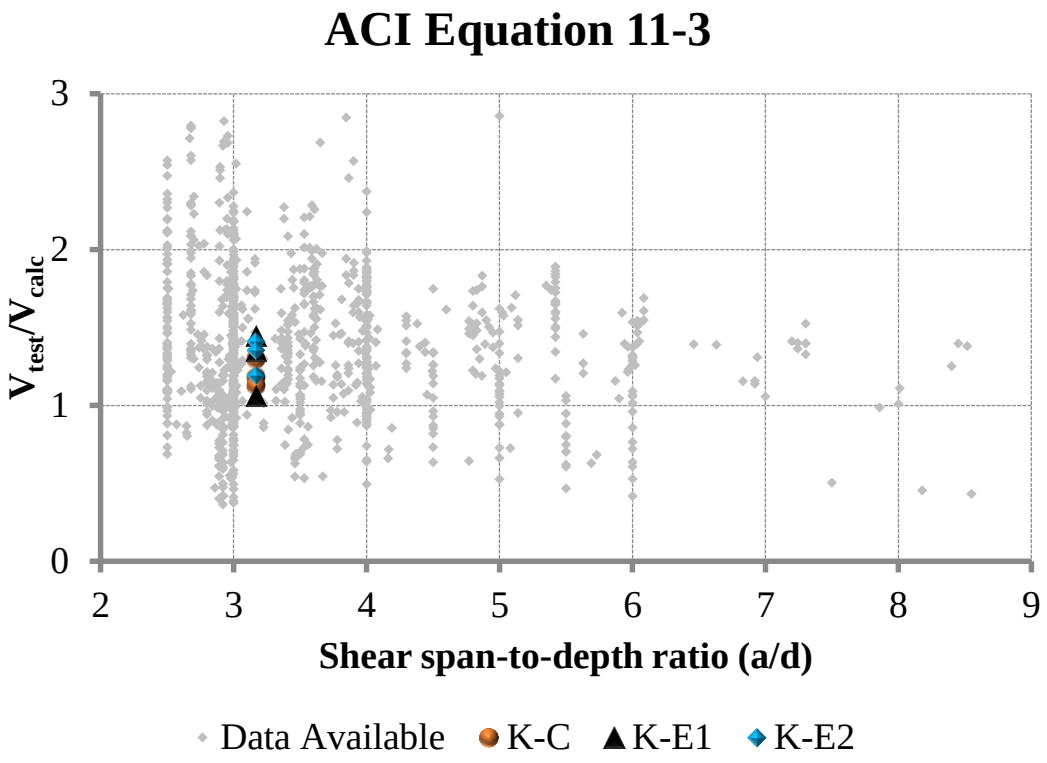

(a) Normalized Shear Strength versus Shear Span-to-Depth Ratio (Reineck et al. 2013)

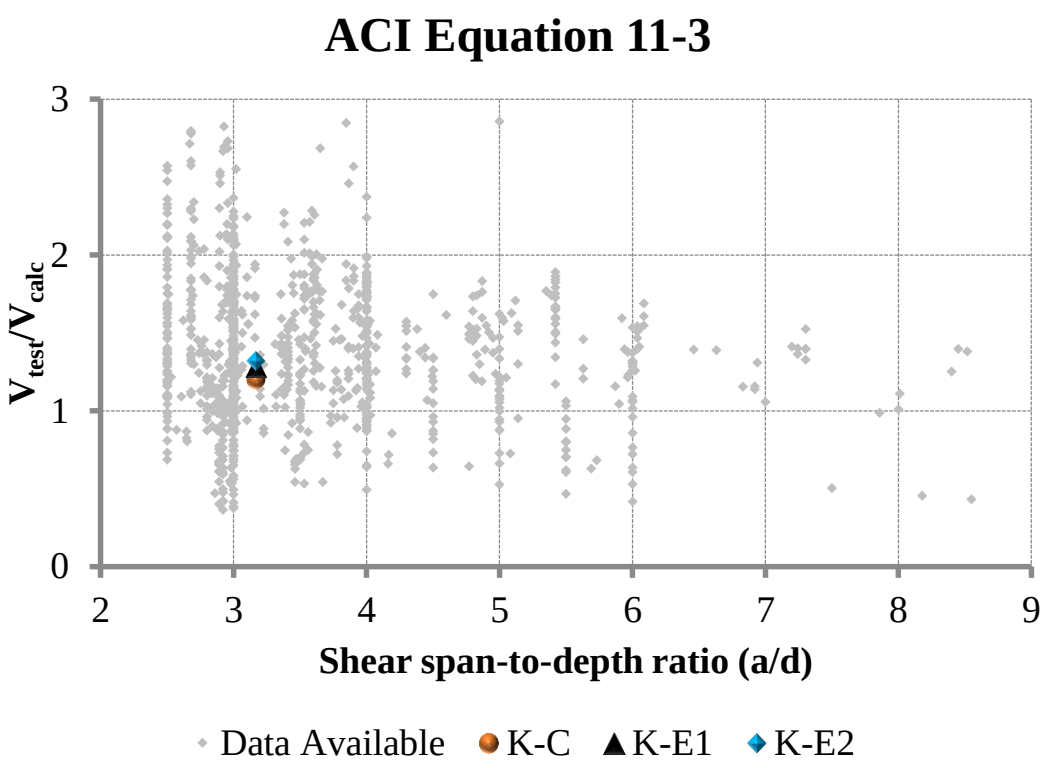

(b) Normalized Shear Strength Averages versus Shear Span-to-Depth Ratio (Reineck et al. 2013)

Figure 5.11: Normalized Shear Strength versus Shear Span-to-Depth Ratio

6. Findings, Conclusions, and Recommendations

6.1 Introduction

The objective of this study was to evaluate the shear performance of economically friendly concrete. The following section presents the findings, conclusions, and recommendations of this research. This research compared two different Eco-Bridge-Crete mixes to a standard ODOT Class AA mix.

6.2 Findings

6.2.1 Fresh Concrete Properties. The fresh properties analyzed were slightly impacted by the changing of the cementitious content, aggregate distribution, and addition of fibers. The unit weight decreased slightly for the Eco-Bridge-Crete mixes. The air content for the Eco-Bridge-Crete 2 mix was slightly below the required value, but slightly more air entraining admixture would correct that shortcoming. The slump decreased for the Eco-Bridge-Crete mixes compared to the control mix primarily due to the addition of fibers. However, the Eco-Bridge-Crete mixes were visually more cohesive and stable, most likely due to the improved aggregate gradation. Slightly more water reducing admixture would increase the slump to the desired amount. These results can be found in **Table 6.1**.

Table 6.1: Fresh Concrete Properties

Mix Design	Slump (in.)	Air Content (%)	Unit Weight (lb/yd3)
K-C	6	6	143.08
K-E1	3	7.2	141.08
K-E2	5.25	3.6	146.00

6.2.2 Hardened Concrete Properties. The hardened concrete properties showed a change in compressive strength of -310 psi and 58 psi, a gain of 13 psi and 40 psi in splitting tensile strength, a decrease in modulus of rupture of 159 psi and 123 psi, and a decrease in modulus of elasticity of 650,000 psi and 200,000 psi.

6.2.3 Shear Capacity. A total of nine full-scale beams were tested for this project. For each mix, three beams were constructed. The load-deflection response, cracking morphology, and type of failure were consistent between the three concrete types. Comparing the average shear failure capacity for the control and Eco-Bridge-Crete 1 mixes reveals that the Eco-Bridge-Crete 1 mix had a slightly higher capacity than the control mix. The control mix averaged a capacity of 30.1 kips, while the Eco-Bridge-Crete 1 mix averaged a capacity of 31.1 kips. This totals a 3% increase in capacity.

For the control mix versus Eco-Bridge-Crete 2, the Eco-Bridge-Crete 2 mix also had a slightly higher capacity than the control mix. The control mix had an average shear capacity of 30.1 kips, while the Eco-Bridge-Crete 2 mix had an average shear capacity of 33.2 kips. This totals a 10% increase in capacity.

A statistical data analysis of the normalized shear test results indicated that the three mixes were essentially equal in capacity.

6.3 Conclusions

The eco-friendly concrete mixes performed at the same level as the ODOT Class AA mix design in terms of fresh and hardened concrete properties and shear strength. As a result, the use of an optimized aggregate distribution can help reduce the cementitious content of concrete mixes by 12% without sacrificing performance.

The use of micro- and macro-fibers had no apparent effect on shear performance. However, fibers can reduce early and late age cracking, which will improve the durability performance of the material, making it even more sustainable.

6.4 Recommendations

Based on the results of this study, the following recommendations are presented:

- Incorporate aggregate optimization techniques into mix design development to reduce the cementitious content, which will reduce the cost while increasing the sustainability of concrete
- Perform additional research on the possibility of further reducing cementitious contents through the use of aggregate optimization techniques
- Examine the durability of the eco-friendly concrete mixes developed in this study
- Develop optimized aggregate gradations that incorporate a larger range of potential sieve sizes
- Examine the three aggregate optimization techniques used in this study to determine if improvements can be made to better predict performance

- Test additional full scale beam specimens with the mixes developed in this study using different longitudinal reinforcement ratios and beam sizes

References

AASHTO LRFD, (2007). Bridge Design Specifications and Commentary (4th Ed.). American Association of State and Highway Transportation Officials. Washington, DC.

ACI Committee 318, (2008). Building Code Requirements for Structural Concrete and Commentary (ACI 318-08). American Concrete Institute, Farmington Hills, MI.

Al-Nasra, M., and Asha, N. (2013). "Shear Reinforcements in the Reinforced Concrete Beams." American Journal of Engineering Research 2.10: 191-99. AJER. 2013. Web. 18 Nov. 2015. <http://www.ajer.org/papers/v2(10)/V0210191199.pdf>.

Cook, M., Ghaeezadeh, A., Ley, T., and Russell, B. (2013). *Investigation of Optimize Graded Concrete for Oklahoma - Phase 1*. Rep. no. 2160. *Optimize Graded*. Oklahoma Department of Transportation.

CSA Committee A23.3 (2004). Design of Concrete Structures (CSA A23.3-04). Canadian Standards Association. Rexdale, ON, Canada.

Dokken, D. (1996). (M. Zinyowera, R. Moss, & R. Watson, Eds.). 20.3.4.1 Cement and Concrete. *Climate Chage 1995: Impacts, Adaptations and Mitigation of Climate Change.* 661-662. New York, NY: Press Syndicate of the University of Cambridge.

EIA (2014). *U.S. Energy-Related Carbon Dioxide Emissions, 2014*. Web. 4 Dec. 2015. https://www.eia.gov/environment/emissions/carbon/

Iowa Department of Transportation (2007). *Aggregate proportioning guide for portland cement concrete pavement*. Office of Materials, Matls. IM 532.

Khayat, K. (2014). *Economical and Crack-Free High Performance Concrete.* Proposal to U.S. Department of Transportation.

Ley, T., & Cook, D. (2014). Aggregate Gradations for Concrete Pavement Mixtures. *CP Road MAP Brief*.

Mehta, P., & Monteiro, P. (2006). Concrete: Microstructure, Properties, and Materials. Web 16 Nov. 2015. http://www.ce.berkeley.edu/~paulmont/165/review2.pdf

Nilson, A.H., Darwin, D., and Dolan, C.W. (2004). Design of Concrete Structures (13th Ed.). McGraw Hill.

NRMCA, National Ready Mixed Concrete Association (1994/2014). *CIP 24 – Synthetic Fibers*. Concrete in Practice What, Why, and How?. Web. 1 Dec. 2015. http://www.nrmca.org/aboutconcrete/cips/24pr.pdf

Obla, K., Lobo, C., Lemay, L., NRMCA (2005). Specifying Concrete for Durability: Performance-Based Criteria Offer Best Solutions. *Concrete InFocus, December 2005.*

Oklahoma Department of Transportation (ODOT) (2009). *Section 701 Portland Cement Concrete.* ODOT Specifications. 551-581.

Rached, M., Fowler, D., and Koehler, E. (2010). *Use of Aggregates to Reduce Cement Content in Concrete*. Tech.

Reineck, K. H., Kuchma, D. A., Kim, K. S., and Marx, S. (2003). "Shear database for reinforced concrete members without shear reinforcement." ACI Struct. J., 100(2), 240–249.

Richardson, J. (2006). "Design of Beams for Shear." N.p., Web. 18 Nov. 2015. <http://richardson.eng.ua.edu/Former_Courses/CE_433_fa06/Notes/Design_for_Shear.pdf>.

Rubenstein, M. (2012). Emissions from the Cement Industry. *State of the Planet.* Earth Institute: Columbia University.

Transportation Research Board. (2006). Control of Cracking in Concrete. *Transportation Research Circular, E-C107*.

Transportation Research Board (2013). Durability of Concrete: Second Edition. *Transportation Research Circular, E-C171*.

USGS (2015), *U.S. Geological Survey, Mineral Commodity Summaries*. Web 4 Dec. 2015. http://minerals.usgs.gov/minerals/pubs/commodity/cement/mcs-2015-cemen.pdf

Vic Roads (2010). Crack in Concrete. Technical Note 38.

Wight, J.K., and MacGregor, J.G., (2009). Reinforced Concrete Mechanics and Design (5th Ed.). Pearson-Prentice Hall.

Yurdakul, E. (2010). "Optimizing concrete mixtures with minimum cement content for performance and sustainability". Graduate Theses and Dissertations. Iowa State University. Paper 11878. http://lib.dr.iastate.edu/cgi/viewcontent.cgi?article=2880&context=etd

APPENDIX A

CONTROL BEAM TEST SPECIMENS

Figure A.1: K-C-1 Test Setup

Figure A.2: K-C-1 Crack Propagation 55 kips

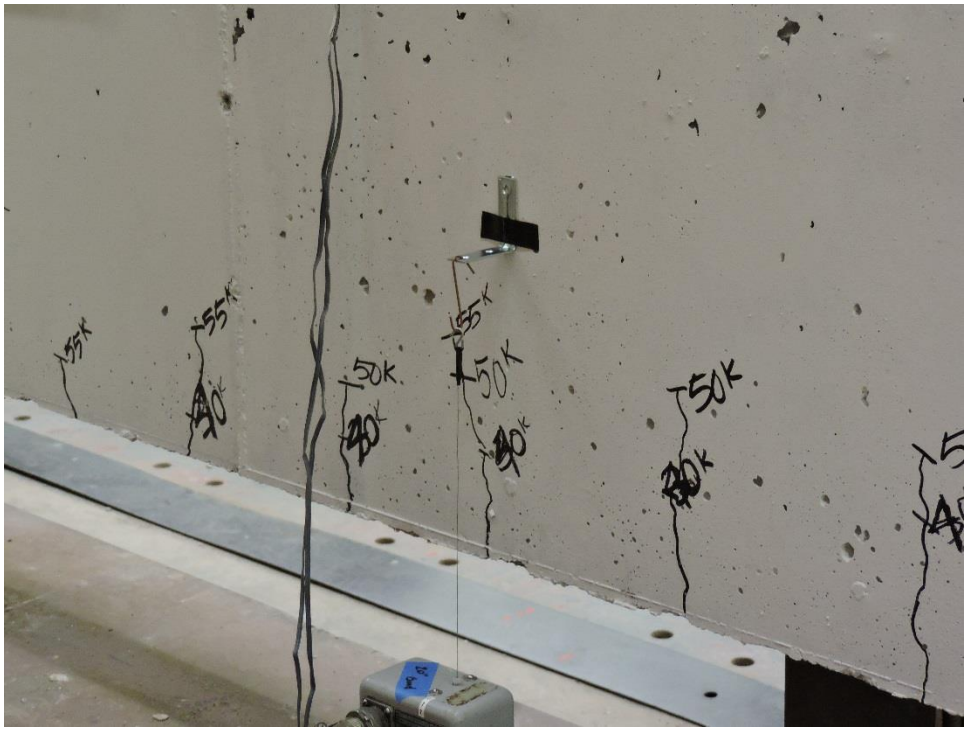

Figure A.3: K-C-1 Crack Propagation 55 kips

Figure A.4: K-C-1 Failure Crack Left View

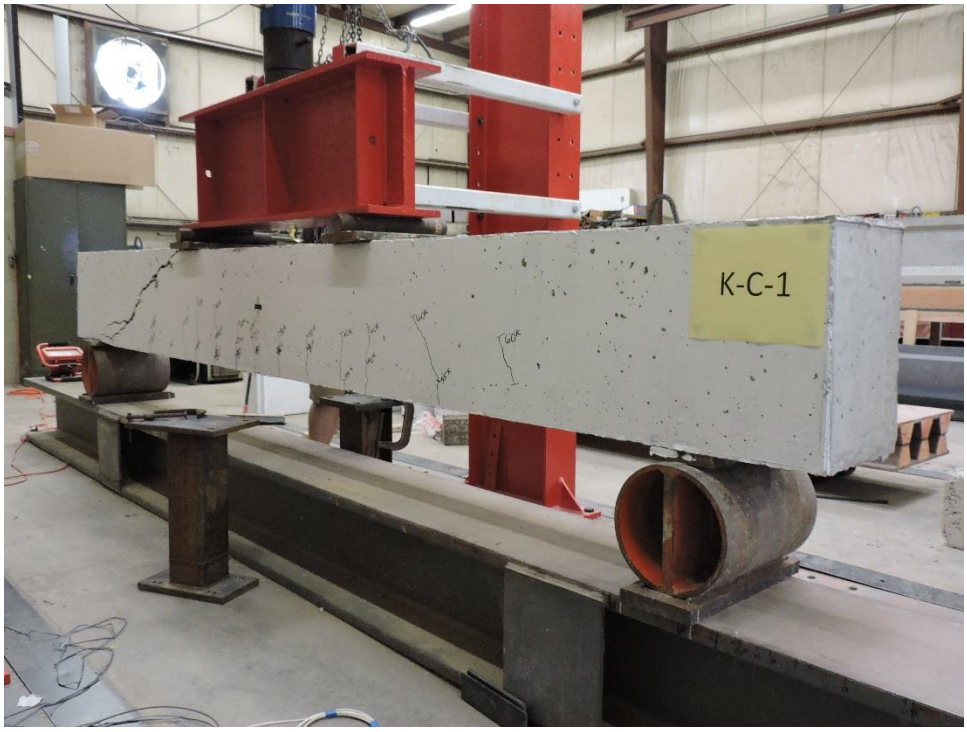

Figure A.5: K-C-1 Failure Crack Right View

Figure A.6: K-C-1 Failure Crack Front View

Figure A.7: K-C-1 Failed Beam

Figure A.8: K-C-2 Test Setup

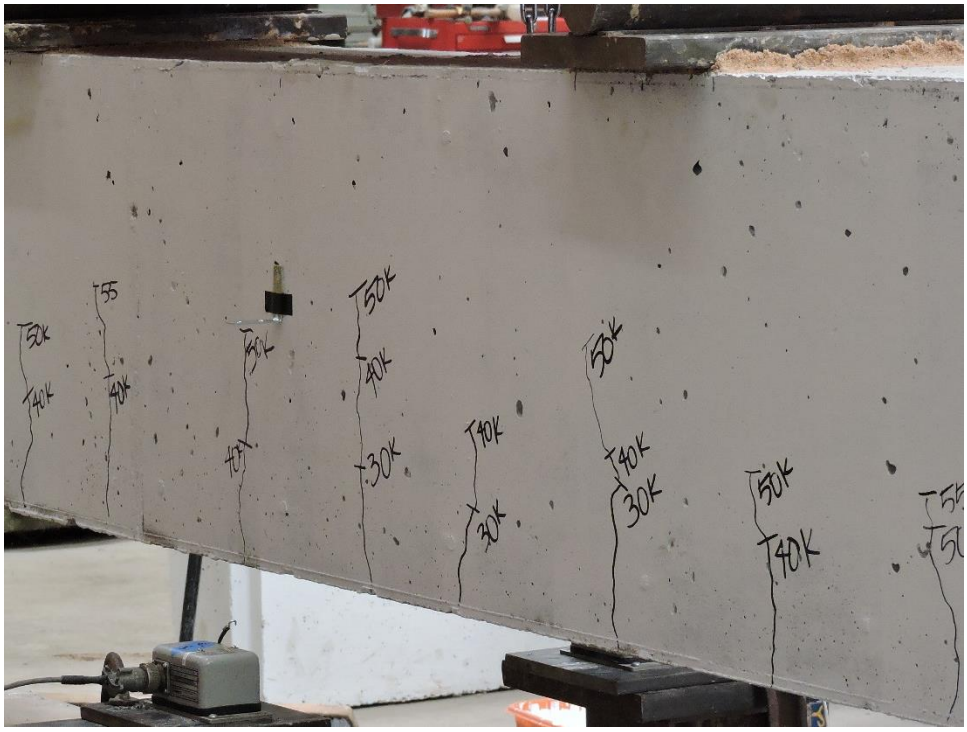

Figure A.9: K-C-2 Crack Propagation 50 kips

Figure A.10: K-C-2 Failure Crack Left View

Figure A.11: K-C-2 Failure Crack Right View

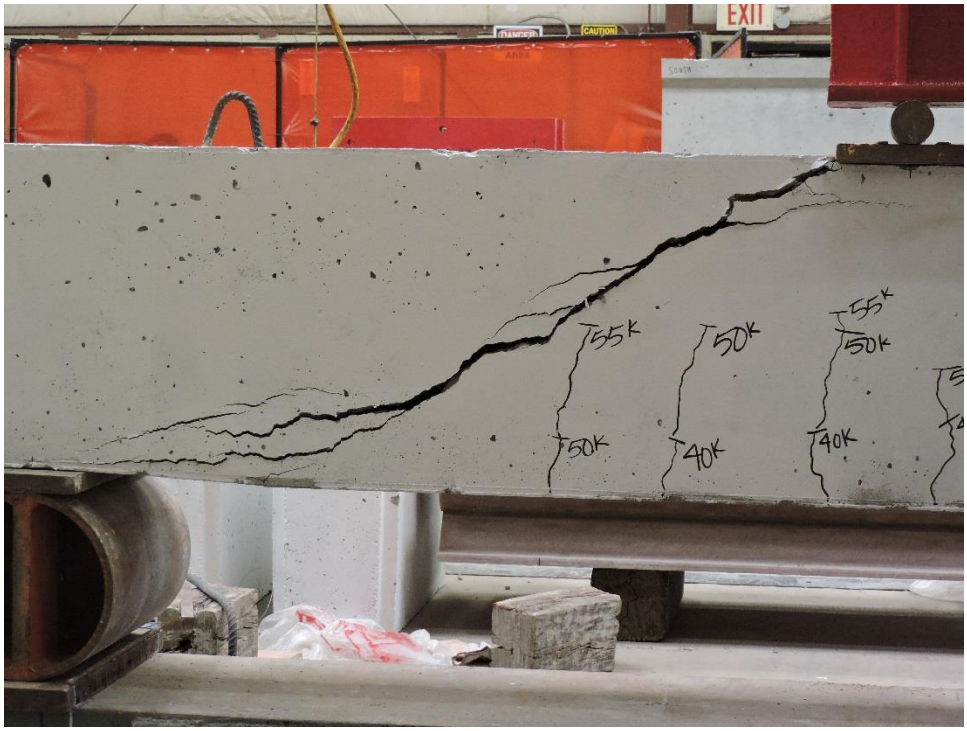

Figure A.12: K-C-2 Failure Crack Front View

Figure A.13: K-C-2 Failed Beam

Figure A.14: K-C-3 Test Setup

Figure A.15: K-C-3 Crack Propagation

Figure A.16: K-C-3 Failure Crack Left View

Figure A.17: K-C-3 Failure Crack Right View

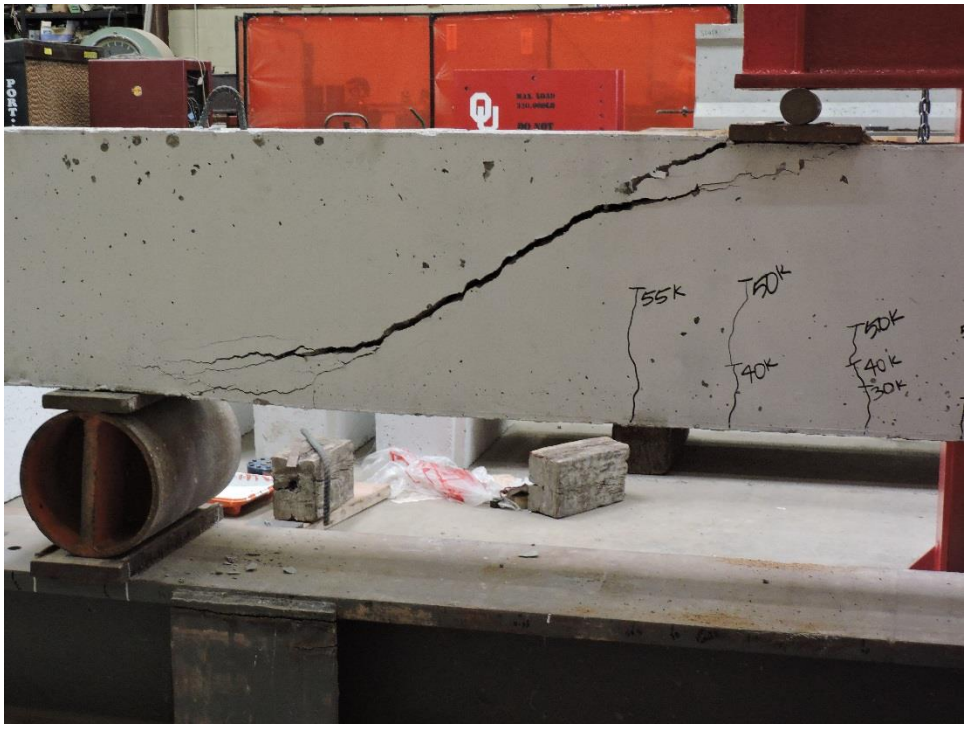

Figure A.18: K-C-3 Failure Crack Front View

Figure A.19: K-C-3 Failed Beam

APPENDIX B

ECO-BRIDGE-CRETE 1 TEST SPECIMENS

Figure B.1: K-E1-1 Test Setup

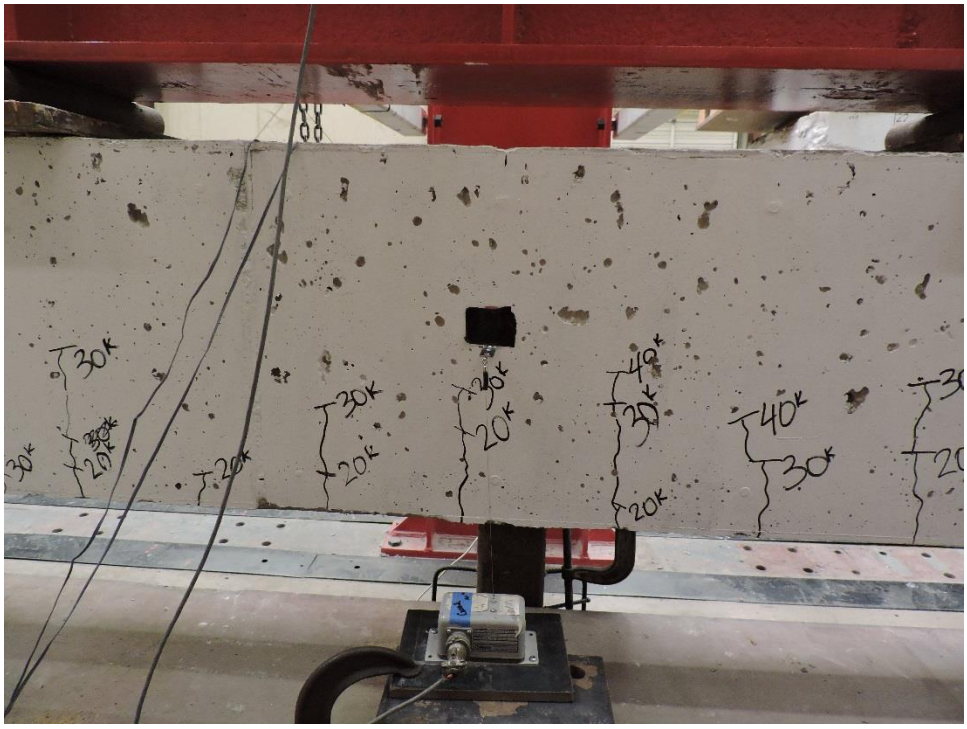

Figure B.2: K-E1-1 Crack Propagation 40 kips

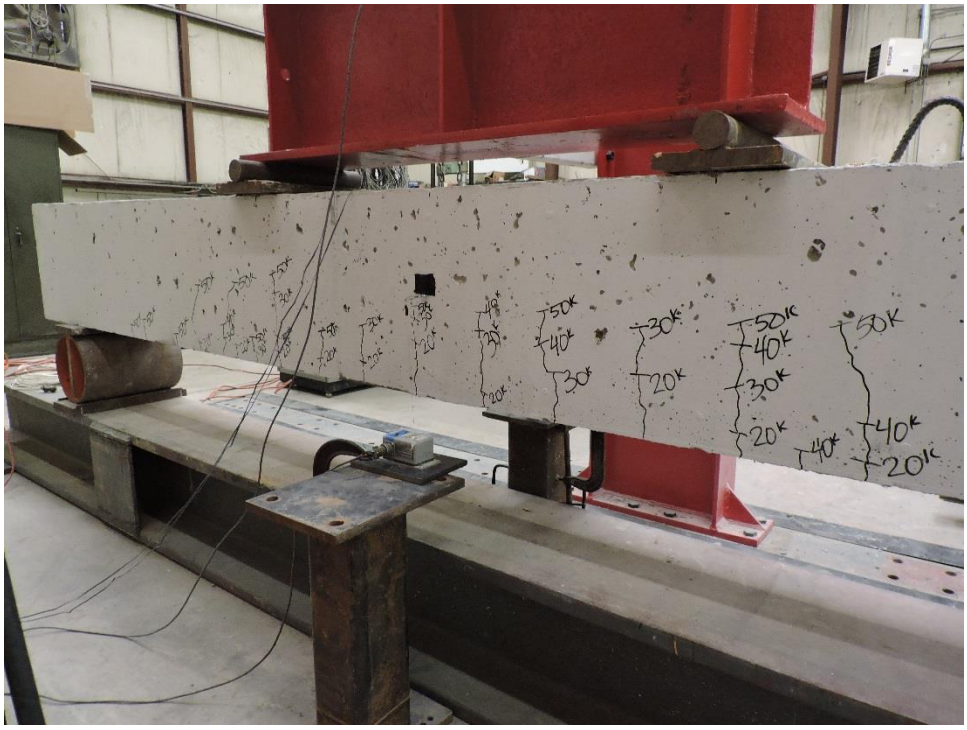

Figure B.3: K-E1-1 Crack Propagation 50 kips

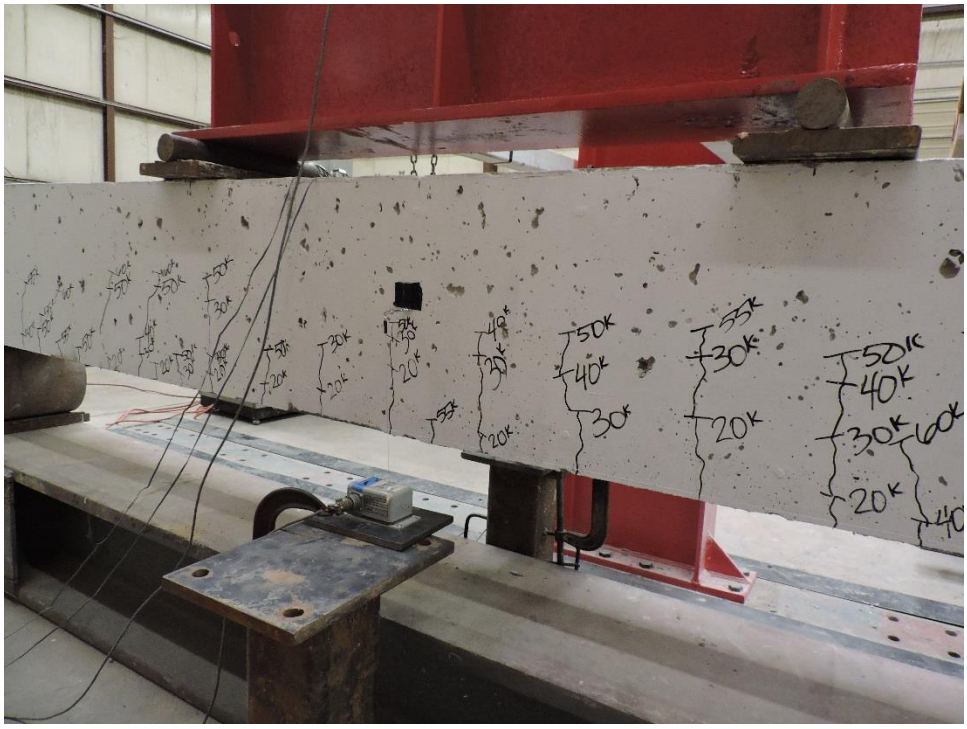

Figure B.4: K-E1-1 Crack Propagation 55 kips

Figure B.5: K-E1-1 Failure Crack Left View

Figure B.6: K-E1-1 Failed Beam

Figure B.7: K-E1-2 Crack Propagation 50 kips

Figure B.8: K-E1-2 Crack Propagation 50 kips

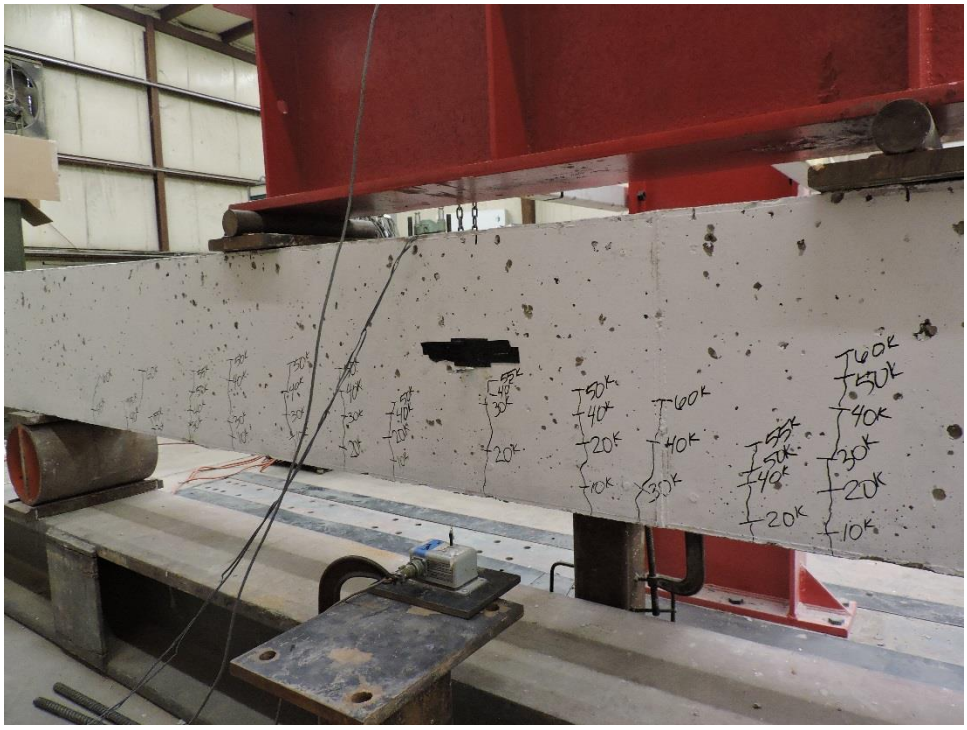

Figure B.9: K-E1-2 Crack Propagation 60 kips

Figure B.10: K-E1-2 Failure Crack Right View

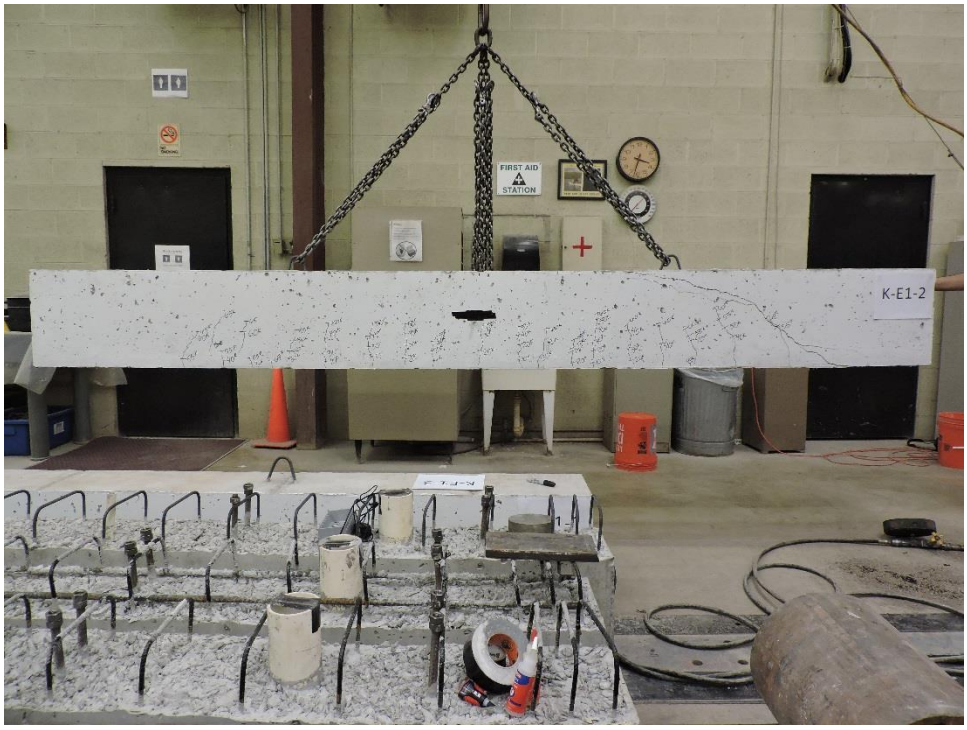

Figure B.11: K-E1-2 Failed Beam

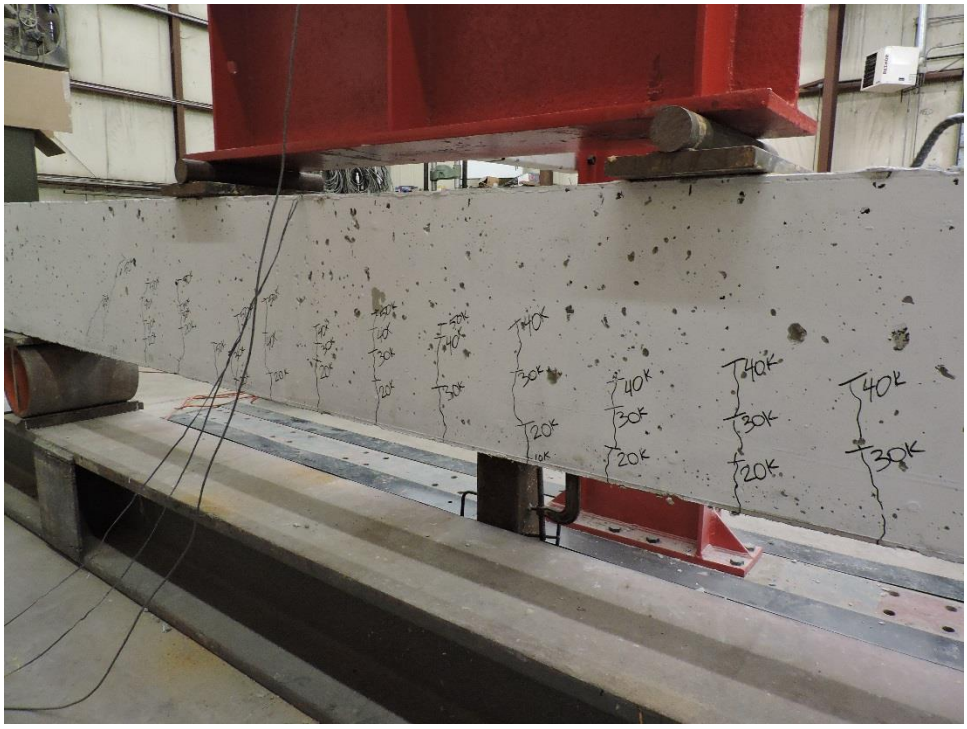

Figure B.12: K-E1-3 Crack Propagation 40 kips

Figure B.13: K-E1-3 Failure Crack Left View

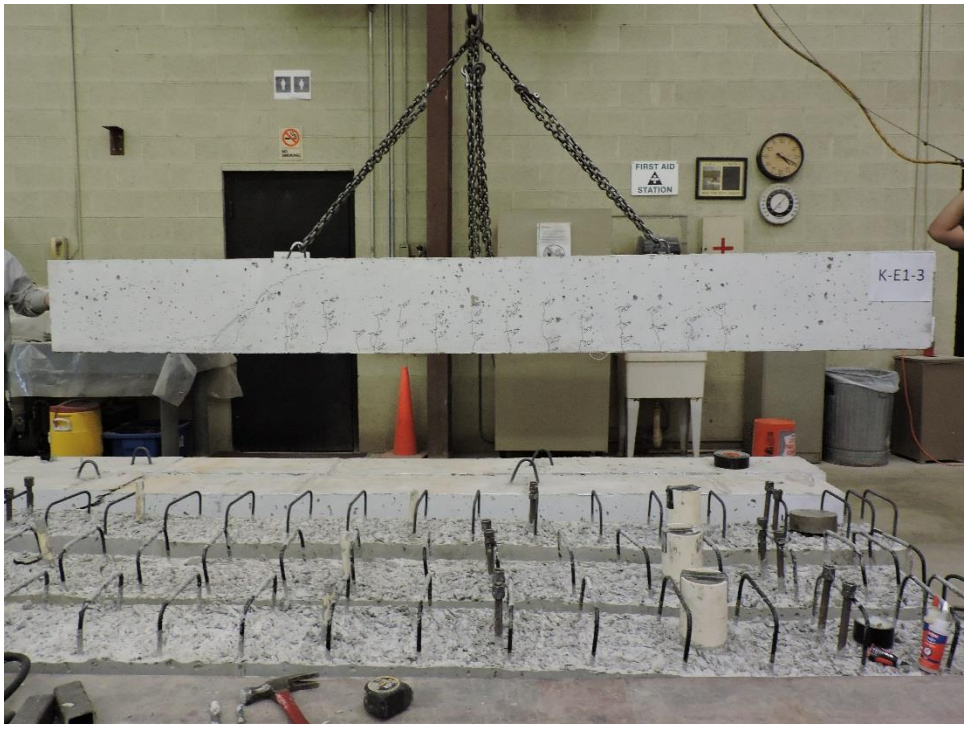

Figure B.14: K-E1-3 Failed Beam

APPENDIX C

ECO-BRIDGE-CRETE 2 TEST SPECIMENS

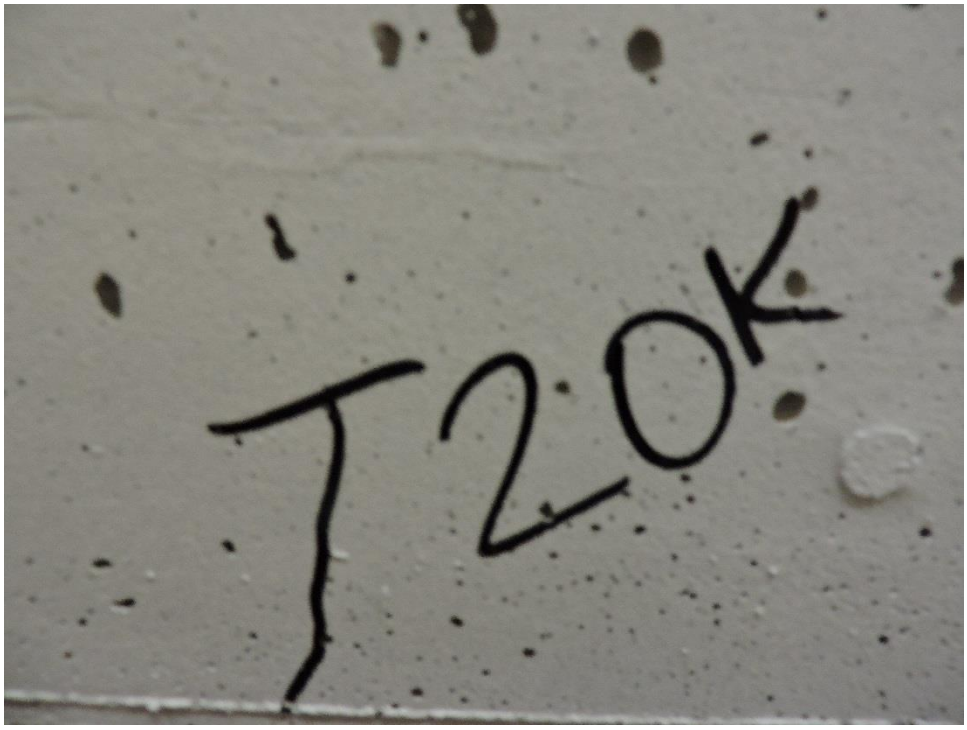

Figure C.1: K-E2-1 Crack Propagation 20 kips

Figure C.2: K-E2-1 Crack Propagation 20 kips

Figure C.3: K-E2-1 Crack Propagation 30 kips

Figure C.4: K-E2-1 Crack Propagation 50 kips

Figure C.5: K-E2-1 Failure Crack Right View

Figure C.6: K-E2-1 Failure Crack Left View

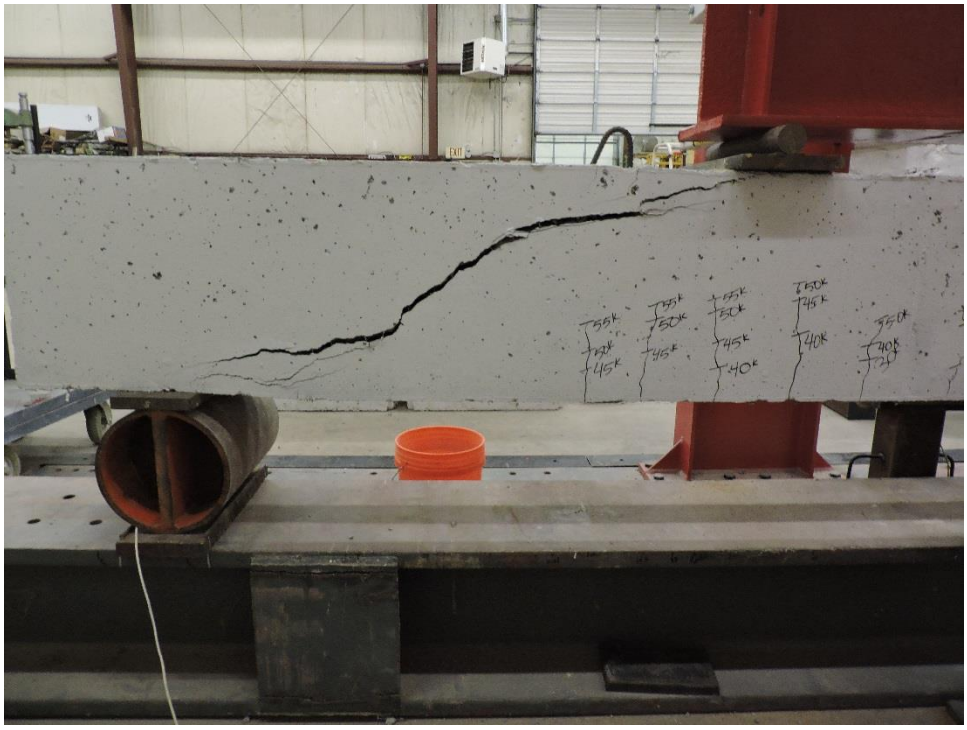

Figure C.7: K-E2-1 Failure Crack Front View

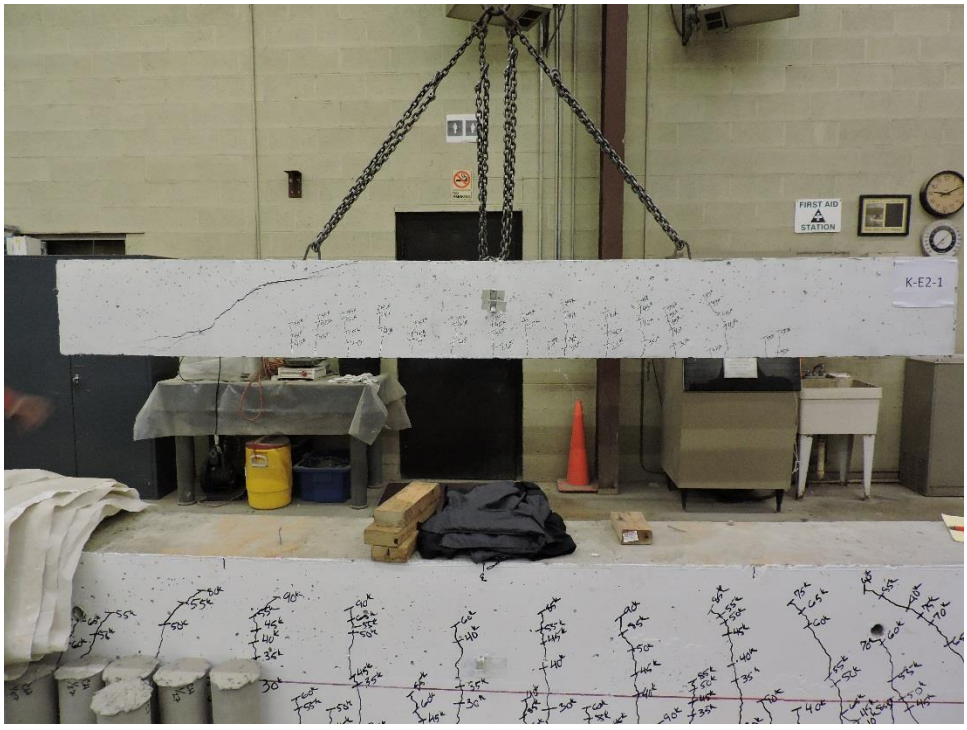

Figure C.8: K-E2-1 Failed Beam

Figure C.9: K-E2-2 Crack Propagation 35 kips

Figure C.10: K-E2-2 Crack Propagation 45 kips

Figure C.11: K-E2-2 Crack Propagation 65 kips

Figure C.12: K-E2-2 Failure Crack Right View

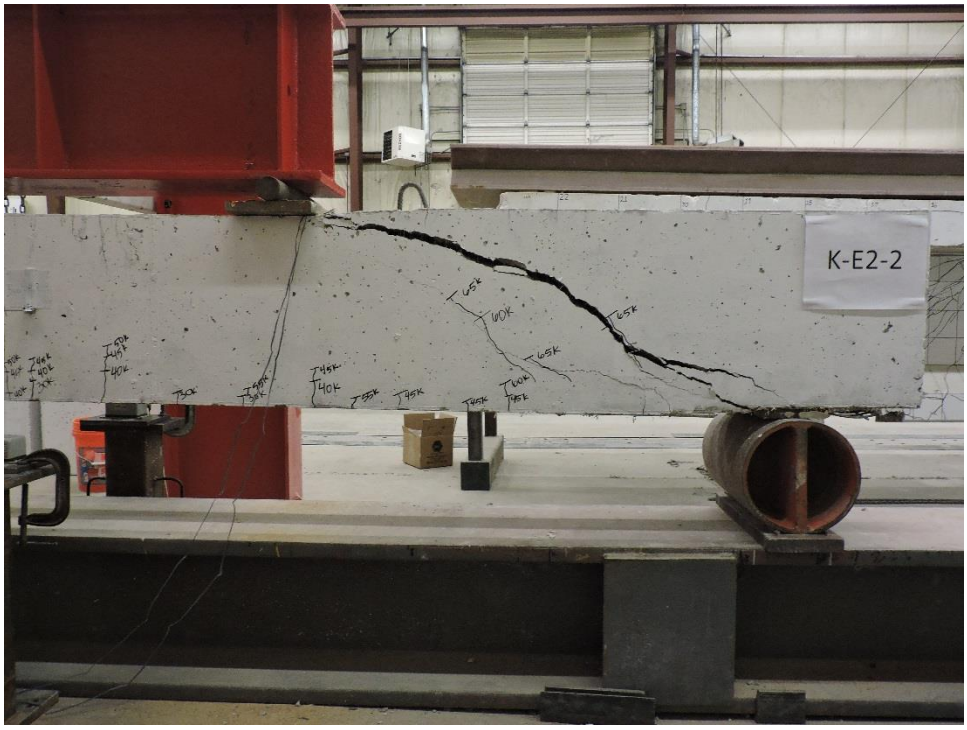

Figure C.13: K-E2-2 Failure Crack Front View

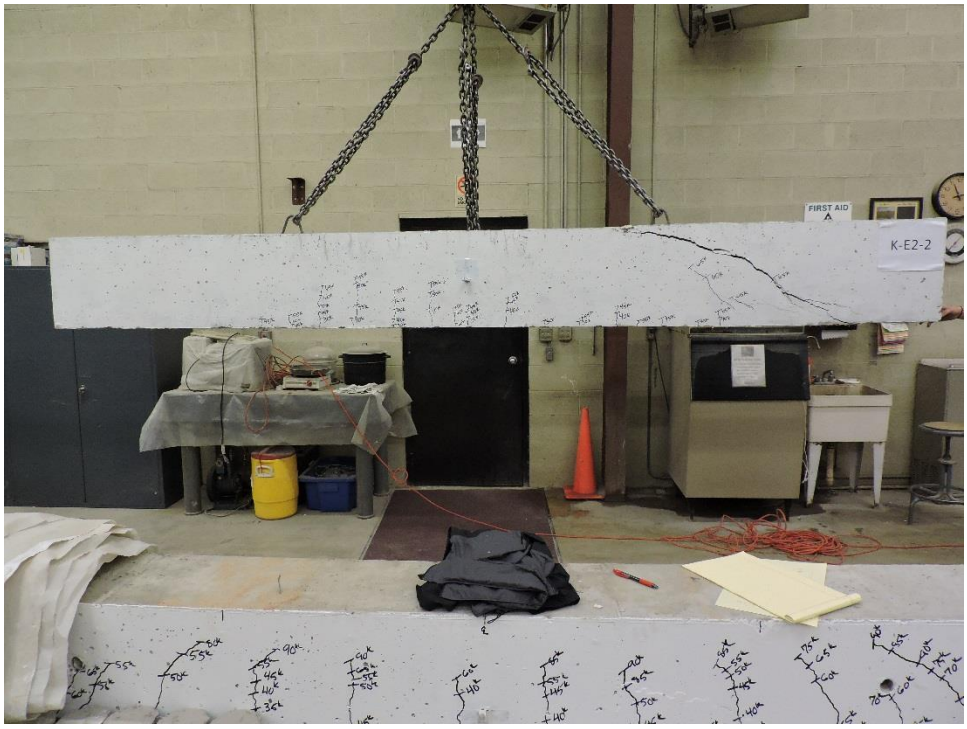

Figure C.14: K-E2-2 Failed Beam

Figure C.15: K-E2-3 Crack Propagation 40 kips

Figure C.16: K-E2-3 Crack Propagation 50 kips

Figure C.17: K-E2-3 Crack Propagation 65 kips

Figure C.18: K-E2-3 Failure Crack Right View

Figure C.19: K-E2-3 Failure Crack Front View

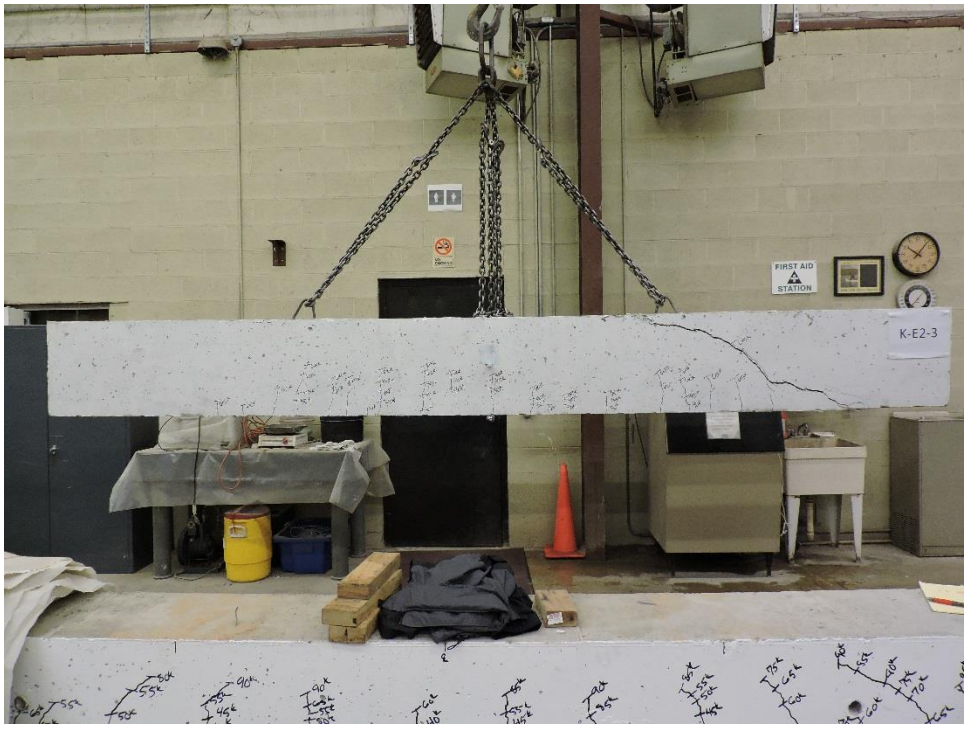

Figure C.20: K-E2-3 Failed Beam

APPENDIX D

LOAD DEFLECTION DATA FOR FULL-SCALE SPECIMENS

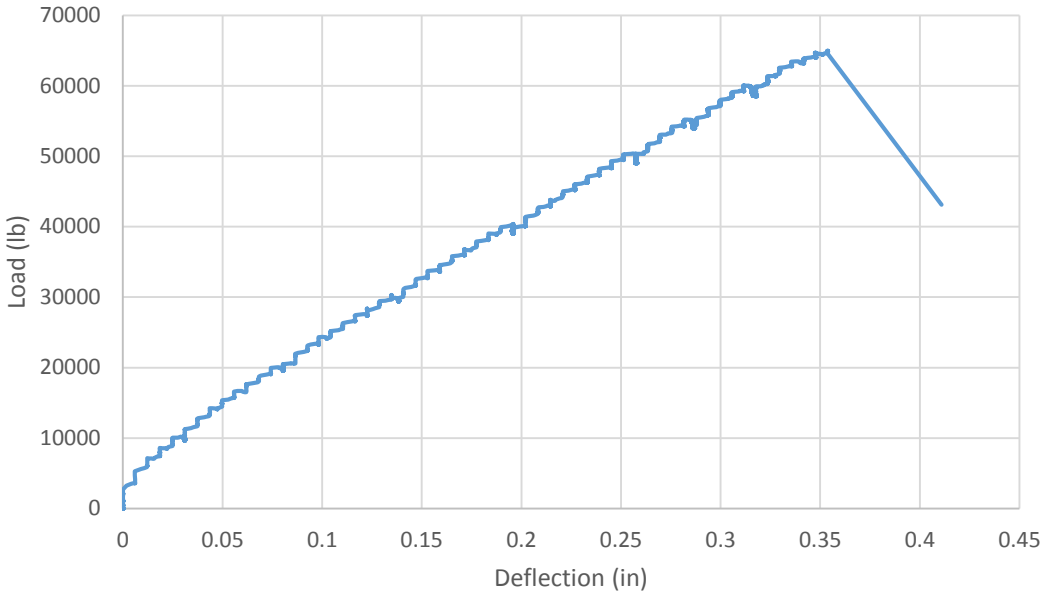

Figure D.1: K-C-1 Load Deflection Plot

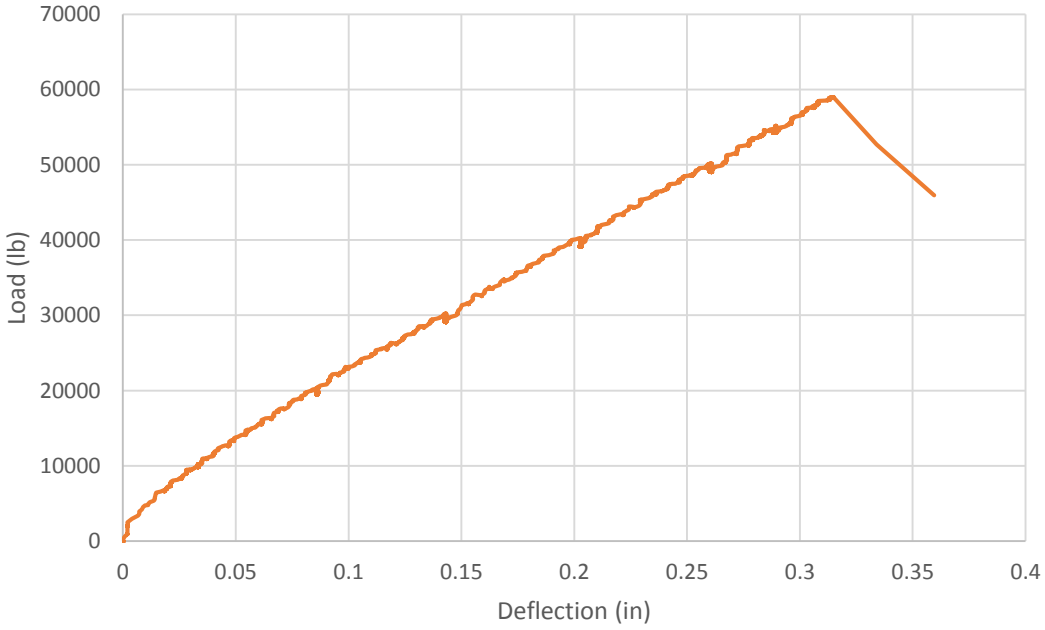

Figure D.2: K-C-2 Load Deflection Plot

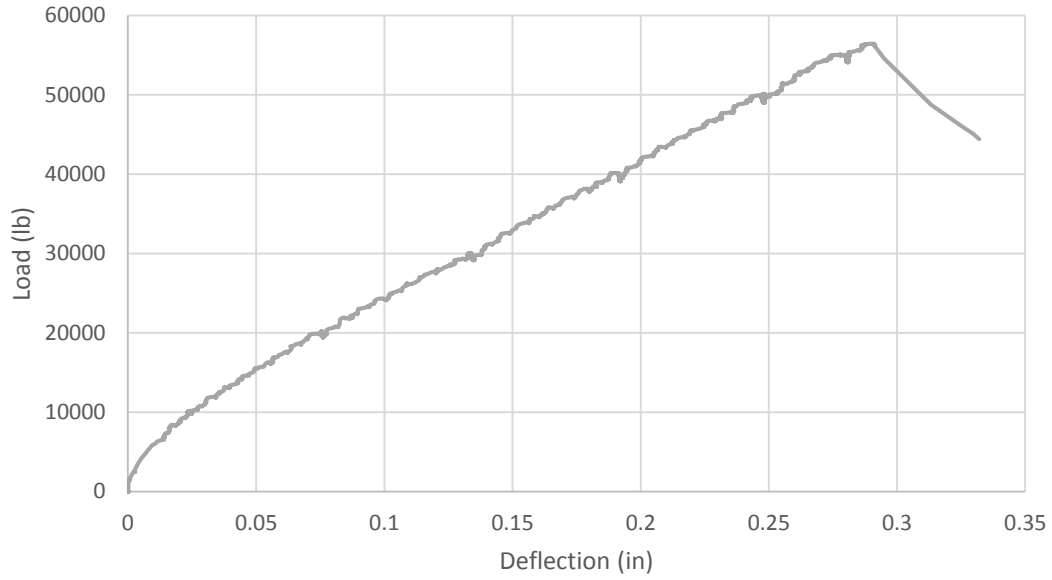

Figure D.3: K-C-3 Load Deflection Plot

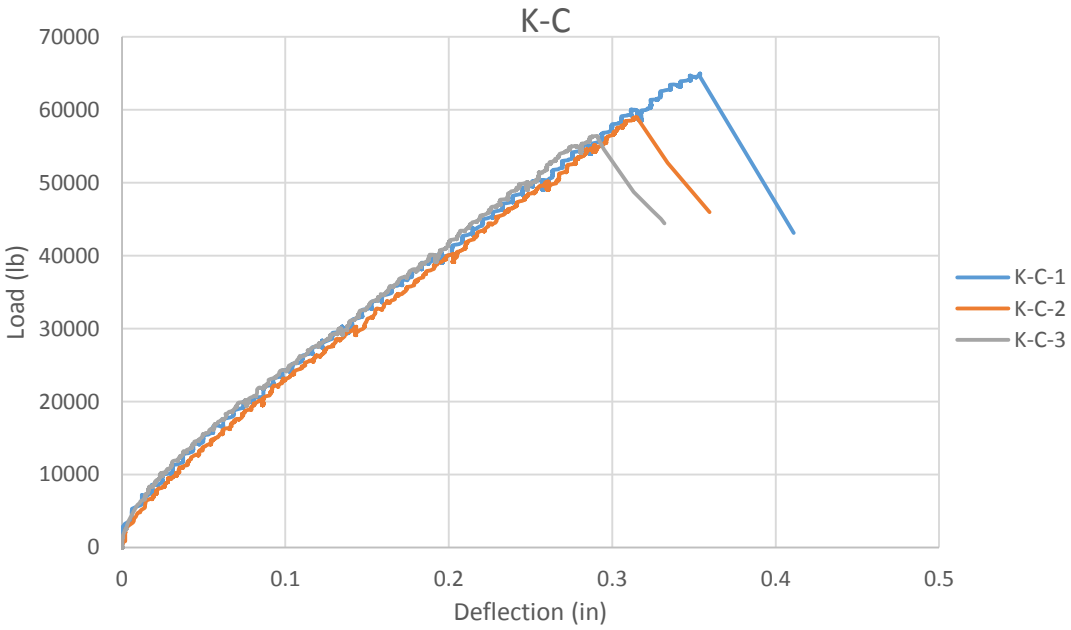

Figure D.4: K-C Combined Load Deflection Plot

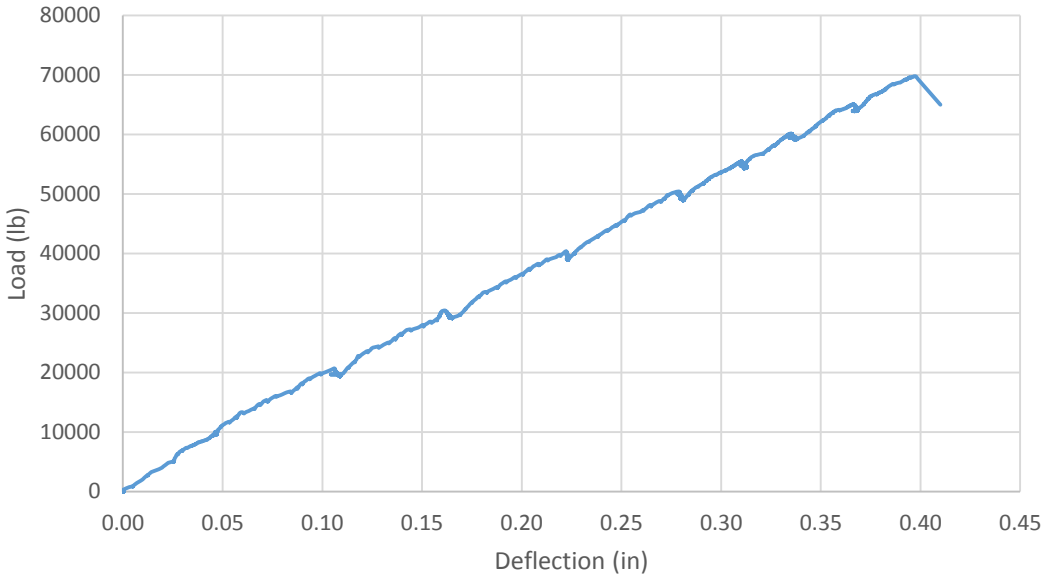

Figure D.5: K-E1-1 Load Deflection Plot

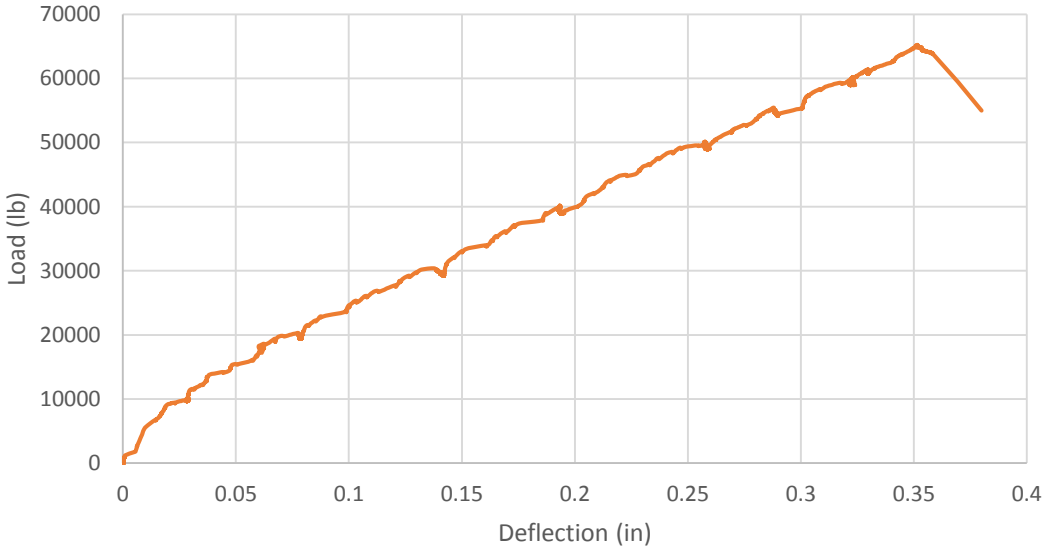

Figure D.6: K-E1-2 Load Deflection Plot

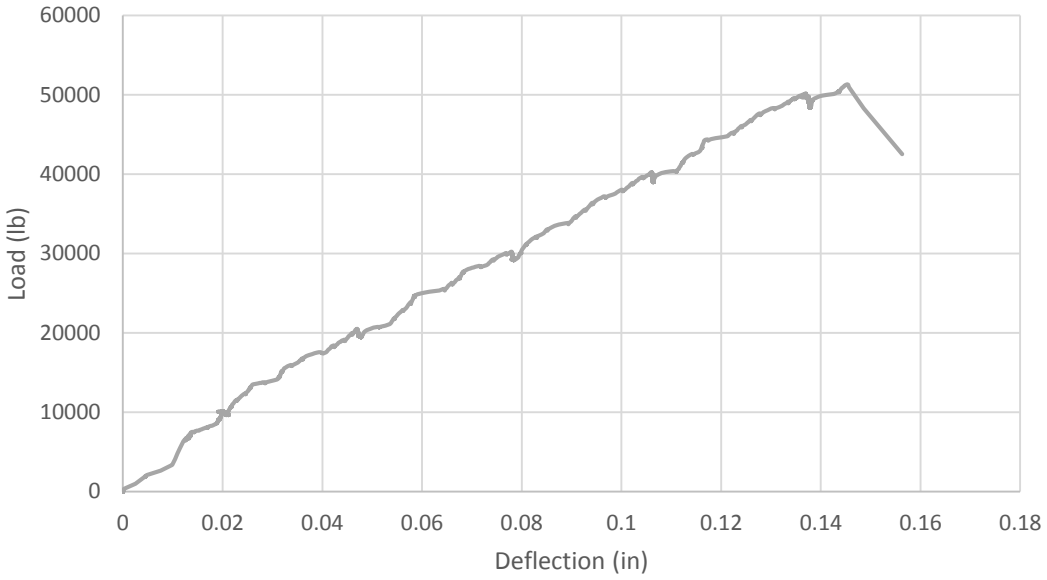

Figure D.7: K-E1-3 Load Deflection Plot

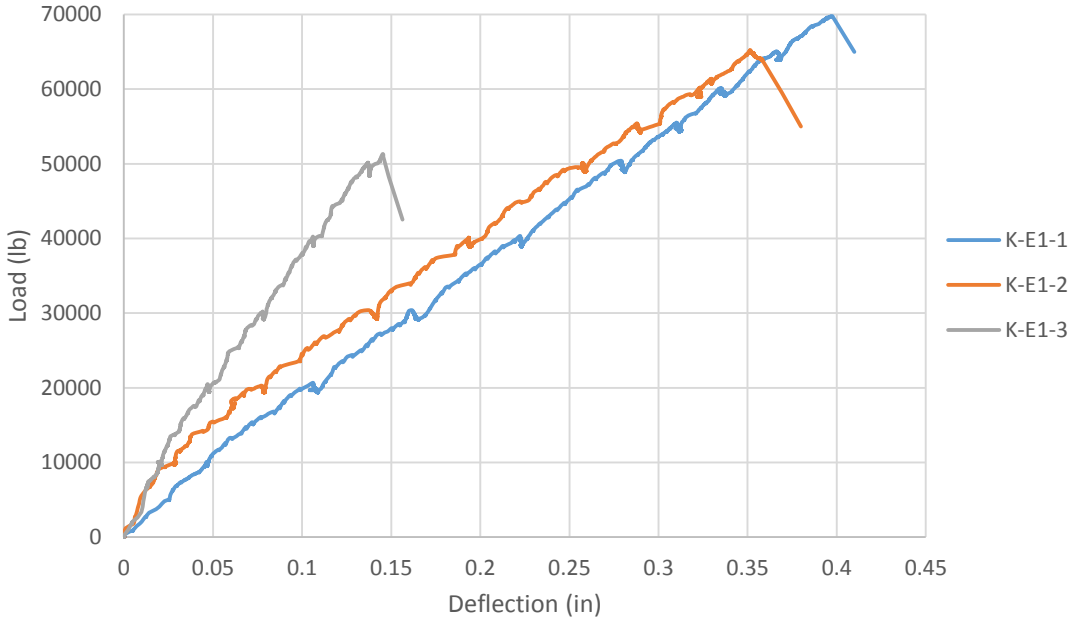

Figure D.8: K-E1 Combined Load Deflection Plot

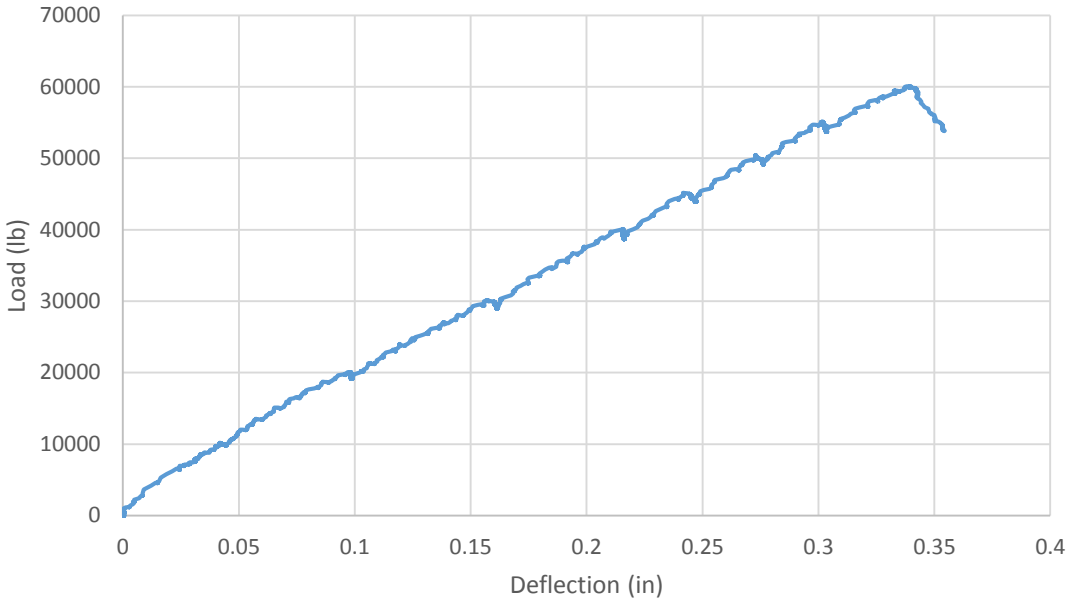

Figure D.9: K-E2-1 Load Deflection Plot

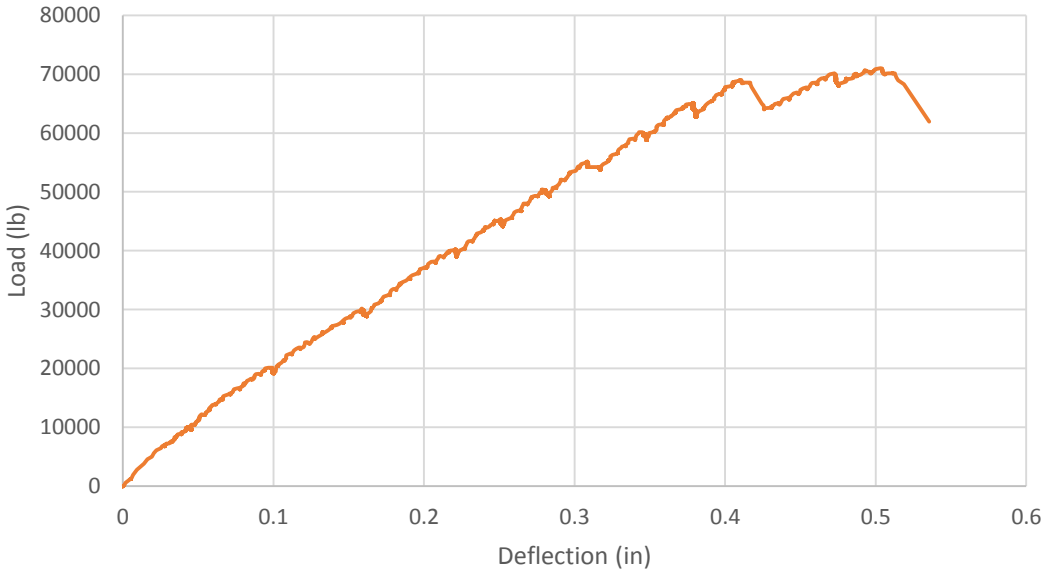

Figure D.10: K-E2-2 Load Deflection Plot

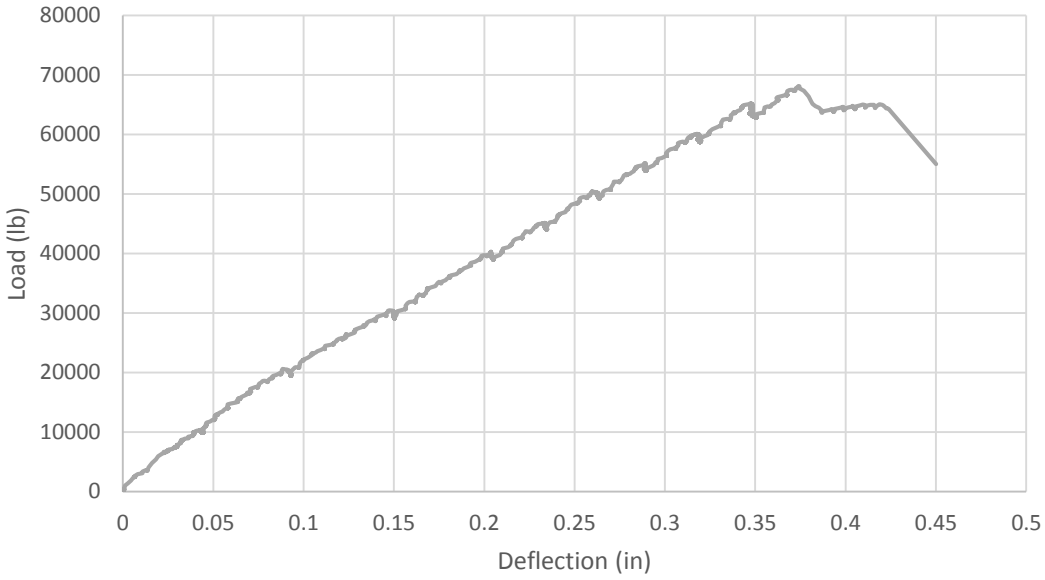

Figure D.11: K-E2-3 Load Deflection Plot

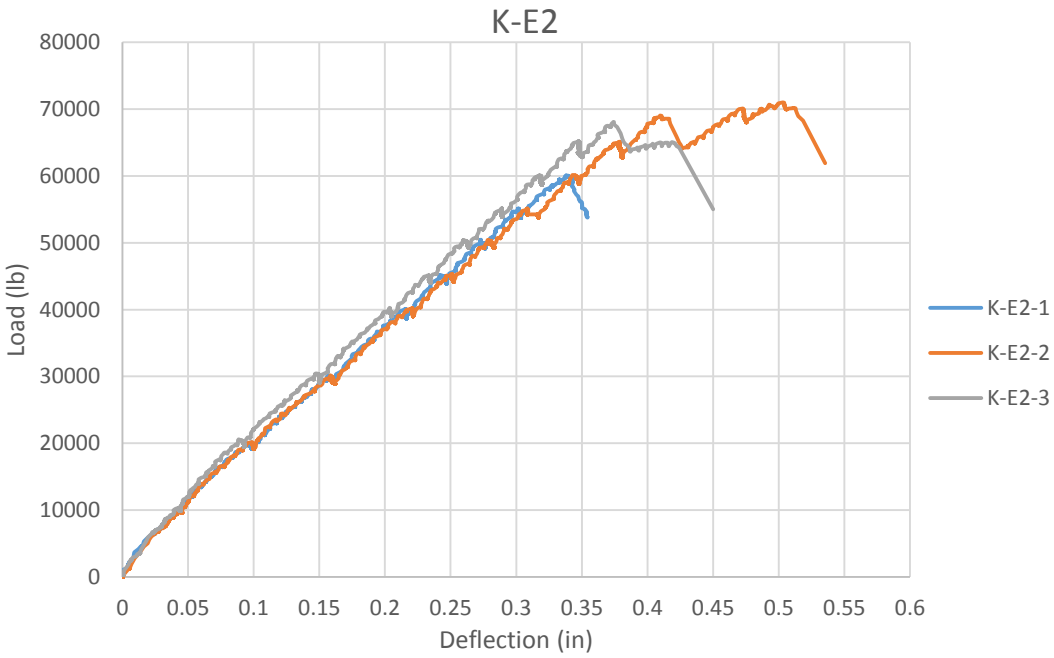

Figure D.12: K-E2 Combined Load Deflection Plot

APPENDIX E

SMALL-SCALE SPECIMEN DATA

Table E.1: K-C Compressive Strength Data

	Stress	Load	Average Stress	Average Load
1 Day	1,710	21,520	1,735	21,807
	1,695	21,302		
	1,800	22,600		
3 Day	3,390	42,030	3,360	42,030
	3,210	40,350		
	3,480	43,710		
7 Day	3,345	42,010	3,508	44,075
	3,365	42,280		
	3,815	47,935		
14 Day	4,595	57,740	4,498	56,540
	4,495	56,505		
	4,405	55,375		
Day of Testing	4,565	57,395	4,747	59,668
	4,870	61,210		
	4,805	60,400		
21 Day	4,595	57,780	4,642	58,360
	4,540	57,075		
	4,790	60,225		
28 Day	4,835	60,735	4,805	60,372
	4,500	56,565		
	5,080	63,815		

Table E.2: K-C MOR, Split Cylinder Data

	Load (lb)	Average Load (lb)
MOR	8,085	7757
	7,685	
	7,500	
Split Cylinder	14655	17668
	17400	
	20950	

Table E.3: K-C Prism Data

	b	d	Average b	Average d
Prism 1	6.202	5.988	6.202	5.996
	6.194	6.005		
	6.211	5.996		
Prism 2	6.313	5.995	6.288	5.993
	6.29	5.99		
	6.262	5.995		
Prism 3	6.271	6.025	6.270	6.029
	6.247	6.027		
	6.292	6.036		

Table E.4: K-E1 Compressive Strength Data

	Stress	Strain	Average Stress	Average Load
1 Day	1,465	18,420	1,445	18,165
	1,445	18,180		
	1,425	17,895		
3 Day	2,855	35,860	2,888	32,948
	2,900	26,430		
	2,910	36,555		
7 Day	3,470	46,635	3,460	44,488
	3,480	43,750		
	3,430	43,080		
17 Day	4,295	53,955	4,362	54,795
	4,460	56,035		
	4,330	54,395		
22 Day	4,665	58,600	4,438	55,773
	4,410	55,440		
	4,240	53,280		
28 Day	4,040	50,765	4,222	53,065
	4,170	52,425		
	4,455	56,005		
Day of Testing	4,330	54,395	4,437	55,752
	4,695	59,000		
	4,285	53,860		

Table E.5: K-E1 MOR, Split Cylinder Data

	Load (lb)	Average Load (lb)
MOR	7,065	6,842
	6,955	
	6,505	
Split Cylinder	17,010	18,352
	20,040	
	18,005	

Table E.6: K-E1 Prism Data

	b	d	Average b	Average d
Prism 1	6.148	6.314	6.075	6.325
	6.073	6.333		
	6.004	6.327		
Prism 2	5.979	6.306	5.987	6.284
	5.991	6.298		
	5.991	6.249		
Prism 3	6.001	6.166	6.015	6.179
	5.999	6.138		
	6.045	6.233		

Table E.7: K-E2 Compressive Strength Data

	Stress	Strain	Average Stress	Average Load
1 Day	1,840	52,005	1,833	51,845
	1,835	51,915		
	1,825	51,615		
3 Day	3,215	90,880	3,112	87,977
	3,035	85,840		
	3,085	87,210		
7 Day	3,660	103,510	3,587	101,402
	3,660	103,455		
	3,440	97,240		
14 Day	4,690	132,670	4,665	131,950
	4,595	129,930		
	4,710	133,250		
21 Day	4,645	131,330	4,620	130,650
	4,585	129,660		
	4,630	130,960		
Day of Testing	4,650	131,475	4,805	135,860
	4,840	136,800		
	4,925	139,305		
28 Day	5,030	142,280	4,945	139,857
	5,125	144,900		
	4,680	132,390		

Table E.8: MOR, Split Cylinder Data

	Load (lb)	Average Load (lb)
MOR	6,485	6,778
	7,365	
	6,485	
Split Cylinder	38,795	44,358
	46,005	
	48,275	

Table E.9: K-E2 Prism Data

	b	d	Average b	Average d
Prism 1	6.244	6.011	6.249	6.047
	6.269	6.098		
	6.233	6.031		
Prism 2	6.111	6.02	6.158	6.022
	6.184	6.031		
	6.179	6.016		
Prism 3	6.186	6.034	6.181	6.020
	6.179	5.994		
	6.178	6.031		

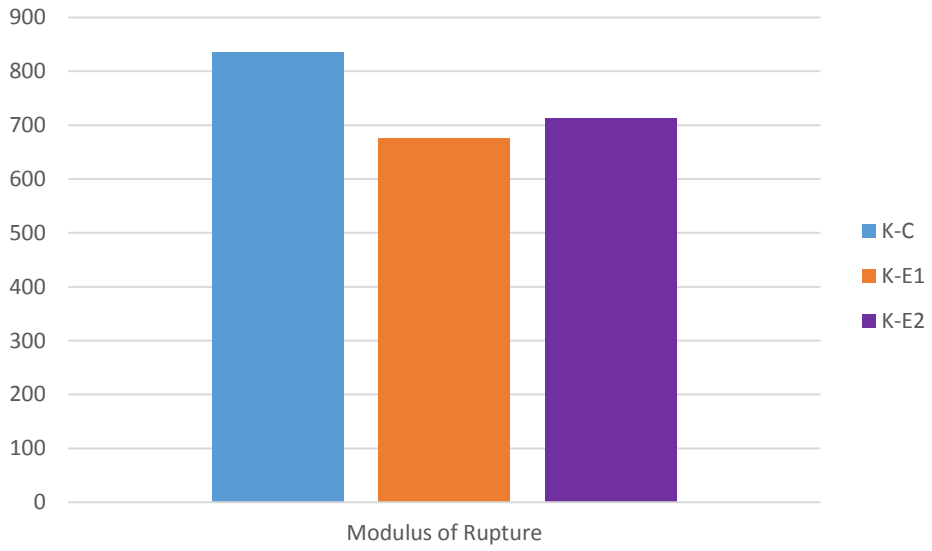

Figure E.1: Modulus of Rupture Comparison Chart

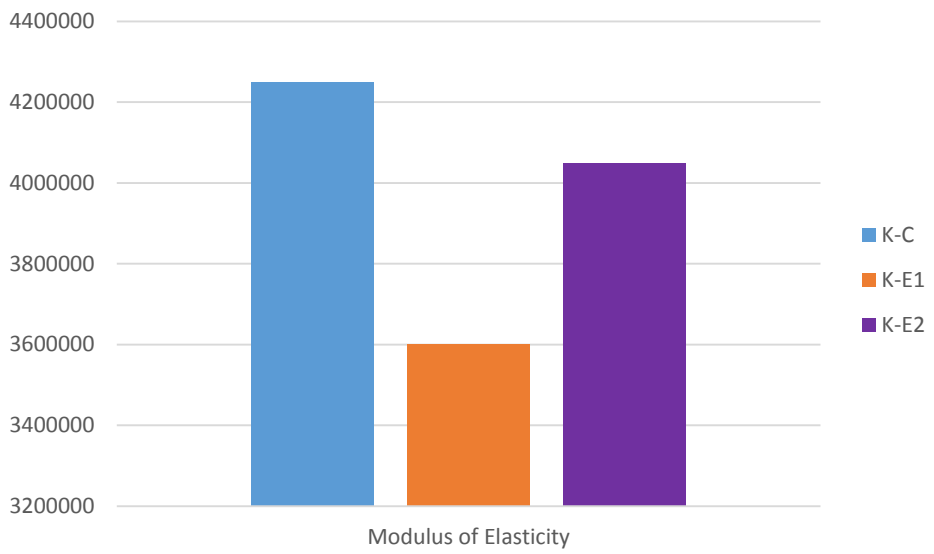

Figure E.2: Modulus of Elasticity Comparison Chart

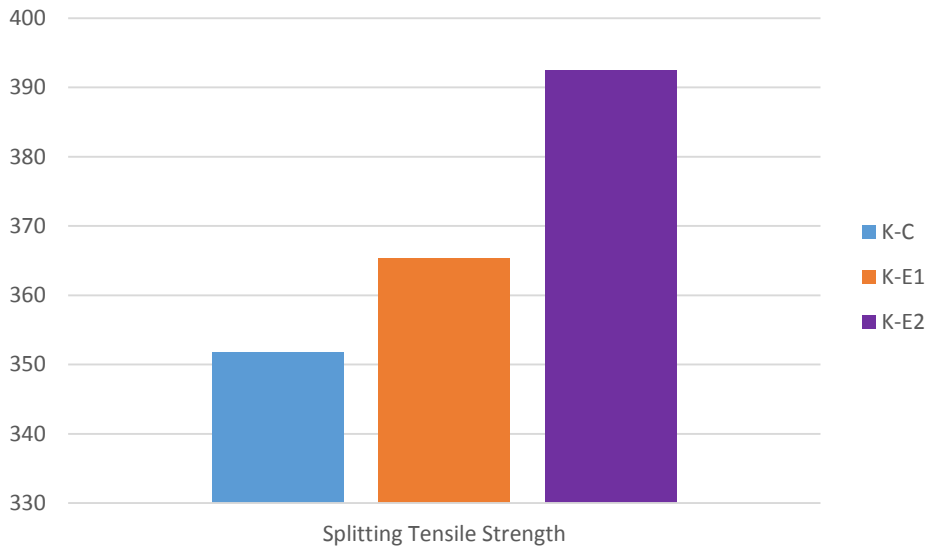

Figure E.3: Splitting Tensile Strength Comparison Chart